MᴄNᴀɪʀ Sᴄʜᴏʟᴀʀs Rᴇsᴇᴀʀᴄʜ Jᴏᴜʀɴᴀʟ

2014

A MESSAGE FROM THE WSU MCNAIR SCHOLARS PROGRAM

The Ronald E. McNair Postbaccalaureate Achievement Program is one of eight Federal TRIO educational access and equity initiatives. The Wayne State University McNair Scholars program is funded by a $1,125,000 grant from the U.S. Department of Education, Office of Postsecondary Education.

The McNair Scholars program is designed to prepare the next generation of scholars, professionals and leaders for doctoral study in the nation's top research universities. The purpose of the program is to increase the number of academically talented persons from low income/first generation and or underrepresented backgrounds with an earned Ph.D. McNair Scholars programs currently exist at over 200 colleges and universities.

The McNair Scholars program attracts applications from a highly competitive pool of undergraduate students with strong interest in research and graduate studies. Throughout the program year, McNair Scholars begin preparing for graduate school, receive research training and instruction and develop research proposals. The experiences prepare students for the Summer Research Experience where students conduct research projects under the guidance and mentorship of a faculty member. Scholars also complete an intensive research course, obtain GRE test preparation and engage in professional development workshops.

McNair Scholars present their research at the WSU Undergraduate Research Conference and select National McNair Conferences held throughout the nation.

The 2014 edition of the Wayne State University McNair Scholars Research Journal highlights the accomplishments of our Scholars and reflects the work of a wide variety of academic disciplines.

Please join the McNair Staff in congratulating the Scholars on their contributions to the advancement of knowledge in their respective fields of interest.

GO WARRIORS!!!!!

The Wayne State University McNair Scholars Staff

TABLE OF CONTENTS

MCNAIR PROGRAM STAFF

Henry L. Robinson
Director
Office of Federal TRIO-McNair Scholars
Co-Principal Investigator

Dr. Joseph Dunbar, Ph.D
Associate Vice President for Research/Graduate School
Co-Principal Investigator

Julianne Vernon, Ph.D
Research & Graduate School Coordinator

Carolyn Porter
Counselor

Marie Elena Villanueva
Secretary

FABRICATION AND ELECTRICAL CHARACTERIZATION OF NOVEL 2D MATERIAL-BASED ELECTRICAL DEVICES

By Hassan M. Barade
Major: Biomedical Physics
Mentor: Dr. Zhixian Zhou, Department of Physics & Astronomy

In today's world of constant achievement, seldom do we stop and admire tools which have helped make technology like the Hubble telescope, and mars rover possible. Many of these very important tools fall under the category of 2D material-based electronic devices. These devices utilize certain characteristics of molecules organized into very thin sheets. Looking deeper into the structure we see that these thin sheets are composed of many layers of highly organized molecules, each layer only as thick as the molecules it is composed of. Different types of compounds utilized for these 2D material-based electronic devices include Graphene (Figure 1), Hexagonal Boron (Figure 2), and Molybdenum Disulfide (Figure 3).
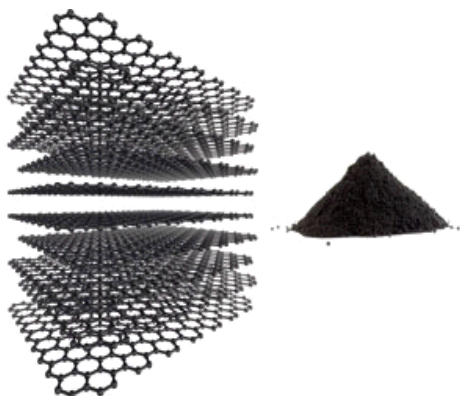
Figure 1: the figure depicts sheets of Graphene layered atop one another. Each sheet is composed of Carbon atoms bonded together in a hexagon. When multiple layers of Graphene are combined they form Graphite.

Hexagonal boron nitride structure
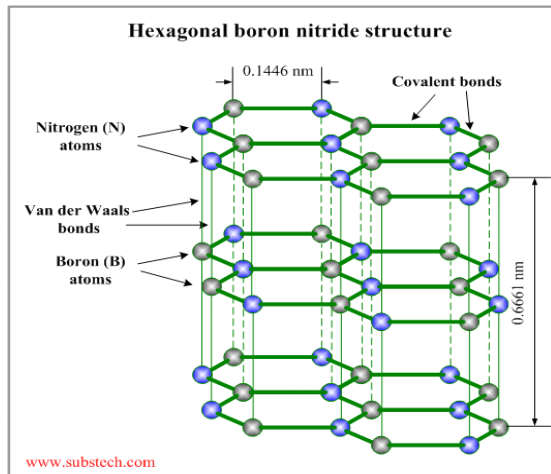
Figure 2: The figure shows the structure and shape of hexagonal boron nitride. The nitrogen atoms are seen in blue, while the boron atoms are shown in grey. Each sheet is composed of altering Nitrogen-Boron covalent bonds.
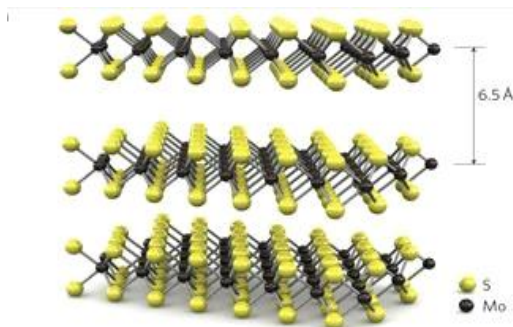
Figure 3: shown in this figure is the structure and layering of Molybdenum Disulfide (MoS_2). The yellow spheres represent Sulfur, while the black spheres represent Molybdenum. The sheets are separated from one another by a distance of 6.5A.

Graphene is essentially a one atom thick layer of mineral graphite, composed of many carbon molecules bonded together in a hexagon shape. Graphene has a long and successful history as a component of 2D material-based electronic devices, Experiments conducted with Graphene sheets show that the electron mobility value can reach values of 15,000 $cm^2.V^{-1s-1}$ at room temperature.[1] The mobility of a Graphene sheet is nearly independent of the temperature, between values of 10 K and 100 K.[1] Graphenes mobility, combined with its low resistance value of approximately 10^{-6} $\Omega \cdot cm$, shows how superb of a conductor it really is.[2-4] There are some electrical devices that cannot utilize Graphene due to the lack of certain properties, One device is the transistor.

The transistor works as a three terminal, solid state electronic device.[5] Electrical current and voltage between two of the terminals can be controlled and amplified in this device.[5] This is done by applying a current or voltage to the third terminal of the transistor, which will work to amplify the existing voltage.[5] The high conductivity of Graphene is mainly due the overlapping of the valance band with the conduction band, which results in the lack of a band gap. A band gap is the amount of energy required for an electron to move from the valance band of the molecule to the conduction band. Without a band gap Graphenes application in transistors is limited at best.

Transistors mainly utilize the band gap of a material to create electric switches. Electrical switches allow current and voltage rates to be controlled throughout a circuit. Cascading of these electrical switches allows for large electrical output with a small electrical input, which has many applications in logic circuitry. Altering the properties of Graphene is one proposed solution to the band gap problem, but any efforts to add a band gap are met with extreme resistance in the form of electron mobility retardation. This leaves no choice but to find a viable replacement for Graphene.

One viable replacement for Graphene is Molybdenum Disulfide (MoS_2). The physical characteristics of Molybdenum Disulfide are very similar to graphite, with only a few key differences. The structure of MoS_2 consists of layered sheets of Molybdenum sandwiched between two sulfur monolayers. Between these sheets is a relatively weak Van Der Waals attraction which allows samples of MoS_2 to be retrieved through mechanical cleavage. When in bulk Molybdenum Disulfide delivers a band gap of 1.2eV.[6,7,8] But when found in only a few layers this band gap has a value of 1.8eV, similar to Graphene.[6,7,8]

The use of MoS_2 in transistors has been demonstrated with very successful results. MoS_2 based transistors could have various application in integrated circuits, which could lead to its application in high performance low energy nanotechnology. One drawback to MoS_2 based transistors is the low electron mobility MoS_2 offers at room temperature, typically in the range of $.1 - 10$ cm^2 $s^{-1}V^{-1}$.[6, 9-12] This extreme limitation of the electron mobility has been attributed to the MoS_2 and SiO_4 substrate interface. To allow electrons to pass through this contact point a Schottky barrier must be overcome, which is a potential energy barrier formed at the metal-semiconductor junction.
Research efforts to reduce the Schottky barrier at the metal and semiconductor junction have been done with much success. One method to reduce the Schottky barrier was electrostatic doping using an ionic liquid. This method gave very impressive results, increasing the mobility from $.1 - 10$ cm^2 $s^{-1}V^{-1}$ to $63 - 293$ cm^2 $s^{-1}V^{-1}$.[6, 9-12] With these results MoS_2 proves to be a viable replacement to Graphene. Synthesis of a MoS_2 based circuit is required for testing purposes. We begin with sample preparation and characterization.

The Circuit begins with a piece of Silicon/Silicon Dioxide dielectric substrate. Samples of MoS_2 are applied by Mechanical Exfoliation. This process begins with applying a thin layer of MoS_2 onto a piece of tape, then attaching the tape to the SiO_2 substrate. After the tape is applied to the substrate it is slowly removed leaving traces of the MoS_2 on the substrate. The tape used during ME is a special type, which will not leave as much adhesive on the layer of MoS_2 as normal scotch tape would. At this point we have a substrate made up of 300nm of Silicon, 180 nm of SiO_2, and small samples of MoS_2 applied to the surface.

The samples of MoS_2 applied to the substrate are located through a coordinate system coated onto the Si/SiO_2 substrate. The coordinate system centers at zero in the very center of the substrate. Through the use of these coordinates samples of the MoS_2 samples, which are on the nanometer scale, can be observed and relocated. The coordinate system consists of large crosshairs organized as the corners of individual squares on the substrate. Within a square of the large crosshairs are smaller crosshairs, which section off individual units of the square. This allows you to take the coordinates of the upper left large crosshair, and inside the square created by the upper left large crosshair the coordinate of the lower right small cross hair can be taken. With these coordinates one can easily record the exact location of a MoS_2 sample.
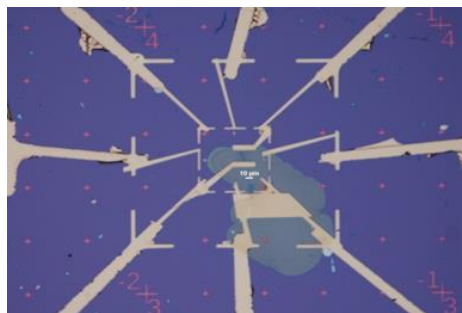

Figure 4: this figure shows the coordinate system mentioned above. The large crosshairs are shown with the coordinate -2/4, -1/4, -2/3, and -1/3. If all four cross hairs are connected the form the corners of a square which is sectioned off by even smaller crosshairs.

The next step in this process is to find samples adequate enough to be used in the circuit. Adequate samples are ones that are rectangular, have sharp edges, smooth surface area, and are less than 15nm in height. Samples are initially observed through a normal optical microscope, than an Atomic Force Microscope is used to further observe the sample. The coordinates of the samples that meet the standards are recorded, so they can be further observed by AFM.

The AFM is used to observe the characteristics of the MoS_2 samples that we are not able to see through a normal optical microscope. Characteristics being by the AFM include the samples height, and surface texture. Because the samples shape and size are important noncontact mode AFM is used. During noncontact mode AFM the samples are scanned by a cantilever. This cantilever never makes contact with the sample; instead it oscillates above the sample. As the cantilever oscillates microscopic forces between it and the sample are recorded, and with the help of a precise laser a highly detailed image is created.

After AFM is completed and a sample is found, a layer of PMMA is applied to the entire surface of the substrate. This layer acts a type of icing which can be drawn into. The Pattern being drawn can be thought of as a stencil or outline for the circuits' metal pathways. The pattern is created by drawing it into some software called Nano pattern generating system. The pattern drawn will have three layers the first layer is located at the center of the second layer, and the second layer within the center of the third.

The first layer consists of a top gate, and two cathodes. Of the two cathodes one is a drain cathode, and the other is a source cathode, both of which are in direct contact with the MoS_2 sample. The purpose of this layer is to make contact with the MoS2 sample. The second layer consists of the first layer at its center, and electron paths that lead to larger structures. The purpose of the second layer is to make contact between the small first layer and the much large third layer. The third layer consists of the first and second layers within its center, and some Electrode pads. The purpose of the third layer is to have electrode pads large enough for an actual sized electrode to be placed on.

When the pattern is completed it can be drawn into the layer of PMMA applied to the entire substrate. The pattern is drawn through a constant bombardment of electrons, using a scanning electron microscope with Nano pattern generating software attached to it. The coordinate square which the MoS_2 sample is found in is aligned with the crosshairs of the SEM, then using the Nano pattern generating software a pattern is drawn into the surface of the PMMA. The electrons from the SEM collide with the surface of the PMMA, effectively digging into it. What is left after the pattern is drawn is a layer of PMMA with a hollowed out pattern.

The hollowed pattern will soon be become the tracts by which metal conductors allow current to travel to the MoS_2 sample. The process by which the metal tracts are created is called Evaporation Metal Deposition. In this process a metal is heated in a vacuum until it evaporated. Its vapors are allowed to travel upwards to where the entire substrate, still coated with the PMMA, is held face down. The evaporated metal evenly distributes itself across the entire substrate surface, even in the hollowed patterns created by the SEM. The metal is then allowed to cool and the PMMA is washed away leaving nothing on the substrates surface but the metal tracks and the MoS2 sample. The metal tracts in our case are created from two types of metal; gold and titanium.
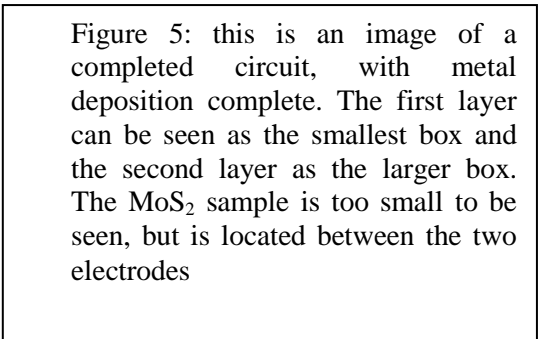
Figure 5: this is an image of a completed circuit, with metal deposition complete. The first layer can be seen as the smallest box and the second layer as the larger box. The MoS_2 sample is too small to be seen, but is located between the two electrodes
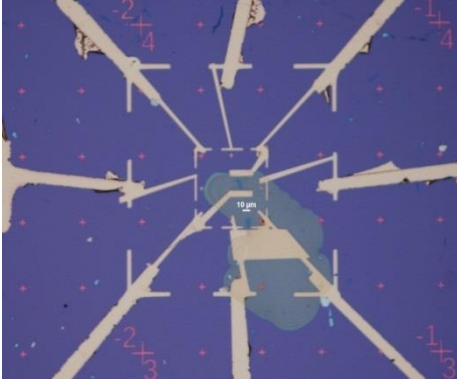
The first metal to be deposited onto the tracts is titanium. The titanium metal is evaporated in a vacuum allowing a 10nm layer of titanium to form on the substrate. The metal is allowed to cool and then gold is allowed to evaporate creating another uniform layer to form, this one is roughly 50nm. The PMMA is then dissolved away using acetone, leaving 60nm tall metal tracts comprised of 10nm of titanium, and 50nm of gold. With the circuit complete we can now begin testing it.

The circuit is tested by applying two voltages and determining the output current. One of the voltages is applied through the Si/SiO2 substrate; this is called the back gate voltage. The other voltage is applied from an electrode in contact with the electrode pad in the third layer of the circuit, which is indirectly in contact with the source electrode attached to the MoS_2 sample. The voltage applied to the MoS_2 is drained through a grounded drain electrode. The difference in voltages between the drain electrode and the source electrode is called the drain-source voltage.

The purpose of this setup is to test how much carriers are introduced to the MoS_2 sample through the Si/SiO$_2$ substrate. This is done by plotting multiple graphs of the drain-source voltage Vs. the Drain source current and determining the change in current as different back gate voltages are applied to the circuit. The experiment was conducted and the following results were obtained.
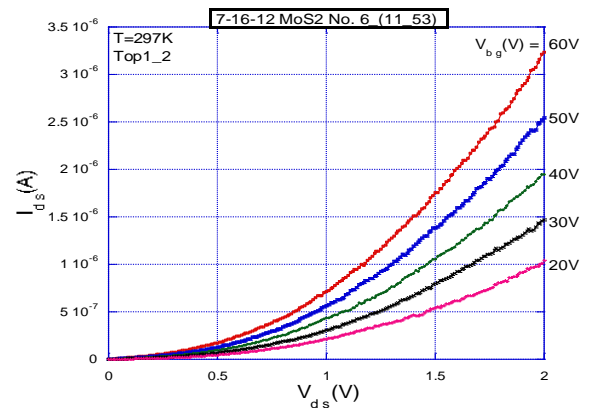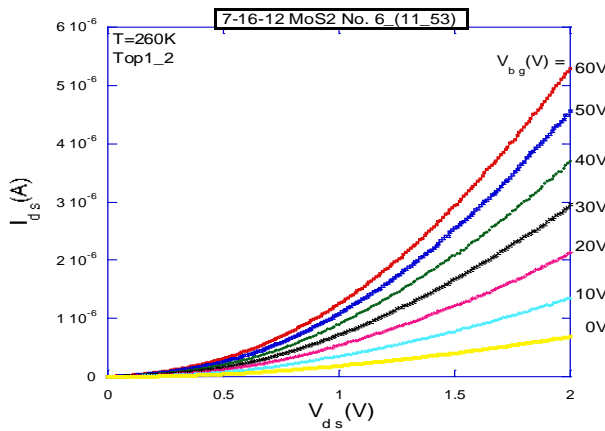
These are two graphs of the voltage drain-source vs. the current drain source. Multiple graphs are combined on these graphs, with each color representing measurements of voltage drain-source vs. the current drain

taken at different applied back gate voltages. From the graph one can easily see that as the back gate voltage is applied the current drain-source increases. This is because as the back gate voltage is increased the ability of the SiO_2 to introduce more carriers into the system is increased as well. With an increase in carriers the current of the system will increase as well. This is why the current is higher on the graphs with larger back gate voltages.

REFERENCES

1. "Graphene." *Wikipedia*. Wikimedia Foundation, 08 Sept. 2013. Web. 10 Aug. 2013. <http://en.wikipedia.org/wiki/Graphene>.
2. Nosolev, K.S, Geim, A.K, Morozov, S.V, Jiang, D, Katsnelson, M.I, Grigorieva, I.M, Dubonos, S.V and Firsov, A.A, Nature 438, 197 (2005).
3. Geim, A.K and Novoselov, K.S, Nature 6, 183-191(2007).
4. Akturk, A and Goldsman, N, J. Appl. Phys. 103, 053702 (2008).
5. Haviland, David B. " The Transistor in a Century of Electronics." The Transistor. N.p., 19 Dec. 2002. Web. 03 Aug. 2013. <http://www.nobelprize.org/educational/physics/transistor/history/>.His article]
6. Meeghage Madusanka Perera,† Ming-Wei Lin,† Hsun-Jen Chuang,† Bhim Prasad Chamlagain,† Chongyu Wang,† Xuebin Tan,‡ Mark Ming-Cheng Cheng,‡ David Toma´ Nek,§ and Zhixian Zhou. "Improved Carrier Mobility in Few-Layer MoS2 Field-Effect Transistors with Ionic-Liquid Gating." (2013): 1. Web.
7. Yoon, Y.; Ganapathi, K.; Salahuddin, S. How Good Can Monolayer MoS2 Transistors Be? Nano Lett. 2011, 11, 3768–3773.
8. Mak, K. F.; Lee, C.; Hone, J.; Shan, J.; Heinz, T. F. Atomically Thin MoS2: A New Direct-Gap Semiconductor. Phys. Rev. Lett. 2010, 105, 136805.
9. Balandin, A. A.; Ghosh, S.; Bao, W.; Calizo, I.; Teweldebrhan, D.; Miao, F.; Lau, C. N. Superior Thermal Conductivity of Single-Layer Graphene. Nano Lett. 2008, 8, 902–907.
10. Novoselov, K. S.; Jiang,D.; Schedin, F.; Booth, T. J.; Khotkevich, V. V.; Morozov, S. V.; Geim, A. K. Two-Dimensional Atomic Crystals. Proc. Natl.Acad. Sci. U.S.A. 2005, 102, 10451–10453.
11. Wang, H.; Yu, L.; Lee, Y.-H.; Shi, Y.; Hsu, A.; Chin, M. L.; Li, L.-J.; Dubey, M.; Kong, J.; Palacios, T. Integrated Circuits Based on Bilayer MoS2 Transistors. Nano Lett. 2012, 12, 4674– 4680.
12. Liu, H.; Neal, A. T.; Ye, P. D. Channel Length Scaling of MoS2 MOSFETs. ACS Nano 2012, 6, 8563–8569.

Infrared Filtering via Sub-Wavelength Gratings for Hyperspectral Imaging

By Arthur Bowman III

Major: Physics

Mentors: Jamie Phillips, PhD, Electrical Engineering & Computer Science, University of Michigan
Justin Foley, Applied Physics, Electrical Engineering & Computer Science, University of Michigan

Abstract

Fabry-Perot cavities are an attractive method of infrared filtering, provided they are made of broadband, lossless reflectors. A long wavelength infrared region (LWIR, 8-12 μm) broadband reflector is demonstrated using a high-index contrast sub-wavelength grating (HC-SWG) based on a suspended silicon system. The expected grating field response was simulated using COMSOL Multiphysics to exhibit greater than 90% reflectance in the LWIR, for transverse magnetic polarization. An un-switched C_4F_8 /SF_6 reactive ion etch was characterized, and showed improved sidewall profile compared to previously used etch chemistry. Fabricated gratings demonstrate greater than 85% reflectance between 8 μm and 14 μm, with the response agreeing well with simulations incorporating as-built dimensions.

Introduction

Hyperpsectral techniques are needed to advance to the next generation of thermal imaging systems. A hyperspectral image contains the electromagnetic spectrum for every point in an imaging plane, providing a "fingerprint" for different objects. These fingerprints improve object discrimination, which is useful in a wide array of applications including satellite analysis of climate change, military surveillance, and biological and chemical sensing. Hyperspectral images are formed from intensity acquired at each wavelength, which requires narrowband filters such as interference-based Fabry-Perot cavity filters. A Fabry-Perot cavity is composed of two parallel reflectors separated by a set distance, and transmits light when a standing wave can be established between the two mirrors. To ensure highly efficient and selective filters, the reflectors must exhibit very high reflectance and be non-absorbing. In this work we designed, fabricated and characterized a low loss reflector using a high-contrast grating .

It was first shown by Mateus [1] using a system of poly-Si gratings (n=3.48) on top of SiO_2 (n=1.4) that high-contrast-gratings could function as broadband and lossless reflectors. "High-index-contrast" refers to the large difference between the refractive indices of the grating and surrounding media. Figure 1 shows a schematic of a high-contrast-grating with dimensions and polarization defined as well as a corresponding fabricated grating. The parameters necessary to optimize the response are the grating period (Λ), Fill Factor (FF), which is the ratio of a grating's width to the period, and thicknesses of the high and low index layers, (t_h and t_l).

Experimental Procedure

We optimized the design of a silicon (n=3.4) grating suspended in air (n=1) using commercial finite element analysis software for transverse magnetic (TM, electric field directed along the grating periodicity) polarized light. A single grating period was used as the computational domain assuming periodic boundary conditions and

material optical properties from Palik [2]. Iterative optimization showed an expected reflectance greater than 90% between 8μm and 12 μm, an important spectral range for thermal imaging.

We used a commercial Silicon-on-Insulator wafer as the platform for fabricating our suspended grating using photolithography and reactive ion etching (RIE). Subsequent wet etching of the sacrificial SiO_2 layer with hydrofluoric acid suspended the gratings as shown in Figure 1b. We characterized the grating response using polarization dependent Fourier transform infrared spectroscopy (FTIR) in transmission mode using an aperture to constrain the focused light.

RESULTS

We compared the sidewall profiles of a fluorine-based RIE chemistry (C_4F_8/SF_6) to a previously used bromide-based etch chemistry (H_2/HBr) using scanning electron microscopy (SEM). The fluorine-based plasma etching improved sidewall profiles over the bromide-based chemistry, as shown in the micrographs of figure 2. The sidewalls produced by the C_4F_8/SF_6 RIE are more vertical and have minimal bowing compared to the H_2/HBr profiles, both of which are expected to improve the structure response. We further characterized the etch rate dependence on open area of the C_4F_8/SF_6 RIE as shown in figure 3, which shows larger periods, with larger open areas, exhibit higher etch rates. These results were used to optimize the grating fabrication process.

FTIR characterization of our gratings indicated less than 15% of incident light was transmitted in the spectral range of 8-14 μm. The expected transmittance, obtained from simulation with the as-built dimensions of the structure (Λ=5.3 μm, FF=0.7, t_h=3.3 μm, and t_l=4.3 μm) agreed well with the experimental transmittance, indicating the reflectance may be approximated as R+Loss=1-T, where the Loss term is small. Figure 4 shows the derived reflectance and simulated response of the gratings as well as the reflectance of a control silicon wafer. The derived reflectance agrees well with the simulation further suggesting loss in the materials does not significantly affect the response. The agreement between the expected reflectance and experimental data indicate the grating is acts as a broadband reflector, with greater than 85% reflectance between 8 μm and 14 μm.

CONCLUSIONS AND FUTURE WORK

We fabricated and characterized a high-contrast grating reflector that exhibits greater than 85% reflectance between 8 μm and 14 μm. We improved the fabrication procedure using a C_4F_8/SF_6 etch chemistry, which improved sidewall profiles over a previously used H_2/HBr etch. Future work includes design and fabrication of a polarization independent high-contrast-grating consisting of a two-dimensional layout. Initial design optimization shows a response with greater than 80% reflectance between 9 and 12 μm.
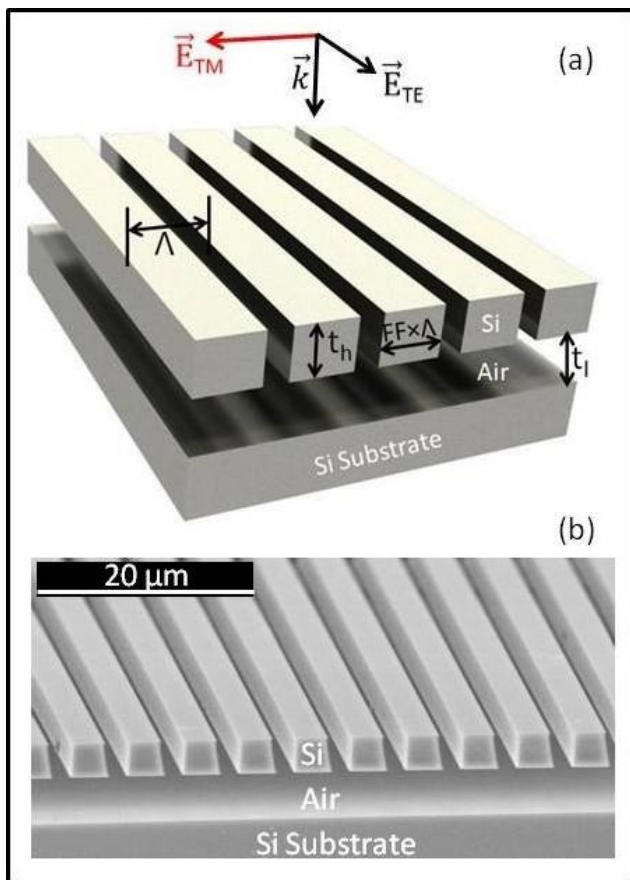
Figure 1: a) A suspended silicon grating schematic and b) A representative fabricated suspended silicon grating
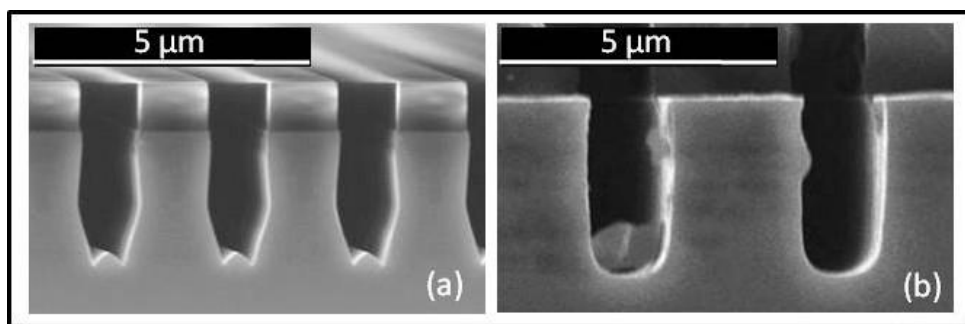
Figure 2: Grating cross-sectional profiles after a) H_2/HBr and b) C_4F_8/SF_6 reactive ion etches
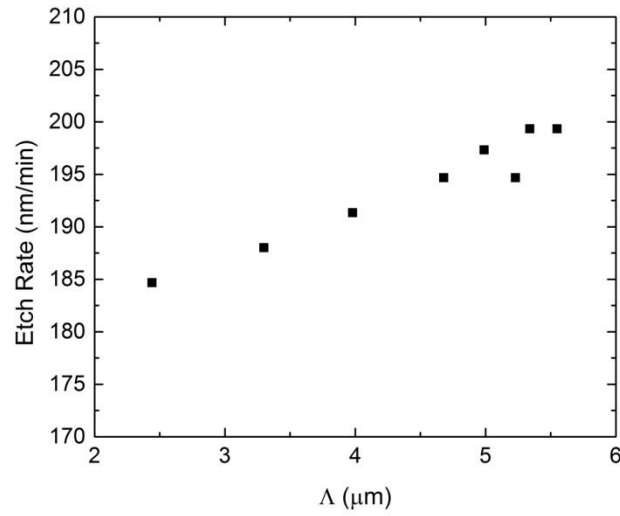
Figure 3: Etch-rate dependence on period for C_4F_8/SF_6 reactive ion etching
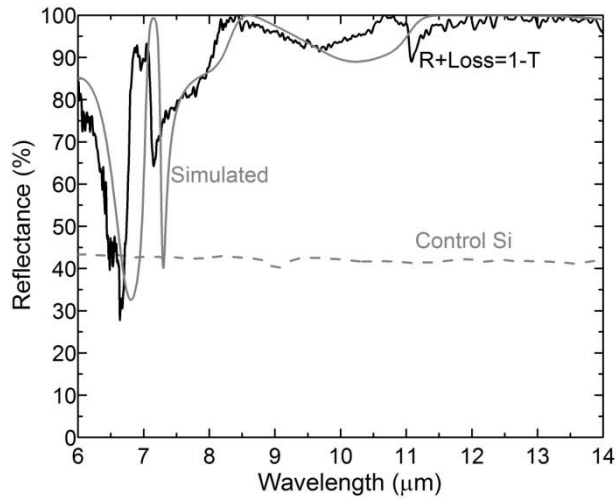
Figure 4: Derived experimental reflectance spectra, simulated reflectance of as-built structure, and the experimental reflectance of a control silicon wafer

REFERENCES

1) C.F.R. Mateus, M.C.Y. Huang, L. Chen, C.J. Chang-Hasnain, and Y. Suzuki. "Ultrabroadband Mirror Using Low-Index Cladded Subwavelength Grating". IEEE Photonics Technol. Lett. 16, (2004)**.**

2) Palik, E. D., "Handbook of optical-constants," J. Opt. Soc. Am. 1, 1297-1297 (1984).

PHYSICAL ACTIVITY PREVALENCE IN DETROIT AFRICAN AMERICAN HIGH-SCHOOL AGED YOUTH

By Khari S. Dickey
Major: Kinesiology – Exercise & Sports Science
Mentor: Dr. Qin Lai, Department of Kinesiology, Exercise & Sports Science

ABSTRACT

Though the advantages of physical activity are extensive, there is an overwhelmingly large presence of physical inactivity within the United States. The Lack of physical activity is linked to an increasing obesity epidemic, as well as an overall increase in preventable chronic disease. Physiologic, environmental, and psychosocial/ sociodemographic factors play an important role in influencing physical activity behaviors. These factors interact in various combinations to "cause" a physical activity behavior. Information collected thus far suggests a call for more research in subgroups at risk of being inactive, including minority ethnic groups. The Incorporation of variables such as benefits, socioeconomic status, and peer modeling in a research study may improve the indication of which factors specifically plague African Americans high school-aged adolescents in Detroit. Cultural and gender differences are present that suggest it would be feasible and beneficial to identify factors that influence activity level and activity choice in Detroit adolescents. The purpose of this study is to test for possible cultural and gender differences within Detroit high school aged adolescents that may be specific to the city and have an effect on physical activity participation.

Physical activity is defined as any activity that enhances or maintains strength, endurance, or overall health. There are many benefits to physical activity that are vital to improving or maintaining quality of life. Some important benefits of exercise are weight control, decreased risk for cardiovascular disease, type II diabetes, metabolic syndrome, and some cancers. Other benefits are elevated bone and muscle strength, positive mood (mental health), and increased chances of living longer (Healthy People 2020). Not only does it improve circulation, increase blood flow to the brain, and raise endorphin levels, which all help to reduce stress, improve mood and attitude, and calm children, physically active students may also achieve more academically (Speregen, 2005). Though the advantages of physical activity are extensive and heavily weighted, there is an overwhelmingly large presence of physical inactivity within the United States. Lack of physical activity is linked to an increasing obesity epidemic as well as an overall increase in preventable chronic disease. More than 60 percent of American adults are not regularly active. In addition, about 25 percent of the adult population is not active at all. Only about 15 percent of adults engage in regular vigorous physical activity. Research data shows that the trends in adolescents are very similar (Center for Disease Control).

The American College of Sports Medicine recommends that children and youth participate in at least 60 minutes of physical activity per day. Physical education is a traditional aspect of grade school education. Physically fit students are less likely to miss school, partake in risky behaviors, get pregnant, or attempt suicide, which are all associated with better outcomes in school (Taras, 2005) (not sure of the structure of this sentence or if it needs to be 2 sentences). Over the past decade physical education participation in schools has decreased. Only 41 percent of Detroit schools require students to participate in physical education without exemption. Additionally, only 51 percent of Detroit schools have a health education curriculum that addresses all 8 national standards for health education. (CDC, School Health Profiles 2010)

The Center for Disease Control conducted the High School Youth Risk Behavior Survey in 2011. The Youth Risk Behavior Surveillance System (YRBSS) monitors six types of health-risk behaviors that contribute to the leading causes of death and disability among youth and adults, which includes behaviors that contribute to unintentional injuries and violence; sexual behaviors that contribute to unintended pregnancy and sexually transmitted diseases. The survey also collects responses regarding HIV infection, substance use, tobacco use, unhealthy dietary behaviors and inadequate physical activity. YRBSS includes a national school-based survey conducted by CDC and state, territorial, tribal, and local surveys conducted by state, territorial, local education, health agencies and tribal governments (Center for Disease Control, 2013). The Center for Disease controlled performed this survey to collect data concerning the state of Michigan and the city Detroit as an individual site.

LITERATURE REVIEW

Kohl and Hobbs (1998) investigate the potential behavioral determinants needed for understanding the influences from three fundamental areas in their article (name article here if you want). These fundamental areas are physiologic and developmental factors, environmental factors, and psychological, social, and demographic factors. This article reviews evidence of potential predictors of potential determinants of physical activity in children and adolescents and provided recommendations for future research. This study takes into account the current difficulties in accurate assessment of physical activity among children and adolescents. The authors recognize the lack of evidence for tracking physical activity may be a problem of assessment as much as it is one of tracking. As a whole, the studies suggest that physical activity has positive consequences in relation to growth and maturation. Physically active children exhibited higher scores on motor, strength, and cardiovascular fitness tests than their inactive peers. Physical health status is likely an important determinant of physical activity behavior among children and adolescents. Physiologic, environmental, and psychosocial/ sociodemographic factors play an important role in influencing physical activity behaviors. These factors interact in various combinations to "cause" a physical activity behavior. The team recommends a standardization of methods to increase accuracy and future studies focusing on the determinants physical activity.

A review of correlates of physical activity of children and adolescents (Sallis et al., 2000) details a study performed to further understand the factors that influence physical activity. The identification of these factors can aid in the design of more effective interventions. Reviews previous to this experiment concerning correlates of youth physical activity have produced conflicting results. MEDLINE and PsychoInfo are the computer searches used by Sallis et. al. The target articles include factors such as ages ranging from 3-18 and a dependent variable of overall physical activity; moreover, the association of these variables is tested with physical activity. 54 studies from the sample focused on correlates among adolescents 13-18 years old.

The review identifies nine demographic and biological variables. These variables are studied three or more times. The most consistent finding is that boys were more active than girls. Ethnicity is consistently causative, with non-Hispanic Caucasians being more active than other ethnic groups. Body weight and composition are found to be unrelated to physical activity participation. Socioeconomic status is also found to be unrelated. Of seventeen psychological variables, the only ones with consistent and positive associations with participation are achievement orientation, perceived competence, and intention to be active. Depression is negatively correlated. Behavioral variables are positively connected with physical activity levels. Positive behaviors that correlate are sensation seeking, previous physical activity, and participation in community sports. Healthy diet is found to be unrelated. Sedentary after school and weekend activities are consistently and inversely effective in relation to adolescent exercise participation. Interaction in the forms of parental support, help from parents, and the support of others are consistently proven to be related to adolescent physical activity. The Sample size is critical to the likelihood of declaring a statistically significant result. A reason for inconsistent findings may be sample characteristics such as the size and population being studies.

More studies should be conducted involving sex specific analysis, ethnicity, socioeconomic status, and academics. The authors suggest that variables classified as consistently connected with physical activity should be used to improve physical inactivity intervention.

How We Play- Cultural Determinants of Physical Activity in Young Children (2010) details a study conducted by the National Center for Physical Development and Outdoor Play. The organization conducted an analysis from a systematic review of research related to cultural determinants. The keywords included in the search are physical activity, movement, exercise play, preschool, early childhood, young children, culture, socioeconomic, ethnicity, parent, and teacher. Studies investigating the relationship among screen time, physical activity, and obesity are excluded due to inconsistent findings in a small body of research focused on pre-school-age children (Burdette & Whitaker, 2005). The team includes definitions to guide the literature search and review to narrow the literature featured in the analysis. The analysis is based on the ecological systems theory. This theory organizes socio-cultural factors into a several nested environments that influence the child and interact throughout their lifespan. There is a relationship between the child's family, educational setting, community, and society. Findings suggest that the beliefs of adults and their behaviors about physical activity may hinder or promote a child's physical activity level. Goodway and Smith (2005) and Lindsay et al. (2009) suggest that cultural beliefs and values do in fact impact adult engagement in physical activity with young children. Individuals who are from Latino, African American, and low-income socio-cultural groups are at increased risk for obesity (Ogden et al. 2006). Studies conducted with children older than six years of age from African American and Latino backgrounds have reported a relationship between race/ethnicity and physical activity (Troiano, Berrigan, Dodd, et. al, 2008). Though there is evidence of a relationship, there is not a body of evidence that accurately explains the interaction. The majority of studies considered in the analysis are culturally, socially, economically, and linguistically diverse families.

The organization focuses on socioeconomic status as part of the analysis. The studies that were reviewed in the literary analysis established the relationship between socioeconomic status and the physical activity of young children. The data suggests that children from low-income families tend to be more sedentary than middle- or upper- income families; furthermore, this increases their obesity risk (U.S. Department of Health and Human Services, 1997). The Campaign for Healthy Kids compiled a fact sheet regarding the rate of overweight and obesity among African American youths. 35.9 percent of African American children ages 2 to 19 are overweight or obese compared to the 31.7 percent of all children of those ages (Campaign for Healthy Children, 2010).

STATEMENT OF THE PROBLEM

The previous studies conducted in children's physical activity have found that ethnicity, socioeconomic status, single parent status, previous physical activity, social/cultural factors, and parent involvement are correlated with children's physical activity participation. Recommendations for future studies suggest that it be a priority to specifically classify variables associated with physical activity and apply them to improve physical activity interventions. Information collected thus far suggests a call for more research in subgroups at risks for being inactive, including minority ethnic groups. Incorporation of variables such as benefits, socioeconomic status, and peer modeling may improve the indication of which factors specifically plague African Americans high school-aged adolescents in Detroit.

Thus, the primary purpose to the present study was to test for possible effects of cultural differences on physical inactivity between Detroit high school aged adolescents and their Michigan counterparts through analyzing the published data from the Centers for Disease Control and Prevision (CDC). The secondary purpose of the study was to analyze the gender differences on physical inactivity. The purpose to this study is to test for possible cultural and gender differences within Detroit high school aged adolescents. If differences

are present, it would be feasible and beneficial to identify factors that influence activity level and activity choice in Detroit adolescents. Future research should be conducted to determine the relationship between socioeconomic status, single parent status, previous physical activity, social/cultural factors, parent involvement, and physical activity preference. In addition to this, to determine the extent to which components influence low levels of physical activity in African Americans.

HYPOTHESIS

Based on the purposes of the present study and the previous research findings that social-culture, financial status, and regional location affect participation of physical activity, the following hypotheses were provided:

1. Detroit high-school aged youth tended to participate in less physical activities compared to their Michigan counterparts.
2. Detroit high-school aged youth tended to spend more time in sedentary activities compared to their Michigan counterparts.
3. There will no sex difference in physical activity participation.

METHODS

The Center for Disease Control's High School Youth Risk Behavior Survey, 2011 is used as second-hand data to conduct a statistical analysis. The surveyed data from African American high school-aged youth from the City of Detroit and the general high school-aged of the state of Michigan is used for gaining information in order to conduct a statistical comparison. Microsoft Excel is used as the mathematical program. The Michigan data is compared to the city of Detroit using standard error and the independent t-test. The independent t-test is used to determine if two sets of data are significantly different from each other. The independent t-test is a test of choice because the Michigan and Detroit data collected are two separate surveys with different sample populations. The statistical significance level is set at 0.05 which translates as a 1.96 confidence level. There are four survey questions compared using these methods: 1. Did not participate in at least 60 minutes of physical on any day, 2. Did not attend physical education classes 5 days in an average week, 3. Watched television 3 or more hours per day, 4. Used computers 3 or more hours per day. The t-test was estimated as the following equations:

$$ t = \frac{\bar{x}_1 - \bar{x}_2}{\sqrt{\frac{s_1^2}{n_1} + \frac{s_2^2}{n_2}}} \qquad SE_{\bar{x}} = \frac{s}{\sqrt{n}} $$

RESULTS

Physical Inactivity Differences between Detroit Adolescences and Michigan Adolescences

The notation p<.05 indicates a significant difference between the factors being compared where p>.05 means that there is no significant difference. As Table 1 demonstrated, Factor 4, *Used computers 3 or more hours per day* was found to be insignificant for the City of Detroit versus State of Michigan high school- aged youth comparison. The other three factors demonstrated a significant difference between the Detroit African American high school-aged youth in comparison with the state of Michigan general population. The city of Detroit had high incidence of not participating in at least sixty minutes of physical activity, physical education attendance, and more teens spending three or more hour watching television.

TABLE 1: City of Detroit versus State of Michigan High School- Aged Youth Comparison	Mean	SE
1. Did not participate in at least 60 minutes of physical on any day		
City of Detroit	20.7	1.122449
State of Michigan	14.8	1.27551
t	3.4725	p<.05
2. Did not attend physical education classes 5 days in an average week		
City of Detroit	81.2	1.836735
State of Michigan	73.3	2.346939
t	2.65081	p<.05
3. Watched television 3 or more hours per day		
City of Detroit	45	1.734694
State of Michigan	29.5	1.938776
t	5.958008	p<.05
4. Used computers 3 or more hours per day		
City of Detroit	28.6	1.530612
State of Michigan	27	1.173469
t	0.829583	p>.05

Sex Differences of Physical Inactivity in Detroit and Michigan Adolescences

Detroit's African American high school-aged males spend more time watching television and using the computer than their female counterparts. There is no significant difference between males and females in regards to physical activity participation (see Table 2). The state of Michigan's data shows that there is no significant difference in females and males with television watching. The other factors are consistent with the analysis of the Detroit specific behavior (see Table 3).

TABLE 2: City of Detroit African American High School-Aged Female vs. Male Comparison	Mean	SE
1. Did not participate in at least 60 minutes of physical on any day		
Female	22.7	1.479592
male	18.5	1.683673
t	1.873815	p>.05
2. Did not attend physical education classes 5 days in an average week		
Female	81.9	1.938776
male	80.4	2.5
t	0.474132	p>.05
3. Watched television 3 or more hours per day		
Female	40.2	2.040816
male	50.2	2.602041
t	-3.02399	p<.05

4. Used computers 3 or more hours per day		
Female	25.4	1.683673
male	31.9	2.193878
t	-2.35041	p<.05

TABLE 3: State of Michigan High School- Aged Male vs. Female Comparison	Mean	SE
1. Did not participate in at least 60 minutes of physical on any day		
Female	17.3	1.428571
male	12.4	1.27551
t	2.558566	p<.05
2. Did not attend physical education classes 5 days in an average week		
Female	81.3	2.295918
male	65.5	2.908163
t	4.264254	p<.05
3. Watched television 3 or more hours per day		
Female	28.5	2.244898
male	30.4	2.040816
t	-0.62626	p>.05
4. Used computers 3 or more hours per day		
Female	23	1.428571
male	30.9	1.785714
t	-3.45456	p<.05

DISCUSSION

The data collected demonstrated that there are some maladaptive practices that lessen physical activity participation. High school-aged African American youth of both the state of Michigan and the city of Detroit spend countless hours partaking in sedentary activities. Both populations spend hours at a time using computers and watching television. Most youth engage in sedentary activities in the place of physical activities. Most spend less than 60 minutes engaging in physical activity. Physical education is not properly implemented in schools to provide adequate amounts of activity. Therefore, students must use time outside of school to take part in physical activity. Limiting computer usage and television watching would allow more time to engage exercise alone or with peers.

The differences highlighted by a statistical difference between the city of Detroit and the state of Michigan suggest that there are factors effecting physical activity participation that are specific to Detroit. Based on the data collected through this second-hand data analysis, there are significant differences between Detroit African American high-school aged youth and the collective population of Michigan African American youth

of the same age group. Detroit is socially, economically, and culturally unique in relation to other areas within the State of Michigan.

Therefore, research to examine ethnicity, socioeconomic status, single parent status, previous physical activity, social/cultural factors, and parent involvement and their effect on physical activity participation in Detroit youth would be essential to creating successful exercise intervention programs. The goals of extending knowledge specific to Detroit will better construct and organize physical activity reform programs. Future research must take into consideration the specific characteristics defining Detroit and its citizens in order improve health through increasing physical activity.

REFERENCES

Andersen, R. E., Crespo, C.J., Bartlett, S.J., Cheskin, L.J., & Pratt, M. (1998). Relationship of physical activity and television watching with body weight and level of fatness among children. *Journal of the American Medical Association 279*, 938-942.

Anderson, D.R. (2012). The death of play is U.S. culture. *The National Academy of Kinesiology 1,* 59-65.

Brody, G.H., McBride-Murry, V., Kim, S., & Brown, A. (2002). Longitudinal pathways to competence and psychological adjustment among African American children living in rural single-parent households. *Child Development 73,* 1505-1516.

Lorelei, E. &Jarrett, M. (2005) How We Play- Cultural Determinants of Physical Activity in Young Children. Tech. no. 90YD0274/01. *National Center for Physical Development and Outdoor Play.*

Haerens, L., Aelterman, N., & Van Den Berghe, L. (2013) Observing physical education teachers' need-supportive interactions in classroom settings." *Journal of Sport & Exercise Psychology* 35 3-17. Web.

Kohl, H. W., & Hobbs, K.E. (1998) "Development of Physical Activity Behaviors Among Children and Adolescents." *Pediatrics: Official Journal of the American Academy of Pediatrics 101: 549-54.*

Pate, R. R., Davis, M.G., & McKenzie, T.L. (2006) "Promoting Physical Activity in Children and Youth." *Circulation: Journal of the American Heart Association 114: 1214-224.*

Sallis, J. F., Prochaska, J.J. & Taylor, W.C. (2000) "A Review of Correlates of Physical Activity of Children and Adolescents." *Medicine & Science in Sports & Exercise: 963-75.*

"Youth Risk Behavior Surveillance System (YRBSS)." *Centers for Disease Control and Prevention.* Centers for Disease Control and Prevention, 04 June 2013.

METABOLIC AND CELLULAR PLASTICITY OF ADIPOSE TISSUE

By Lahib H. Douda
Major: Biomedical Physics
Mentors: Dr. James G. Granneman, Department of Psychiatry & Behavioral Neurosciences
        Dr. Yun-Hee Lee, Department of Psychiatry & Behavioral Neurosciences

ABSTRACT

Fat tissue is comprised of two major types of fat: white adipose tissue (WAT) and brown adipose tissue (BAT) that can be found in various regions throughout mammals in depots. WAT's function is to store lipid energy and is much more abundant than BAT. BAT's function is to produce heat by oxidizing lipids. Although BAT is the main cell type of classical BAT, these cells can be found in WAT and their presence in WAT is metabolically favorable (Cinti, 2005). The aim of our study is to understand what conditions increase the presence of BAT in WAT, and other factors that contribute to the variability between the two tissues. This renewed interest in BAT and catabolic remodeling of WAT can potentially be significant in treatments of disorders related to obesity such as diabetes and cardiovascular disease. Brown adipocyte function is largely controlled by the sympathetic nervous system and we hypothesize that differences in inducibility may relate directly to the level of innervation.

Two kind of variability were explored in this study. First we explored brown adipocyte variability, or "browning," among three fat depots: classic BAT, highly-inducible inguinal WAT, and poorly-inducible epididymal WAT. There exists genetic variability between the two inbred strains that were research: the highly-inducible S129 strain (S1) and the poorly-inducible C57BL/6J strain (Xue, 2005). We evaluated sympathetic innervation by probing tissue extracts for Tyrosine Hydroxylase (TH), a well-known marker of sympathetic neurons, using the western blot technique. Our results showed a significant variation in amount of innervation across various fat pads in the strains with BAT displaying two to three times the density of innervation as measured by TH versus inguinal white adipose tissue (iWAT) and epididymal white adipose tissue (eWAT). The level of innervation varies across pads, but this alone cannot explain the differences in browning, as indicated by the brown adipocyte marker Uncoupling protein 1 (Ucp1). Even though the two strains differ in their susceptibility to induction, they have similar levels of innervation.

INTRODUCTION

Obesity, defined as an excess of adipose tissue, is a huge medical problem and the thermogenic tendencies of BAT serve to offer obesity related treatments for this and other related ailments. There has been substantial research stemmed from this understanding of the types of fat and their characteristics (Cinti, 2005). Recent work has shown that the adipocytes within adipose tissue are metabolically flexible, and can adopt a range of phenotypes, including those that are dedicated to fat oxidation (brown adipocytes). Studies indicates that it is not the mass of adipose tissue that causes disease, rather, it is the function of adipose tissue. In particular, adipose tissue dysfunction is related to the inability of fat cells (adipocytes) to properly handle toxic fatty acids. One therapeutic approach to the problem of obesity-related disease is to generate metabolically beneficial adipocytes, that is, those that can properly oxidize or sequester toxic fatty acids.

The S1 are a strain of mice that are unphased by a high fat diet (HFD) (Xue, 2005). The mice have the ability to induce brown adipose and their resilience to obesity is strengthened along with our interest in this

innervation. Using prior research as the basis of the strain and fat pad choices, we aim to contribute to this understanding to benefit individuals. The protocol for protein analysis is to use the western blot to isolate proteins from total tissue, and resolve them by gel electrophoresis. After the proteins are resolved by gel electrophoresis the procedure is to probe the proteins for TH as a measure of the level of sympathetic innervation. The aim of this study was to investigate factors that promote the appearance of metabolically-beneficial brown adipocytes in typical white adipose tissue.

BACKGROUND

With further regards to the types of adipocytes, white are unilocular (consisting of one cavity or single chambered) while brown adipocytes are multilocular (Multiple lipid droplets). WAT facilitate fatty acid accumulation and distribute these fatty acids between meals. They contain a gene called leptin which is believed to have a role in not only regulating energy intake, expenditure, appetite, and metabolism, but also behavior. BAT are likely to undergo thermogenesis, otherwise known as heat production, which consumes energy while WAT's store energy. Within these fat depots there are numerous vessels and nerve fibers with BAT containing a denser composition than WAT. Browning's prevalence increases when norepinephrine binds to receptor sites in cells. The adrenoceptor is β3AR which exists in adipose tissue (Cinti, 2005). There are a range of metabolic phenotypes of adipose tissue (eWAT, iWAT and BAT) and BAT is preferred due to its thermogenic nature. This thermogenic characteristic of the BAT is caused by a protein called Uncoupling protein 1 (Ucp1). As its name implies, the Ucp1 serves the function of uncoupling oxidative phosphorylation. Oxidative phosphorylation is a metabolic pathway which cells, specifically mitochondrial cells, oxidizes nutrients in order to conserve energy by reforming ATP. Ucp1 uncouples and allows substantial amounts of substrates to be oxidized without generating ATP (Cinti, 2005). In other words, mice and other mammals are able to experience browning of their WAT and expel energy via oxidative phosphorylation. The question then is, "under what conditions does this browning occur?"

Two factors were examined in conjunction with one and other in hopes to answer this question: the type of fat pad and a genetic factor or difference between the two strains of mice. The types of fat pads vary from BAT to epididymal white adipose tissue (eWAT) and inguinal white adipose tissue (iWAT). Inducibility also directly varies among the three fat pads. BAT is highly inducible due to Ucp1's presence and therefore favorable. IWAT has metabolic flexibility; it consists of brown or white adipose tissue and serves as a good bridge between the highly inducible brown and the resistant eWAT. EWAT, or abdominal fat, is categorized as classic white adipose tissue. EWAT's ability to display browning differs dramatically from the other types of fat depots because it is composed of mostly white fat that is resistant to browning. EWAT lacks the ability to express Ucp1and serves as a strong candidate of Ucp1 independent processes (Granneman 2005).

Different strains of mice have different susceptibility to diet induced obesity. The inducibility is directly related to level of innervation. The level of innervation between B6 and S1 strains varies. It has been shown that B6 is highly susceptible to a HFD and the S129 strains of mice are more resistant. It has been shown that the B6 mice are poorly inducible while contrarily S1 mice are very inducible (Xue 2005). The S1 strain of mice is able to express Ucp1 much more readily than B6 is able to. Ucp1 was thought to be affected by a few molecules; however Xue showed that small changes in the pathway from receptor to Ucp1 were sufficient enough to cause dramatic reductions in Ucp1 levels. Xue's aim was to identify which genes controlled induction of BAT (Xue 2005). It was proved to be difficult to determine which genes controlled induction of BAT due to the fact that genes interact with one and other. In addition to genes interacting with each other, epistasis occurs. Epistasis is the phenomenon that a gene could have an opposite effect given a particular background. Given epistasis, we know for certain that the levels of innervations these strains display differs and due to this contrast they were chosen for this study.

The level of innervation refers to the sympathetic nervous system's ability to drive metabolism in brown fat and can convert white fat into a brown fat phenotype. The sympathetic nervous system is a branch of the

central nervous system and a part of the autonomic nervous system. The strain difference in innervation is driven by neurotrophic factors, which are proteins that maintain the health of developing neurons and of mature neurons. These neurons, as a part of the sympathetic nervous system are involved in brown adipocyte generation. The mice release neurotrophins that specify how much innervation they get. There are many conditions that increase the presence of BAT in WAT: the location of fat pads to strains of mice, the level of innervations the mice display and their inner workings.

Sympathetic innervation was evaluated by probing tissue extracts for Tyrosine Hydroxylase. The best marker of sympathetic innervation is the rate limiting enzyme for catecholamine biosynthesis which is tyrosine hydroxylase. TH is a well-established marker of sympathetic neurons and is the rate limiting enzyme for the production of the neurotransmitter that is being released, norepinephrine. This was done first by the western blot: a method of identifying proteins via specific antibodies. The various proteins are separated by gel electrophoresis, a method of separating proteins (or DNA/RNA) by size and charge.

METHODS

Fat pad samples from eWAT, iWAT and BAT were carefully dissected from euthanized mice and stored for further analysis. They were placed in tubes marked with the details of what strain of mice they originate from and what type of fat pad they are. Depending on the size (full or half) of the samples they receive either 100µL or 200µL of lysis buffer that acts as a method of breaking down the cells for further analysis. The sample is then cut with surgical scissors to a size of roughly 1 cubic millimeter. The samples are kept on ice and each sample is carefully sonicated which is the process of further physical breakdown of tissue via a sonicator that uses high frequency sound waves to achieve this. They appear as a slurry fluid of tissue and buffer and are then briefly vortexed to further mix the buffer with the sample. After, the samples are placed in a centrifuge (which induces forces of up to 14,000 X gravity) at 4^0 C for 10 minutes in order to separate the layers. From top to bottom the layers consist of fat, cytosolic protein, and cell debris on the bottom. Carefully, we transferred the middle protein layer into new but similarly marked tubes and then vortex again and spin them down (10 second centrifuging). Afterwards the samples are placed in a 90^0 C water bath for three minutes in order to denature the proteins and are once again spun down.

After this, we prepared the buffers that will be used for running and transfer of the proteins. Reagents for protein analysis and western blotting were obtained from Thermo Scientific. One such reagent is the BCA Protein Assay Reagent that was used with specific amounts of protein from the samples to determine protein concentration. A 10X running buffer was made comprised of 14.4 grams of glycine, 2.92g of tris base, 1g of SDS and 1 L of distilled water. This was used to rinse the tank and gel prior to gel electrophoresis. The gel used is comprised of precast polyacrylamide gel for protein electrophoresis; this study used the 4-20% that contained 12 wells. The first and last wells were filled with a marker and the sample was carefully loaded into the remaining wells, placed in a tank filled with running buffer and attached to the Bio-Rad brand power pack that supplied the gel with a constant 85 volts. After five minutes we checked for separation, found none and upped the voltage to a constant 120 volts for 40 minutes.

After gel electrophoresis was complete we then began the process of transferring the proteins from the gel onto a methanol activated immobilon transfer membrane by a company called Milipore. This was accomplished by filling a glass dish with transfer buffer and carefully sandwiching the gel against the transfer membrane and blotter paper. From top to bottom we placed a sponge, two sheets of blotter paper, the membrane, gel, then another sheet of blotter paper and finally another sponge. Every layer was rolled with a test tube to remove bubbles that would interfere with the final outcome. The transfer buffer consisted of 14.4 grams of glycine, 2.92g of tris base, 200mL of methanol and 800mL of distilled water. The layers were clamped down and placed in a tank full of transfer buffer that sat in a bucket of ice; again the Bio-Rad

machine was used however this time it was set to a constant 0.28 amperes for one hour. A magnetic stir bar was placed in the tank. This part serves to transfer the sample from the gel to the membrane.

Upon completion of the transfer, we were careful to only handle the membrane with forceps as protein from our gloves or elsewhere could skew data. In the mean time we prepared a 5% milk solution consisting of 2.5g of non-fat dry milk powder and 50ml of Tris buffer $((HOCH_2)_3CNH_2)$. Then after the hour elapsed the membrane was removed and rinsed with buffer solution and placed in a small plastic tray with 15ml of the 5% milk, the tray was placed on a shaker for 30 minutes. The milk blocks all the binding sites on the membrane so antibodies don't stick to membrane (membrane contains nonspecific sites) and blocks nonspecific sites. A half hour later, we discard the 5% milk solution and pour 8ml of 5% milk and 4μL of primary Donkey anti-mouse (HPR conjugated) antibodies and let that shake overnight.

The next morning the membrane is washed three times for 10 minutes each time with a tris buffer. After the third wash, 1μL of secondary Donkey anti-rabbit (HPR conjugated) antibodies are added to 5ml of 5% milk and the membrane and shaken for 30 minutes. The membrane is again washed three times for 10 minutes each wash and exposed to a 1:1 ratio of SuperSignal West Femto Substrate by Thermo Scientific for 1 minute. It is taken to the ChemiDoc MP imaging system for imaging. The ChemiDoc MP imaging system images western blot membranes via high resolution and high sensitivity detection. The primary probes specific sites with antibodies and we are able to detect primary antibodies with secondary antibodies that are conjugated to an enzyme called horseradish peroxidase (HPR conjugated). This enzyme is able to amplify the small signals we have on our membrane and we are able to later detect them with the ChemiDoc machine via chemiluminescence. Chemiluminescence detects the overall level of TH that's produced by the secondary antibodies binding to primaries. Quantification of the images produced via imaging software gives us our results of the study.

RESULTS AND DISCUSSION

The question of various fat pads differing in the level of adrenergic innervation comes to some resolve from our results. We have found significant variation in the amount of innervation across the three pads we tested; however this does not explain the differences in browning. The brown adipose tissue has by far the most density of innervation as measured by TH, around 2-3 times the level of iWAT and greater still than eWAT. In general iWAT and eWAT surprisingly had similar levels of innervation, even though they're dramatically different in terms of inducibility. We expected eWAT to be much lower than iWAT and iWAT much lower than BAT in a uniformly descending pattern. The results showed BAT constitutively innervated as measured by TH while eWAT and iWAT moderately innervated.

The strains have differences in their ability to induce Ucp1 in white and inguinal fat pads. It seems that the strains that vary in Ucp-inducibility also show differences in innervation. These differences correlate with resistance to HFD and it's thought, but not proven, that there's a connection between the two. Logically if you're able to induce Ucp1 and thermogenesis you can resist HFD as the S1 strain is proficient at doing. Genetically, in general, the level of innervation correlates with Ucp1 (literature reference). As expected, we found no statically difference in the level of innervation in brown among the strains, or surprisingly in the iWAT where differences were expected, however we did in eWAT. In eWAT the S1 mice have a higher level of innervation. Even though this is true of the S1 strain, the B6 strain unexpectedly showed higher, but insignificant, levels of innervation in BAT. The iWAT and eWAT pads in that the S1 strain had greater innervation over its B6 competitor. There was also a great difference in innervation of eWAT between the strains. This variance may influence strain differences in that particular pad.
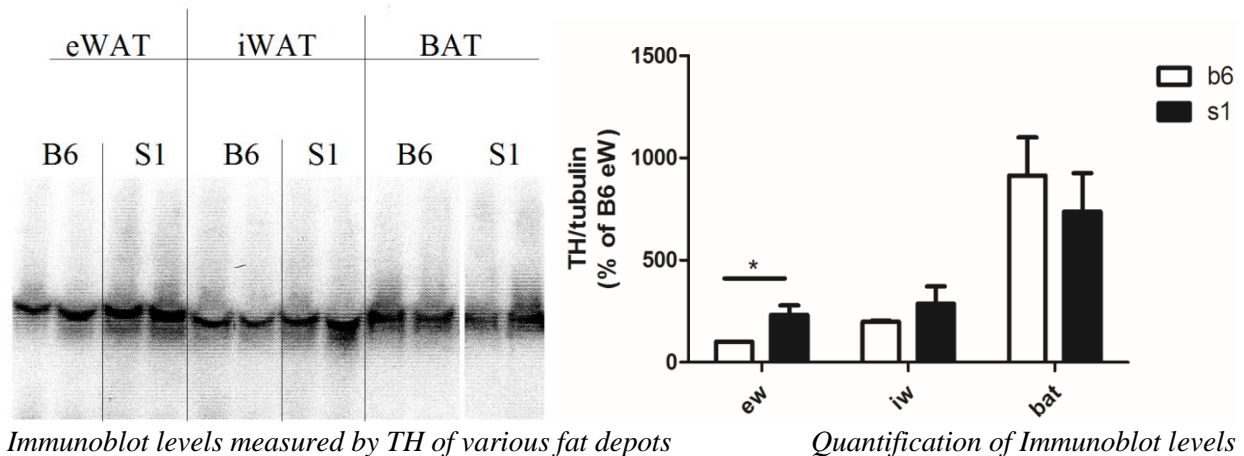
Immunoblot levels measured by TH of various fat depots   Quantification of Immunoblot levels

The first image shows levels captured with the ChemiDoc imaging system. These bands were quantified with software to give the image on the right. This quantification shows the three types of fat pads of both strains vs. the TH level with Tubiline as the common denominator. You can see the level of innervation as measured by TH for BAT is significantly higher than the other two fat depots. What is also significant is the eWAT level of innervation between the B6 and S1 strains.

There are differences among pads and between strains that are related to level of innervation. I measured tubulin content which is considered a house keeping gene in the sense that it's not related to level of innervation. This was used as the common denominator in the analysis (the standard that we divided by) and can correct for variations of protein recovery using tubulin from the different fat pads of the different strains. When Ucp1 is induced, typically in a cold environment, the sympathetic nervous system is major regulator of Ucp1 expression in response to cold stress. Cold induced inducibility was identically in brown and differed in white among the strains (Xue, 2007). In general S1's have greater Ucp1 in all white but not BAT. The innervation level differs from the pad samples (BAT, iWAT, eWAT) but the level of innervation alone can't explain the differences in Ucp1 induction. While the two strains undergo induction differently, they have comparable levels of innervation.

REFERENCES

Cinti, S. (2005). The Adipose Organ. *Science Direct*, 9-15.

Granneman, J. G., Li, P., Zhu, Z., & Lu, Y. (2005, June 7). Metabolic and Cellular Plasticity in White Adipose Tissue I: Effects of β_3-Adrenergic Receptor Activation *AJP-Endocrinology and Metabolism*, *289*, E608-E616.

Xue, B., Coulter, A., Rim, J. S., Koza, R. A., & Kozak, L. P. (2005, September). Transcriptional Synergy and the Regulation of Ucp1 during Brown Adipocyte Induction in White Fat Depots. *American Society for Microbiology*, *25*(18), 8311-8322.

Xue, B., Rim, J. S., Hogan, J. C., Coulter, A. A., Koza, R. A., & Kozak, L. P. (2007). Genetic Variability Affects the Development of BAT in White Fat but Not in Interscapular Brown Fat. *Journal of Lipid Research*, *48*, 41-51.

COMPARING ANTIDEPRESSANT EFFECTS ON ELECTROCHEMICALLY DETECTED SEROTONIN RELEASE IN VIVO

By: Kristin Gallik
Major: Biological Sciences
Mentor: Dr. Parastoo Hashemi, Department of Chemistry

ABSTRACT

Millions of Americans will develop Major Depressive Disorder (MDD) at some point in their lives. Those suffering experience serious disruptions in everyday functions making treatment of MDD a high priority. Serotonin has been linked to the pathophysiology of MDD. Antidepressants that block serotonin reuptake, selective serotonin reuptake inhibitors (SSRIs), are commonly prescribed to treat this mood disorder. However, these drugs produce side effects and have variable clinical efficacy. To compare differences of antidepressants on stimulated serotonin release and uptake, fast-scan cyclic voltammetry (FSCV) was used. The effects that common antidepressants (escitalopram, venlafaxine, fluoxetine, and fluvoxamine) had on stimulated serotonin release and uptake in the Substansia Nigra riticulata (SNr) of the mouse brain *in vivo* were compared between each other and correlated to clinical efficacy (treatment) and acceptability (side effects). Clinically, escitalopram and venlafaxine (serotonin and norepinephrine reuptake inhibitor) are considered to be highly efficacious and were seen to have a significant effect on increasing the release and decreasing uptake of serotonin. Fluoxetine and fluvoxamine, rated as having low efficacy, had a significantly lower effect on serotonin release and uptake in comparison. This study has shown that ratings in clinical trials translate into detectable effects as measured with FSCV. These traits can be further used in the development and screening for new antidepressants, ultimately bettering the treatment available to those effected by depressive disorders.

INTRODUCTION

Approximately 10-25% of women and 5-12% of men will develop Major Depressive Disorder (MDD) in their lifetime. MDD is a mood disorder characterized lack of interest in daily activities, family, and work, reoccurring thoughts of suicide, and lack of energy. Additionally, those with MDD develop an increased chance of substance abuse (American Psychiatric Association. & American Psychiatric Association. Task Force on DSM-IV., 2000). The serotonergic pathways of the brain have been implicated in the pathophysiology of depressive disorders; antidepressants that target serotonin are used as treatment (Lindsley, 2012). Selective serotonin reuptake inhibitors (SSRIs) block the reuptake of serotonin by the presynaptic neuron, thereby prolonging the duration of serotonin's effects in the synapse (Bosker, Klompmakers, & Westenberg, 1995; Ceglia et al., 2004). Serotonin and norepinephrine reuptake inhibitors (SNRIs), another classification of antidepressant, are used in the same manner as SSRIs (Lindsley, 2012). Unfortunately, the ability of antidepressants to effectively treat MDD is variable.

A meta-analysis by Cipriani et al. ranked the clinical efficacy and acceptability, how well symptoms are treated and side effects respectively, of twelve commonly prescribed antidepressants (Cipriani et al.). They can be categorized as effective drugs with little side effects (escitalopram and venlafaxine) and those that are least effective with increased side effects (fluoxetine and fluvoxamine) (Cipriani et al.). Although these

antidepressants target the same neurotransmitter, serotonin, it is clear that the variances in ranking indicate a difference in functionality. In order to develop new antidepressants selective for serotonin pathways, it is imperative that we understand the differences between a more effective SSRI/SNRI from those less effective. Fast-Scan Cyclic Voltammetry (FSCV) can be used to monitor changes in neurotransmitters *in vivo* electrochemically. FSCV scans through a specified range of potentials repetitively oxidizing and/or reducing molecules allowing high temporal resolution and chemical specificity (Michael & Wightman, 1999). Previously, Wood and Hashemi used FSCV to monitor the changes in serotonin post escitalopram administration in the Subtantia Nigra reticulata (SNr) of the mouse brain *in vivo* (Wood & Hashemi, 2013). Wood illustrated that escitalopram increases serotonin concentrations in the SNr by over 400%. The SNr is rich in serotonergic neurons with axon projections running through the Medial Forebrain Bundle (MFB). Electrical stimulation of the MFB forces the release of serotonin in the SNr thus allowing an electrochemical detection of serotonin using FSCV (Hashemi, Dankoski, Wood, Ambrose, & Wightman, 2011). This technique will be used to monitor and characterize the differences between escitalopram, venlafaxine, fluoxetine, and fluvoxamine.

Methods
Animals

Male C57BL/6J weighing between 20-25g were used (Jackson Laboratory, Bar Harbor, ME). Mice were housed in a 12 hour light/dark cycle, food and water were offered *ad libitum*. Housing and procedures were approved by the Institutional Animal Care and Use Committee (IACUC) of Wayne State University.

Surgery
Mice underwent stereotaxic surgery (David Kopf Instruments, Tujunga, CA) after intraperitoneal injection of urethane (25% dissolved in saline solution, Hospira, Lake Forest, IL). Stereotaxic coordinates for MFB (AP: -1.58; ML: +1.10; DV: -5.00) and SNr (AP: -3.28; ML: +1.40; DV: -4.2 to -4.8) were taken from Bregma. A heating pad maintained body temperature around 37 °C (Braintree Scientific, Braintree, MA). An electrodeposited nafion carbon fiber microelectrode was lowered to the DV coordinate of the SNr. The electrode was adjusted in the DV, ML, and AP planes until a desirable serotonin signal was achieved. A stainless steel stimulating electrode was lowered to the DV coordinates in the MFB (diameter: 0.2mm, Plastics One, Roanoke, VA). **Figure 1** illustrates the placement of the stimulating electrode and carbon fiber electrode in the MFB and SNr respectively. Biphasic pulse trains applied through a linear constant current stimulus isolator (NL800A, Neurolog, Medical Systems Corp., Great Neck, NY) evoked serotonin release. The trains were 60 Hz, 350 µA each phase, 2 ms in width, and 2 s in length. A Ag/AgCl reference electrode was placed into the opposite hemisphere of the brain. Chloride was electroplated to silver wire using 0.1 M HCl.
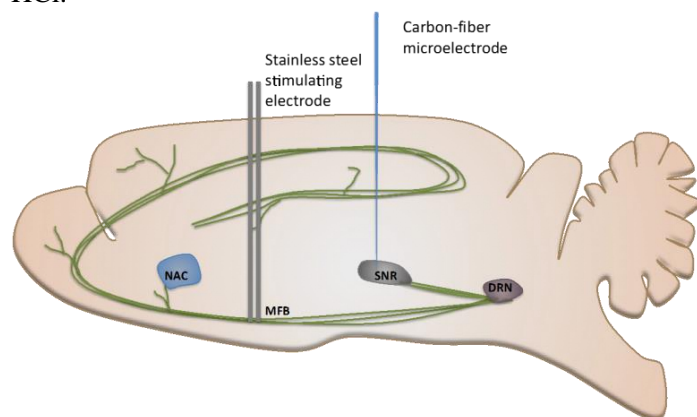

Figure 1: Placement of stimulating electrode in the MFB and carbon fiber microelectrode in the SNr.

Drugs

Escitalopram (Wood & Hashemi, 2013), venlafaxine, and fluvoxamine (Dazzi, Seu, Cherchi, & Biggio, 2005) were all administered at 10 mg/kg dissolved in saline solution (fluoxetine required the addition of ethanol) injected into the intraperitoneal (ip) space (Sigma-Aldrich, St. Louis, MO). Fluoxetine was administered at 20 mg/kg (Kobayashi, Hayashi, Shimamura, Kinoshita, & Murphy, 2008) dissolved in 0.9% saline solution injected into the intraperitoneal space (Sigma-Aldrich, St. Louis, MO).

FSCV Procedures

Fast-Scan Cyclic Voltammetry at nafion coated carbon fiber microelectrodes allows for quantitative measurement of electroactive molecules in the intact brain. Scanning from 1V to -0.1V with a resting potential of 0.2V at 1000 V/s at the carbon fiber microelectrode allows for selective measurement of serotonin (Hashemi, Dankoski, Petrovic, Keithley, & Wightman, 2009). Potentials were measured against a Ag/AgCl reference. Serotonin is oxidized at 0.8V and reduced at -0.1V enabling confirmation of serotonin detection. Data collection lasts for 30s; each file consists of voltammograms taken every 100ms. Files were taken every 5-10 minutes from 0 minutes (control values before drug administration) to 120 minutes. Files are represented as false color plots;reduction is indicated by dark blue, oxidation is green. Data along the horizontal axis is current over time, the vertical axis contains the cyclic voltammogram consisting of the points of oxidation and reduction of serotonin during the potential sweep. **Figure 2** shows the oxidation and reduction of serotonin on the carbon fiber microelectrode, the waveform used, and the generation of false color plots from individual cyclic voltammograms. LABView 2009 software and a PCIe-6341 DAC/ADC card (National Instruments) generated the waveform and collected the data.

Figure 2 A. Oxidized and reduced forms of serotonin during potential sweep from 1.0V to -0.1V on nafion coated carbon fiber microelectrode. **B.** Scanning from 1.0V to -0.1V with resting potential at 0.2V serves as the waveform used for selective measurement of serotonin *in vivo*. **C.** Cyclic voltammograms graphed as potential over current are unfolded and graphed as current over time to be represented in the false color plot. The duration of the file is composed of amalgamated current over time voltammograms. False color plots represent oxidation and reduction readily with green and dark blue respectively. Note: Dopamine is shown in **C**.
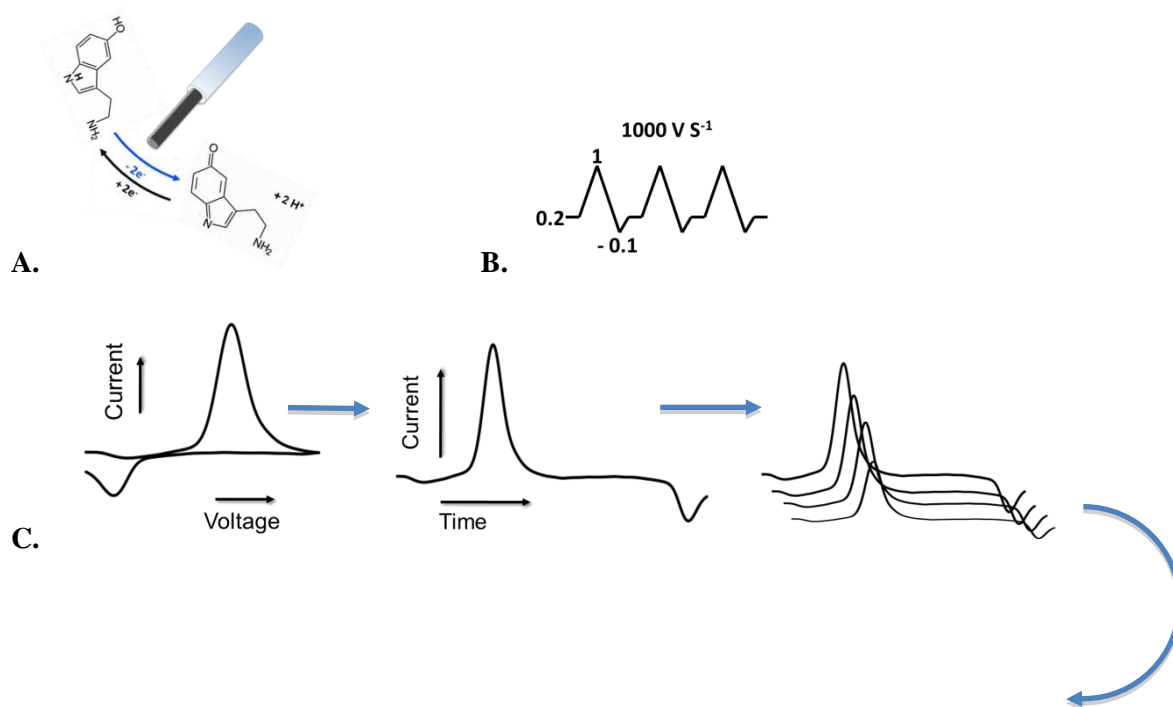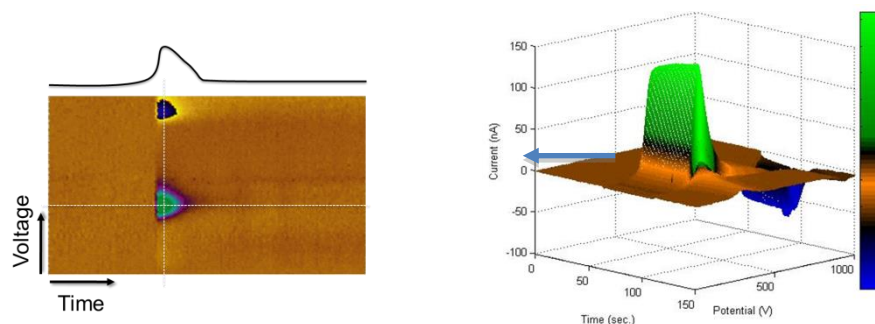
Data Analysis

Software noted in FSCV procedures was additionally used for data analysis, background subtraction, and signal filtering using. Current versus time values were taken at peak amplitude value within the serotonin signal. Five trials were averaged for each drug (fluoxetine had four trials) and converted from current to concentration in nanomolar. The standard error of the mean was calculated from the concentration values and graphed with the average concentration over time responses. Data was analyzed in respect to highest concentrations of serotonin observed after stimulation and the time at which post antidepressant concentrations returned to those observed at 0 minutes. These aspects of the data represent the release of serotonin into the synapse and the rate of clearance from the synapse respectively.

Results
Escitalopram

Figure 3 A shows the effects on serotonin in the SNr after an ip injection of escitalopram. Observed peak effect of escitalopram increased serotonin from 26 ± 5.5 nM at 0 minutes to 96 ± 18 nM at 10 minutes. Peak concentration of serotonin after stimulation decreased to 69 ± 13 nM at 120 minutes. However, decrease in serotonin uptake increases from 23 seconds to 30+ seconds throughout the time trial post-administration. 30 seconds was the limit of file taking for this exploration; it was not tested how long the serotonin signal remained elevated.

Venlafaxine

Response to venlafaxine in the SNr is illustrated in **Figure 3 B**. Greatest increase in serotonin release was observed at 60 minutes. Serotonin concentration increased from 25 ± 6.1 nM (0 minutes) to 120 ± 24 nM. Release after stimulation decreased to 101 ± 23 nM at 120 minutes. Venlafaxine shows a trend of increasing the release of serotonin upon stimulation the most of all the drugs tested in this study. Elevation of serotonin above control values continued to 22 seconds at 5 minutes. Similarly to escitalopram, venlafaxine at 10, 60, and 120 minutes did not return to control values. However, uptake of serotonin from the synapse was greater than escitalopram (the decreasing slope representing clearance from the synapse for venlafaxine is steeper than in escitalopram).

Fluvoxamine

Figure 3 C illustrates the effect of fluvoxamine on serotonin. The greatest increase in stimulated release occurred at 60 minutes with a concentration of 99 ± 21 nM from 37 ± 11 nM at 0 minutes. Stimulated release decreased to 69 ± 14 nM at 120 minutes. The 60 minute file additionally had the longest duration above control values; serotonin concentration did not match 0 minutes till 26 seconds. Fluvoxamine increased release of serotonin more than it decreased the rate of uptake. Uptake remained the greatest of all antidepressants tested.

Fluoxetine

Fluoxetine, shown in **Figure 3 D** had the least effect on serotonin release, and slightly greater effect on uptake from the synapse than fluvoxamine. Increase in release after stimulation was maintained from 60 minutes to 120 minutes at 87 ± 25 nM from 27 ± 5.9 nM at 0 minutes. Fluoxetine's ability to decrease uptake of serotonin was observed from 60 minutes to 120 minutes with values returning to those seen in control at 29 seconds.
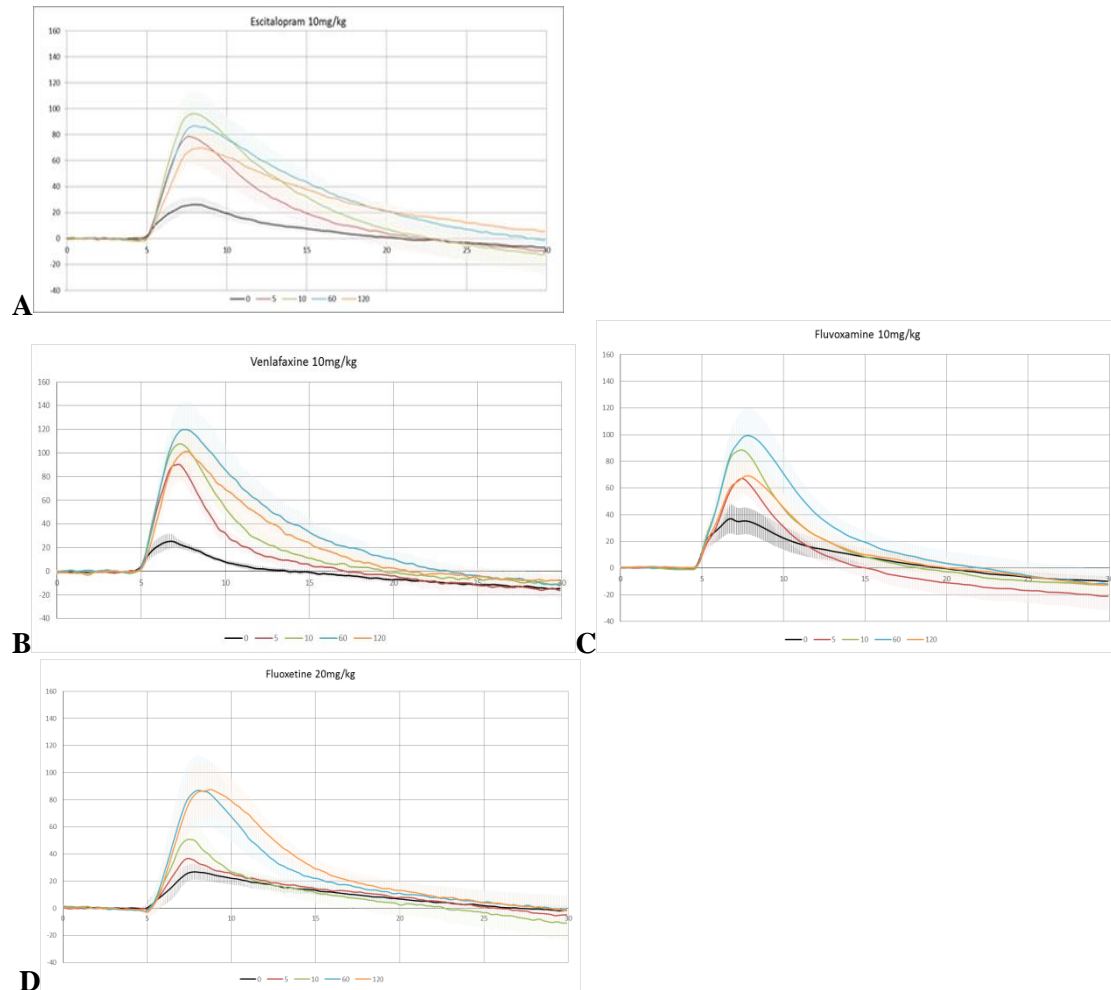
Figure 3: Effects of escitalopram (**A**), venlafaxine (**B**), fluvoxamine (**C**), and fluoxetine (**D**) on serotonin in the SNr of the mouse brain *in vivo*, vertical axis represents concentration in nM, horizontal axis represents time in seconds. Each graph is plotted as the average of n=5 (fluoxetine n=4) with SEM. t=0 represents pre-antidepressant concentration of serotonin.

Discussion

As stated in the introduction, antidepressants targeting serotonin release and uptake are traditionally used in the treatment of MDD. However, the variations in efficacy between antidepressants noted by Cipriani et al. makes it imperative to fully understand the differences between them. Cipriani et al. rated escitalopram and venlafaxine as more efficacious than fluoxetine and fluvoxamine. In this exploration, several distinctions can

be made between escitalopram and venlafaxine, and fluoxetine and fluvoxamine. Additionally, small variances can be observed between antidepressants of similar ranking.

Venlafaxine had the greatest effect on stimulated release of serotonin raising the concentration by 94 nM above control. Escitalopram had the second greatest effect raising control values up to 70 nM post administration. Fluvoxamine and fluoxetine had lesser effect, raising control values 63 nM and 61 nM respectively. This trend of effect on stimulated release of serotonin indicates that antidepressants ranked more efficacious increase stimulated release more than lesser ranked antidepressants. These findings suggest release is one important target in the development of new antidepressants, the second being the drug's effect on uptake, or clearance of serotonin from the synapse.

In this study, the rate of uptake suggested to be the most crucial aspect distinguishing highly efficacious antidepressants from those lesser ranked. Although escitalopram is a very effective antidepressant it did not have the greatest increase in stimulated release, but rather the greatest effect on slowing uptake. An interesting trend that was seen with escitalopram is that a maximum effect on stimulated release was achieved early in the time trial (10 minutes), as the trial progressed the effect on stimulated release lessened in contrast to the effect on uptake. At 120 minutes the slope is significantly elongated horizontally in comparison to fluvoxamine and fluoxetine. Venlafaxine did have effect on uptake, but not as profoundly. Additionally, the same trend in regards to release, as observed with escitalopram, was observed with venlafaxine, this agrees with the findings of Wood and Hashemi in their recent study with escitalopram. This observation identified prolonging the time serotonin remains in the synapse as an important element in the designing of antidepressants.

Increasing the release of serotonin by the presynaptic neuron and decreasing the rate of uptake of serotonin are the two elements suggested to be targeted for effective treatment of MDD. Medically, this information can be used in the development and screening of new antidepressants. Before new drugs move to clinical trials, they can be evaluated through the use of FSCV and their effects on release and uptake can be characterized. Utilizing the known clinical effectiveness of the drugs currently used, and the characteristics of the four seen in this study through FSCV, antidepressants that are in the early stages of development could be predicted to be an efficacious drug or non-efficacious. Adding this step to the development process could save resources, time, and money. Additionally, it could further help to distinguish antidepressants (known and newly developed) that are the most effective in the treatment of MDD, this could assist in improving the therapy of patients. Further studies need to be conducted with additional antidepressants, in addition to more in depth characterization. However, the trends observed in this study suggest that targeting uptake primarily and release could be the ideal mechanism to use in the treatment of depressive disorders such as MDD.

REFERENCES
American Psychiatric Association., & American Psychiatric Association. Task Force on DSM-IV. (2000). *Diagnostic and statistical manual of mental disorders : DSM-IV-TR* (4th ed.). Washington, DC: American Psychiatric Association.

Bosker, F. J., Klompmakers, A. A., & Westenberg, H. G. (1995). Effects of single and repeated oral administration of fluvoxamine on extracellular serotonin in the median raphe nucleus and dorsal hippocampus of the rat. *Neuropharmacology, 34*(5), 501-508.

Ceglia, I., Acconcia, S., Fracasso, C., Colovic, M., Caccia, S., & Invernizzi, R. W. (2004). Effects of chronic treatment with escitalopram or citalopram on extracellular 5-HT in the prefrontal cortex of rats: role of 5-HT1A receptors. *Br J Pharmacol, 142*(3), 469-478. doi: 10.1038/sj.bjp.0705800

Cipriani, A., Furukawa, T. A., Salanti, G., Geddes, J. R., Higgins, J. P. T., Churchill, R., . . . Barbui, C. Comparative efficacy and acceptability of 12 new-generation antidepressants: a multiple-treatments meta-analysis. *The Lancet, 373*(9665), 746-758. doi: http://dx.doi.org/10.1016/S0140-6736(09)60046-5

Dazzi, L., Seu, E., Cherchi, G., & Biggio, G. (2005). Chronic administration of the SSRI fluvoxamine markedly and selectively reduces the sensitivity of cortical serotonergic neurons to footshock stress. *Eur Neuropsychopharmacol, 15*(3), 283-290. doi: 10.1016/j.euroneuro.2004.11.003

Hashemi, P., Dankoski, E. C., Petrovic, J., Keithley, R. B., & Wightman, R. M. (2009). Voltammetric detection of 5-hydroxytryptamine release in the rat brain. *Anal Chem, 81*(22), 9462-9471. doi: 10.1021/ac9018846

Hashemi, P., Dankoski, E. C., Wood, K. M., Ambrose, R. E., & Wightman, R. M. (2011). In vivo electrochemical evidence for simultaneous 5-HT and histamine release in the rat substantia nigra pars reticulata following medial forebrain bundle stimulation. *J Neurochem, 118*(5), 749-759. doi: 10.1111/j.1471-4159.2011.07352.x

Kobayashi, T., Hayashi, E., Shimamura, M., Kinoshita, M., & Murphy, N. P. (2008). Neurochemical responses to antidepressants in the prefrontal cortex of mice and their efficacy in preclinical models of anxiety-like and depression-like behavior: a comparative and correlational study. *Psychopharmacology (Berl), 197*(4), 567-580. doi: 10.1007/s00213-008-1070-6

Lindsley, C. W. (2012). The top prescription drugs of 2011 in the United States: antipsychotics and antidepressants once again lead CNS therapeutics. *ACS Chem Neurosci, 3*(8), 630-631. doi: 10.1021/cn3000923

Michael, D. J., & Wightman, R. M. (1999). Electrochemical monitoring of biogenic amine neurotransmission in real time. *Journal of Pharmaceutical and Biomedical Analysis, 19*(1–2), 33-46. doi: http://dx.doi.org/10.1016/S0731-7085(98)00145-9

Wood, K. M., & Hashemi, P. (2013). Fast-scan cyclic voltammetry analysis of dynamic serotonin reponses to acute escitalopram. *ACS Chem Neurosci, 4*(5), 715-720. doi: 10.1021/cn4000378

Investigation of Three Putative Loci
Involved in Corn Domestication

By Hieu Duc Hong
Major: Biology
Mentors: David Wills, Ph.D & John F. Doebley, Ph.D
           Laboratory of Genetics, University of Wisconsin-Madison

ABSTRACT

Maize (commonly known as corn) is the most productive crop and major food source in the US. Our research is interested in understanding more in corn genetics. In particular we want to investigate the number and the kind of genes responsible for modern, domesticated phenotypes. A set of three transcription factors were investigated to identify the domestication traits they influence. In order to accomplish this, genotyping of 382 F_2 individuals from a knockout line for each of the 3 candidate genes was carried out using PCR. Next, gene expression of mRNA level of three candidate genes in three different tissues (ear, seedling, and leaf) would be done using allele specific expression assays. We found that two of populations did not follow the expected Medelian segregation ratio. In the future, a lot of measurement will be done in the mutant plants that displayed interesting phenotype. This research will help us understanding more in gene expression.

INTRODUCTION

Corn is a staple cereal which has played a large role in providing calories for humans and livestock[2]. It generates billions of dollars of revenue each year in the US economy. Even though much has been learned about the origin and the evolution of corn in the last 50 years, only a handful of the particular genes involved in corn domestication have been identified and studied. Roughly a century ago, the progenitor of maize was a mystery until Beadle proposed the "teosinte hypothesis". He proposed teosinte was the closest, oldest relative of maize[1].

Teosinte refers to four species of the genus *Zea*. *Zea mays* ssp. *parviglumis* has been identified as the progenitor of maize and it is commonly known as the "grain of the gods" by the Nahuatl Indians[1]. Its plant architecture and morphology are completely different from the cultivated maize. The corn we consume typically has one stalk with few branches, whereas teosinte has multiple stalks with many branches (see figure 1). Maize has one male flower at the top and it's the female flower, the ear, is found at the tip of each branch. Teosinte has male flowers at the top of the stalk and the tip of each branch, with multiple female flowers at the internode of the branches. Teosinte has many ears compared to only one or two ears from the domesticated maize. Teosinte's kernels are encased in a lignified fruitcase that is extremely hard for humans to digest while the maize kernel is exposed. In addition, teosinte only has 5 to 12 kernels per ear while corn has more than 500 kernels. Although very different morphologically, teosinte and maize are the same biological species. Crosses resulting in fully fertile offspring can be readily made in either direction. Yet in terms single nucleotide polymorphisms, the genetic distance between two lines in maize is greater than the genetic distance between humans and chimpanzees[2].

It is this great genetic diversity that has been used as a method to identify the genes that were selected upon during domestication. We are interested in answering these following general questions: What are the number and kind of genes that were under selection during domestication and how do we identify and map out those genes? During the process of domestication, what form of mutations occurred yield the variants that we have today? How do we identify the phenotype under selection? To investigate aspects of these questions,

my research involved implementing a special corn model system called the UniformMu Transposon Resource that provides knockout lines for hundreds of genes. The goal of this project is to identify expression differences and the phenotypes controlled by three genes involved in corn domestication.
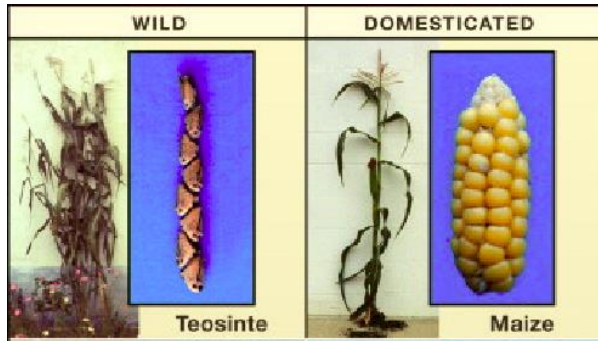
Figure1: differences between teosite and maize[1]

Candidate gene selection:
In prior studies based on locus specific reductions in genetic diversity, over 500 putative domestication loci have been identified[3,4,5,6,7]. Three loci were selected from this candidate list that were transcription factors that had knockout lines availible from the UniformMu Transposon Resource at the University of Florida[8,9]. Mutant seed lines for each putative selected locus were obtained by crossing in an active Mutator Transposon into a W22 background and allowed to insert randomly throughout the genome. F_2 seed and backcrossed seed were obtained for each line. All three selected loci were located on chromosomes three. Each locus has roughly 76-80 seeds planted in 20 kernel rows and were genotyped as described below.

Primer design:
Using NCBI Primer-BLAST (basic local alignment search tool) and Primer3 software, forward and reverse primers were designed to amplify the B73 allele for each locus. The size of the product was neither larger than 600 bp nor smaller than 300 bp. The size of the primer was between 21-32 base pairs, and Tm from 57 to 66.6 °C. These optimal values were used as the default for the further primer design. To identify individuals carrying the transposon insertion in the candidate locus, a partially degenerate primer named TIR6[9], was design by the UniformMu Transposon Resource which binds to the terminal inverted repeat (TIR) sequences and can be used with locus specific forward and reverse primers to indentify individuals with the transposon inserted allele (See Table 1 and Figure 2).

Table1: Primers used to genotype each line.

Mu Primers	5'-DNA-3'	bp	T_m (°C)
G062218MuF02	ACAATTATACTGCCGCGTAAGA	23	54.1
G062218MuR03	GAGGACGAGTAGCAGGACGAC	21	61.9
G104082MuF03	TCTCTGTCTCCTGCTGATTGG	21	56.3
G104082MuR03	ACTGTTTCCTGAACGAGGTCT	21	55.9
G321810MuF02	CTATGCAGGTCGTGGTACTCG	21	57.1
G321810MuR03	GACCACGCTCGGTAACCTCTC	21	59.5
TIR6	AGAGAAGCCAACGCCAWCGCCTCYATTTCGTC	32	66.6

DNA extraction:
A 1 cm^2 piece of leaf tissue for each individual was collected and extracted using a modified cTAB DNA extraction protocol[10].

Genotyping using Polymerase Chain Reaction Screening (PCR):

Figure 2: Working model for Mu Transposable element (TE). The top figure showed the gene without insertion. The middle showed the process of insertion. The bottom one showed the inserted Mu in the gene. The arrows indicated the direction of the primers annealing to the segment of the gene.
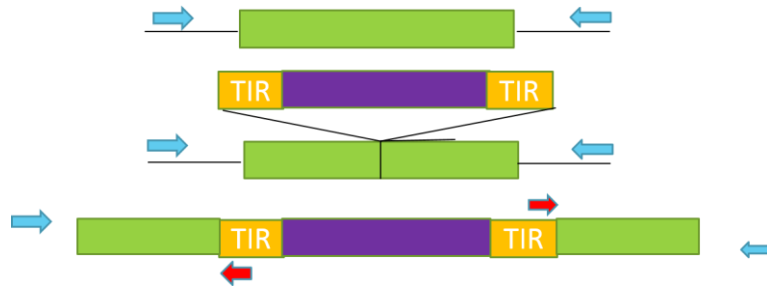
In each PCR reaction, there were three primers: the locus specific forward and reverse primers and the TIR6 primer (see Table 1 and Figure 2). Using GoTaq Kit from Promega (Madison, WI) each individual was amplified with the appropriate set of locus specific primers with the TIR6 primer along with B73 as a positive control and Tris-EDTA buffer (pH 8.0) as a negative control. The PCR products were then separated and visualized using 1.5% TBE argarose gels. Plants homozygous for the wild-type allele should only have a single band from the PCR reaction between the locus specific forward and reverse primers. Plants homozygous for the transposon inserted allele will have two PCR products, one from each locus specific primers and the TIR6 primer. Heterozygous individuals would have all three products. Thermocycler conditions used a two-step protocol as follows: After a 1 minute 94°C incubation, 10 cycles of 94°C for 25 seconds, annealing temperature of 62°C for 30 seconds, then extension at 72°C for one minute. Second, 30 cycles of 94°C for 25 seconds, annealing at 56°C for 30 second, and extension at 72°C for 1 minute. Finally, a 72°C incubation for 5 minutes.

Allele Specific Expression Assay:
Each candidate locus was sequenced and scanned for indel (insertion-deletion) polymorphisms between maize and teosinte inbred individuals present in the exons for each locus. Fluorescently labeled forward primers were ordered to amplify the mRNA transcript for each locus containing the indel polymorphism. ASEAs were run on a panel of cDNAs of 31 F_1 crosses of inbred maize and teosinte. There were zero to three biological reps per sample, and the F_1 parental genomic DNAs were included as 50/50 control for each sample. Each ASEA was diluted and combined with a ROX DNA ladders in formamide. The mRNA abundance for each parental allele was quantified from the PCR products of the cDNAs via gene scan using an ABI 3730 XL DNA Analyzer. Peak areas were measured using the GeneMarker® package (SoftGenetics, State College, PA.) Leaf, seedling and immature ear tissues were previously extracted for each F_1, the mRNA was extracted, and then converted to a cDNA library.

Statistical Analysis:
Chi square test (in Excel) was used to determine whether the result of genotyping was statistical different from the expected Mendelian ratios.

In order to figure out the genotype of the plants, we scored the PCR products of the plants as mutant, wild-type, or homozygous. A single band of the same size as the wild-type allele indicated 2 copies of inserted allele (lane A), or heterozygous with 1 copy of inserted allele and one wild-type copy (lane B), or 2 copies of the wild-type allele (lane C) See Figure 3.
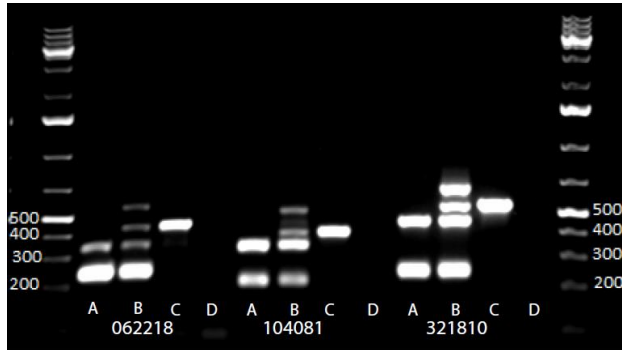
Figure 3: PCR products on 1.5 % TBE Agrose gel

Table 2: Genotyping results

Mu number	ID number	Heterozygous observed	Homozygous with Transposon	Wild-Type
062218	GRMZM2G062218	21	37	19
104081	GRMZM2G104081	39	9	28
321810	GRMZM2G321810	30	29	21

Table 2 summarizes the genotyping of knockout line individuals. There were a total of 77 seeds for locus GRMZM2G062218 in which I observed 21 plants with heterozygous Mu insertion, 37 plants with mutant homozygous on both chromosomes, and 19 wild-type individuals with no Mu insertion. For locus GRMZM2G104081, there were 39 individuals with heterozygous genotype, 9 individuals with the mutant genotype, and 28 individuals with the wild-type genotype. Lastly, for locus GRMZM2G321810, there were 30 individuals with heterozygous genotype, and 29 homozygous knockout individuals, and 21 individuals with the wild-type genotype.

DISCUSSION

There were three genotypic classes: for the homozygous transposon insertion, wild-type (without Mu insertion), and heterozygous. Therefore, we could test for Mendelian inheritance. For F_2 crosses that meant the F_1 parents were heterozygous crossed to each other. A Chi square test was used to determine whether the number of expected offspring fit the standard Mendellian ratio. For locus GRMZM2G062218 and

GRMZM2G321810, the percentage of observed heterozygous plants were 24% and 39% which deviated from the expected 50% heterozygous offspring. The number of homozygous mutant individuals was overwhelming high compared to standard 25% expected number. They were 69% for GRMZM2G062218 and 48% for GRMZM2G321810. The p values indicated they were statistically significant and they did not follow the Mendelian ratio (p=1.23 x 10^{-12} and p=1.25484 x 10^{-4}, accordingly). We believed that our collaborators sent us the homozygous mutant lines instead of the heterozygous seed. After removing the individuals from suspected incorrect crosses, the other crosses followed the expected ratio. To be certain it was not caused by genotyping error, a second DNA extraction was performed for each individual and genotyped. The results were identical. For the locus GRMZM2G104081, the percentage of observed heterozygous plants was 53%. The p value (p=0.215567163) for the locus was not significantly different from Mendelian inheritance.

FUTURE WORK

Allele specific expression assays will be completed for immature ear, leaf, and seedling tissue (see Allele specific assay). Heterozygous plants will be chosen to pollinate in the middle of August for future phenotypic study. In addition, measurements on knockout and wild-type plants with interesting traits will be completed at plant maturity.

HUMAN MACHINE INTERFACE FOR AN UPPER-EXTREMITY SMART ASSISTIVE ROBOTIC ARM (SARA)

By Kayla Jordan
Major: Electrical Engineering
Mentor: Mr. Umer Khalid, Department of Electrical Engineering

INTRODUCTION

For upper limb motions almost all able-bodied humans take for granted, there are some individuals that struggle every day. Arm movements such as holding one's arm horizontal or moving it across the body pose challenges for some of the disabled population. About 250,000 Americans are spinal-cord injured. Approximately 11,000 spinal injuries occur each year. [1] Assistive technology aiding these Americans is spanning from a single limb robotic tech to a full-body application. The reason for this large span is some individuals rely on the technology more than others. Individuals may still have some movement in their limbs while others can barely lift a finger and require a full-body robotic suit. Assistive technology truly depends on the needs of the user. It is not limited to one's needs over another's. Many different machines are created to fit not only a general part of the human body, but also the user's preference as well. From as early as 1918, people have continued striving towards helping the restricted become mobile again. Even more effort has been put towards the enhancement of overall body movement.

One of the first assistive technologies was the package reacher. The package reacher was a simple arm that was used to reach packages from places out of arm's reach. The reacher was patented in 1918, and can be seen as the first for most modern grabbers today as seen below. [3]
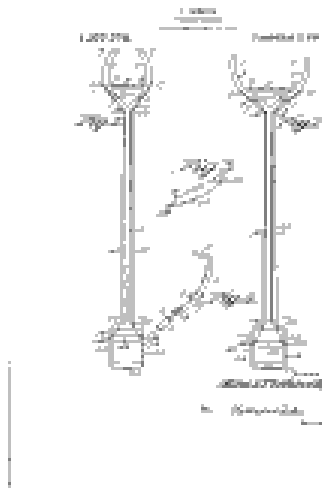
Figure 1: Designs for the first package reacher.

The technology available today can be tailored to the person's specifics. Single limb robotic technology can range from a 20% loss of some limb movement to having no motion at all due to nerve damage or an amputation. An example of a tech that can be used by an amputee is the i-LIMB Prosthetic Hand. The i-LIMB uses myoelectric signals from the remainder of an amputee's limb. The i-LIMB translates those signals into movements for the hand to take. Research has shown that the hand is very accurate in its motions. It provides the user with fine-controlled results. [4]
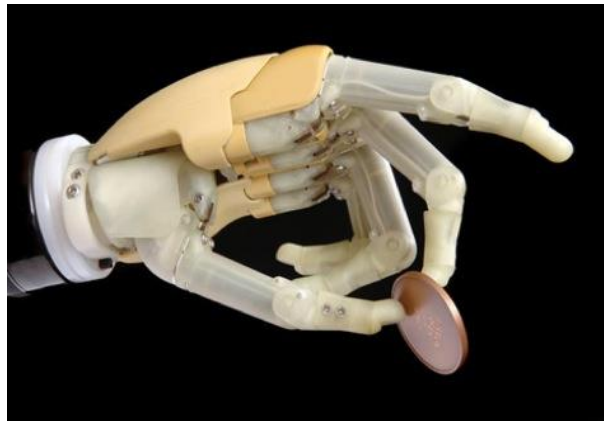
i-LIMB holding a penny, showing precise control.

Full-body exoskeletons have been more so designed for military purposes in the United States, not necessary for the disabled. The SpringWalker is a lower-body exoskeleton that can run at a peak of 24 kilometers. It can also carry a 90-kg load. Already a few exoskeletons have been commercialized to date. [2] In Asia however, exoskeletons have been created to help the elderly and disabled walk. A commercialized example is the HAL-5. It uses electric actuators that is attached to the user's body and help them become more mobile. [2]
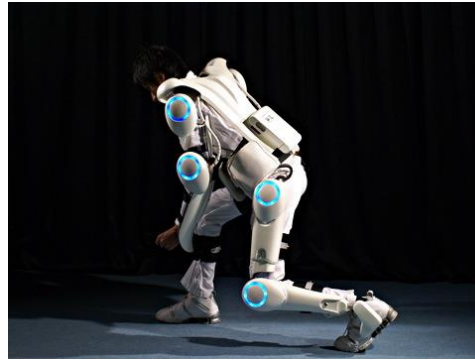
Demonstration of HAL-5. [3]

Some of these exoskeletons have been designed to be relatively lightweight and be able to support themselves so that the user does not experience more weight. However, the difficulty arises with the disabled still needing someone to place them in the equipment and to remove it as well. The exoskeleton may not even reach its full potential if the user only prefers to use the equipment for no longer than five minutes. As stated before, a human assistant will probably still need to be available to support the user. Exoskeletons in consequence require more work and human aid even though they are very supportive.

The variations began to take shape when some people may have some function in their limbs while others may not have any mobility at all. SARA is made for people who still have residual functionality in their arm. SARA can be also applied to persons who have conditions such as extreme arthritis. The amount of dependence on the device is determined by the user. It was built to have more movement than just a simple grabber, but to not be as demanding as a full-body exoskeleton.

SARA 1

SARA 1 was originally an assistive technology that was only voice-controlled and could only grip, not move forward or backward. The design included a suction cup gripper, band springs, a linear actuator, a hand grip, a Velcro attachment strap, and a control circuit pack [Figure 1]. The design of SARA 1 was designed to be low-cost, modest, and lightweight. An individual volunteered to test the equipment. SARA 1 was strapped to his arm, and he was able to pick up a cellphone from the ground voice-controlling SARA 1 with commands such as "grab" and "open", successfully returning it to his lap. [1] SARA 1 was simple in design, having only one modality and built for a person who could still move his or her arm across and away from their chest. Also to note, the user had to still be able to pick up items weighing no more than 2.5 pounds. [1] Shoulder movement was the key for the effective use of SARA 1 as there was no track for extension and retention. The user had to have enough dexterity to be able to move their arm along the vertical axis to return objects to their desired position. Because voice-control was the only available modality for SARA 1, the participant had to have almost clear vocal capabilities. The user had to be able to repeat the same command that was recorded for the memory chip inserted into the circuit board. Otherwise, there was a chance that SARA 1 would not respond. SARA 1's vocal interface only supported the English language a small amount of commands due to the limitation of memory directly on the microchip.
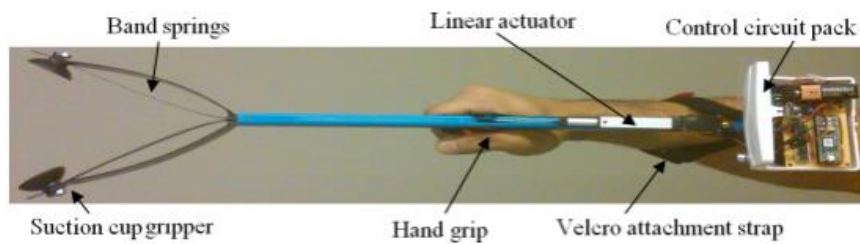
Figure 1: SARA Gen 1
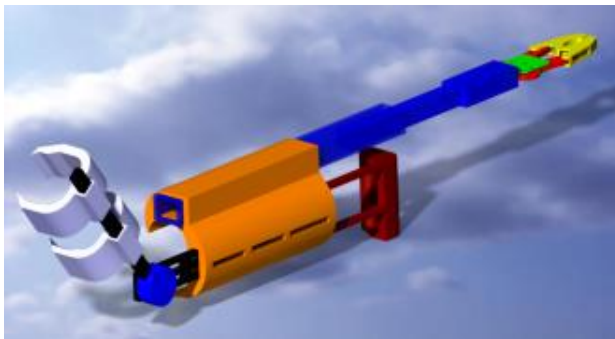
Figure 2: SARA Gen 2 (modeled in AutoCad)

SARA 2

In the ever-growing field of Assistive Technology, researchers of Wayne State University have finished their prototype SARA 2, also titled "MAX", designed to help disabled people with tasks such as picking up objects from a mid-shin level and placing them on surfaces from a sitting eye-level position. MAX in addition had two more modalities added to its design. MAX has a robotic arm that can extend forward and backward almost double the length of the carriage. MAX too has pressure sensors that support angular movements on the vertical plane. Actuators mimic the muscle movements of the triceps and biceps of the upper arm. Pilot tests are being conducted in shaping the final product of the technology.

INCENTIVE

The incentive for the design of SARA 2 was the same as SARA 1. The design was to still be kept low-cost, but to add two more modalities. SARA 2's plan was to stay low-cost because some disabled do not work because of their limited movement. The modalities added were digital and analog. These modalities were added to help SARA 2 become more ergonomic in the future assistive technology market. Personalities and adaptation to certain modalities help make SARA more versatile with its operations. SARA 2 still had the incentive of being user-friendly. The main purpose of the mechanical arm was to reduce the stress on a new user when they were attempting to learn how to use the device. Some people who begin to use assistive technology find it hard to get adjusted to certain equipment because of the mental taxing. By studying the modalities and mental stresses, the creators were able to determine the strengths and weaknesses of SARA 2.

HYPOTHESIS: STUDY

Test subjects included three people with normal arm movement, and seven disabled participants. A bookshelf had 5 different colored markers taped down on each shelf. On each shelf, each color was labeled with a number from one to five. Sitting on a stool, participants would participate in a fine-movement test involving colored pegs from the labeled points on the shelves to their respective receptacles in a peg holder. A gross test involved moving weighted bottles (marked as well) ranging from 0.5 pounds to 2 pounds from one level to another. A third test used voice commands to maneuver MAX to move objects. A method of scoring the placement of the objects determines the timed completion of each test. Drops from the test area (being monitored as "errors") also assisted finding the finished time. The allotted time for testing each participant was approximately 90 minutes and on a voluntary basis. The fine (pegs) and gross (weighted objects) movement tests were measured to gauge the accuracy of using SARA 2 as a prominent assistant. These studies will benefit researchers as they decide on any improving alterations that can be made to MAX.

MATERIALS AND METHODS

The materials used in SARA 2 gave users variability. SARA 2 has the like design of SARA 1, but instead of being made of plastic is made of steel. The peg and gross object tests were implemented using all three modalities. First the digital modality was tested. A participant had to place their arm into SARA 2's Velcro straps and hold the controller in the other. A microchip processor calculated to take signals from the buttons had to be placed on SARA 2's circuit board. Four buttons were used in controlling SARA. Two buttons controlled the forward/backward motion while two more controlled the opening and closing of the gripper. Motions could be controlled simultaneously. The linear actuator would move after one button press and would not stop moving in the carriage until the identical button was pressed again. SARA 2 moved at a constant speed when using the digital modality and did not accelerate or decelerate.

The second modality involved analog signals. Repeating the fine and gross movement tests, the user used an analog controller. The controller involved two "sliders" in a box. One "slider" controlled the forward/backward motion of MAX. The other slider managed the opening and closing of the grabber. Again the four motions could be performed simultaneously. Markings on the controller noted the "safe zone" for a slider to be rested in so action would be taken by MAX.

The third modality was voice. Users would first use a program (insert name of voice program here) to record their voices on a microchip. The command was recorded twice to give a slightly larger range of tone and word speed for MAX to recognize. For the voice modality to stay even more accurate, it was advised that the same tone and word speed be used. SARA 2 would only respond to the voice data on the microchip. This aided in reducing acting movement on other sounds heard. Simple commands such as "grab", "go", and "back" were recorded for the motions. Other command words could be recorded at the user's request. The main command that had to stay the same was "MAX". Likewise the other two modalities, users completed the same two tests.

RESULTS

Due to SARA 2 still being a prototype and in the process of being patented, I cannot release the details of the results. At my mentor's discretion I can give my own thoughts about my participation in the pilot studies. I felt the experiments were simple to conduct once I was adept to MAX. Using the pressure sensors made me feel comfortable in knowing that I would not have to do much arm movement of my own besides pointing MAX in the correct direction to place the pegs and gross objects. I favored the digital modality overall, as it gave me more control than the sliders and I did not have to give a lot of commands such as with the voice modality.

CONCLUSION

With any prototype, there are improvements that can be considered. An improvement that can be made to SARA 2 is the analog modality. For those with not enough dexterity to keep the sliders in a certain position on the remote, this can cause a problem such as battery and equipment wear-down. Future work includes making SARA 2 lighter as the prototype is currently made of steel. A material being considered is a type of plastic.

FINAL WORDS

Some thoughts I took from SARA 2 was how such "easy" motions are taken for granted, even lifting a finger. I hope that one day I can take the experiences I learned from MAX to be able to help people with assistive technology. I would like to thank Umer Khalid for giving me the opportunity to test his research and I would like to thank the McNair Scholars program for giving me the chance to do so.

REFERENCES

Hand-World Pic: http://www.babyboomercaretaker.com/images/Advantages-Of-Robotics.jpg

Pegs http://www.arnoldwood.com/images/category/3/product_largeimg_246.jpg

SARA 1 and Grabot Poster: Umer Khalid et al., *"Multi-Modal Smart Assistive Robotic Arm"*, (I do not know the year this was published).

HAL-5 and SpringWalker Citation: E Guizzo, H Goldstein - Spectrum, **IEEE**, 2005 - ieeexplore.**ieee**.org

HAL-5 Pic: http://images.businessweek.com/ss/06/10/gooddesign/source/15.htm

i-LIMB Pic and Citation: http://hanger.com/prosthetics/services/Technology/Pages/FeatureArea.aspx

Package
Grabber: https://www.google.com/search?hl=en&site=imghp&tbm=isch&source=hp&biw=1304&bih=707&q=j.+tichacek

RECYCLING ROUTE OPTIMIZATION BASED ON TRAVELING SALESMAN PROBLEM WITH MULTIPLE TRIPS

By Vilma Kocllari
Major: Industrial & Systems Engineering
Mentor: Dr. Evrim Dalkiran, Department of Industrial & Systems Engineering

ABSTRACT

In this paper, we study a real-life vehicle routing application based on recycling gondola collection problem faced by an automotive manufacturing facility. The General Motors, Lake Orion Assembly Plant, uses gondolas for collecting cardboard and trash throughout the plant. The gondolas are picked up and dropped off to the depot to be emptied, and then are returned to their original locations by three tugger drivers. At each round, a tugger driver is allowed to pull up to two gondolas. A recent simulation study revealed that the utilization of drivers is no more than 54%. The purpose of this study is to identify an optimal route in order to minimize the total transportation cost (distance) and increase driver utilization. In the classic Travelling Salesman Problem (TSP), the salesman visits each city once and returns to the depot travelling through the shortest route. Our recycling gondola collection problem is similar to TSP with two main exceptions. First, each gondola location is visited twice, during picking-up full gondola and dropping-off empty gondola, where the first visit realizes strictly before the second visit. Secondly, a truck driver may haul up to two gondolas, which sets the capacity of a truck to two. Our study presents a specific case of TSP, where nodes represent a group of two gondolas and each driver performs multiple trips during the working hours. In order to solve this specific case of TSP, we first tackle the assignment of gondolas to groups of up to two. The distances between groups are judiciously defined such that the cost associated by particular link is not affected by and does not affect the cost of other links. We introduce a naïve TSP formulation for the recycling gondola collection, which is applicable to various collection problems in different domains.

1 INTRODUCTION

General Motors is searching for an optimal routing schedule for the recycling process at Lake Orion Assembly Plant. Currently, the cardboard and trash materials are collected in gondolas that are transported to the depot, collecting area, by tugger drivers. Three tugger drivers are assigned to the pick-up and drop-off operations and based on the simulation data provided by Production Modeling Corporation it is known that they are only utilized 54%. In this project, we aim to find an optimum schedule and route for picking-up and dropping-off gondolas using mathematical modeling techniques that would save time and man-power.

According to the plant regulations, the maximum number of gondolas that can be sent to the depot to be emptied cannot exceed two. In this circumstance, the driver has to pick up at most two gondolas at the time and bring them to the depot. After placing back the empty gondolas to their location, the tugger driver picks at most another two gondolas that need to be emptied. At this time, there are a total of 69 locations throughout the plant where the gondolas are placed. This translates in a total of 90 gondolas since a few locations contain more than one gondola. The number of gondolas positioned at the certain locations is based on the amount of cardboard and trash produced by the assembly process. Another important issue related to this problem is the pickup frequency. The cardboard gondolas placed closer to high traffic areas get filled up very quickly. Consequently, the pickup frequency per day changes significantly from location to location. Specifically, our data show a pickup frequency of one time a week up to four times a day.

2 PURPOSE

In this paper, we seek an optimal route from the depot to gondola locations which are scattered throughout the plant. In other words, we aim to identify which gondolas the driver should pick up together and which ones should be next based on cost of traveling, which is distance and pick up frequency. The optimal route will be translated to a pre-determined schedule that the drivers follow in their day-to-day work. The utilization of the drivers will be recalculated after the final results are drawn.

3 LITERATURE REVIEW

In order to formulate and determine an optimal route for the recycling process, it is necessary to understand the history and context of the Traveling Salesman Problem (TSP). TSP is one of the most studied problems in deterministic optimization area since 1950s. In its classic form, given a number of cities and the distances between them, TSP finds the route with minimum travel distance. The salesman from the starting point, the depot, visits each city once and comes back to the depot. In the symmetric TSP the distance from city A to city B is equal to the distance from city B to city A. This means that the tour length stays the same when the route is reversed. Even though a significant amount of literature exists on different solution approaches and special cases for TSP, there are still obstacles related to the number of cities (n) and nodes, since there are $\frac{(n-1)!}{2}$ possible solutions.

The first integer programing formulation was made by Miller and Tucker [9].The TSP formulation problem was also tackled by Lin and Kernighan [8]. The authors generate an effective heuristic algorithm to find optimal or near optimal solutions for the symmetric TSP. A relatively recent approach to an effective solution for both symmetric and asymmetric is given by Dorigo and Gambardella [4] based on ant colony system algorithm (ACS). In other words, a set of agents, in this case ants, search in parallel for good solutions to TSP. The new cites are only added based on the past experience and a greedy heuristic algorithm. The remaining of this section touches upon the literature presenting different branches of TSP such as: TSP with Backhauls (TSPB), TSP with Time Windows (TSPTW), multiple TSP (mTSP), and most importantly Vehicle Routing Problem (VRP) (Bochtis and Sorensen, 2009). The first branch TSPB brings a new set of customers known as backhaul who request their order to be sent to the depot. Ghaziri and Osman [6] introduces a new approach based on the three chains of neurons. The first chain interacts with line haul customers, the second one deals with backhaul customers, both interacting with depot and each other. TSPTW focuses on finding the minimum cost path when visiting a set of cities only once, but each city must be visited on a specific time windows. A merge of Operation Research techniques and scheduling problem were used by Focacci et al. [5] to solve TSPTW. On the other hand, m-TSP is a generalization of the TSP where multiple traveling salesman routes are calculated. Bektas [1] gives a review of the literature dedicated to m-TSP by emphasizing the real life application. When it comes to VRP, which focuses on optimal delivery from one or several depots to a number of geographically cites or customers, Laporte [7] concluded that exact algorithms can only solve small problems and approximate algorithms possess high potential to solving large problems.
In this paper, we will be facing multiple trip problems that can be linked with Vehicle Routing Problem with Multiple trips (VRPM). VRPM investigates cases where vehicles make more than one trip within the working hours. Brandon and Mercer [3], Salhi and Petch [10] test problems from the literature and study a more efficient algorithm, respectively heuristic and a hybrid Genetic Algorithm.

4 MATHEMATICAL FORMULATION

In this section, we will be discussing the mathematical model that includes assignment and TSP formulations to our on recycling gondola collection problem. The assignment formulation forms groups of at most two gondolas and the TSP formulation minimizes the total distances travelled to visit each gondola.

We commence with introducing the assignment formulation. As mentioned in Section 1, tugger drivers are allowed to carry at most two gondolas at a time. Given that there are N_1 gondolas, the total number of groups of size at most two is calculated by $\frac{N_1 * (N_1 + 1)}{2}$, where N_1 of them includes only one gondola and the remaining $\frac{(N_1 - 1) * N_1}{2}$ are of size two, i.e., $(1, 1), (1, 2) \dots (1, N_1), (2, 2), (2, 3) \dots (N_1, N_1)$. Let $N_2 = \frac{N_1 * (N_1 + 1)}{2}$ be the total number of such groups. Next, we introduce the binary parameter a_{ij} which is set to 1 if the gondola i is in group j and is set to 0 if otherwise, as follows:

$$a_{ij} = \begin{cases} 1 & \text{if gondola i is in group j} \\ 0 & \text{o/w} \end{cases}$$

The model should select a subset of groups such that all the gondolas are visited exactly once. In order to formulate this constraint, we introduce an array of binary variables x_j, each of which takes the value one if the group j is selected and 0 if it is not selected, as follows:

$$x_j = \begin{cases} 1 & \text{if group j is picked} \\ 0 & \text{otherwise} \end{cases}$$

Then, the constraint that forces to select a subset of groups to visit each gondola exactly once is formulated as follows:

$$\sum_{j=1}^{N_2} a_{ij} x_j = 1, \quad \forall i = 1, \dots, N_1$$

Note that we formulated the relation as an equality constraint since our assumption is to visit each gondola exactly once. Instead, we may choose to formulate the constraint as a greater than equal to one form, which allows visits more than once. Given that our objective function minimizes the total distance travelled, we may utilize the greater than equal to constraint since the model automatically eliminate visits more than once.

We continue with the TSP formulation for our problem. It is worth noting that the capacity restrictions prevent us to use the classical TSP formulation directly. In order to highlight the modifications and the main contribution of our research, we first introduce the standard TSP formulation below:

$$\min \sum_{i=0}^{N_2} \sum_{j=0, j \neq i}^{N_2} c_{ij} y_{ij}$$

$$\sum_{i=0, i \neq j}^{N_2} y_{ij} = 1 \qquad \forall j = 0, \dots, N_2$$

$$\sum_{j=0, j \neq i}^{N_2} y_{ij} = 1 \qquad \forall i = 0, \dots, N_2$$

$$u_i - u_j + N_2 y_{ij} \leq N_2 - 1 \qquad 1 \leq i \neq j \leq N_2$$

$$y_{ij} \; binary$$

The decision variable y_{ij} is set to 1, if the route leaves group i and enters group j. The model minimizes the total distance travelled, where c_{ij} represents the distance from group i to group j. The first and second set of constraints forces that each group is visited exactly once. The next set of constraints is called the subtour elimination constraints.

It is worthwhile to mention that the optimal tour visits each gondola once, but it does not have to visit each group. Since each gondola is assigned to N_1 different groups, only one of these groups should be visited. Since c_{ij} represents the distances between groups, not the distances between gondolas, we need to formulate the distance. In the sequel, we discuss the modifications and our TSP formulation.

Let the decision variables y_{ij} represent if the path between the groups i and j is included within the route.

$$y_{ij} = \begin{cases} 1 & \text{the path from group I to group j is selected} \\ 0 & \text{o/w} \end{cases}$$

In order to formulate the objective function, we need to calculate the distance from group i to group j. Note that the drivers could only go through the aisles, hence the distance between gondolas a and b is calculated using rectilinear distance formula as follows:

$d_{ab} = |x_a - x_b| + |y_a - y_b|$, where $\qquad d_{ab} = d_{ba}$,

where (x_a, y_a) and (x_b, y_b) are the coordinates of the gondolas a and b, respectively.

We continue with calculation of distance between two groups of gondolas. Assume that gondolas 2 and 4 are in group i and the gondolas 1 and 3 are in the group j Figure 1 below.
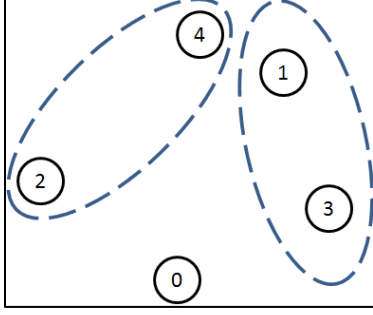
Figure 1: Groupings of four gondolas and the depot.

We first consider visiting the group i and calculate the distance travelled. Next, we study visiting the second group and calculate the distance travelled between groups i and j, which corresponds to c_{ij}. The first gondola to be picked-up while visiting group i can be gondola 2 or gondola 4. Next, the driver picks up the other gondola and drives to the depot. Hence, the driver follows either 2-4-0 or 4-2-0 routes, respectively shown by solid and dashed lines, in Figure 2a. The two routes may give different total distance travelled values, if d_{20} differs from d_{40}.
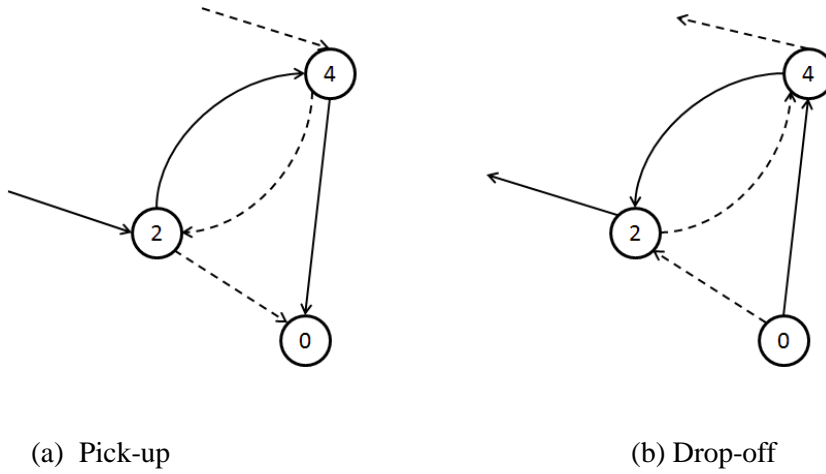
(a) Pick-up   (b) Drop-off
Figure 2: Alternative paths while visiting group i.

After emptying the gondolas at the depot (shown by node 0), the tugger driver chooses to drop-off either gondola 2 (dashed lines) or gondola 4 (solid lines) first and follows the routes either 0-4-2 or 0-2-4, respectively. Again, these two routes may have different lengths.

The route minimization within the group forms a small TSP problem. Since we have at most two gondolas to visit, we calculate the two combinations and find the shortest route. If the capacity of the tugger is larger, another TSP should be solved to minimize the route. In other words, our problem can be classified as a TSP within a TSP.

The first gondola picked-up while visiting a group, affects the total distance travelled as explained above. Additionally, the first gondola dropped-off in the previous group affects the distance travelled from one group to the next one. Hence, the tugger driver's decision at the depot should be based on the location of the gondolas in the next group to be visited. For the case in Figure 2, the tugger driver's decision on dropping-off either gondola 2 or 4 firstly affects the distance travelled from group i to j. In order to calculate c_{ij}, we should consider dropping empty gondolas in group i at their original locations, picking-up the full gondolas in group

j and emptying them at the depot. Dropping the empty gondolas in group j should be included within the cost of c_{jk}, where k is the next group to be visited.

For our example in Figure 1, there are four different routes to select among: 0-2-4-1-3-0, 0-2-4-3-1-0, 0-4-2-1-3-0, and 0-4-2-3-1-0. At the depot, we need to calculate the distance travelled via these four alternatives and select the one having a minimum distance.

$$C_{ij} = min \begin{cases} d_{02} + d_{24} + min \begin{cases} d_{41} + d_{13} + d_{30} \\ d_{43} + d_{31} + d_{10} \end{cases} \\ d_{04} + d_{42} + min \begin{cases} d_{21} + d_{13} + d_{30} \\ d_{23} + d_{31} + d_{10} \end{cases} \end{cases}$$

$= min(d_{02} + d_{24} + d_{41} + d_{13} + d_{30}, \ d_{02} + d_{24} + d_{43} + d_{31} + d_{10}, \ d_{04} + d_{42} + d_{21} + d_{13} + d_{30}, \ d_{04} + d_{42} + d_{23} + d_{31} + d_{10}).$

We now continue with calculating c_{ji}, the total distance travelled while visiting group i, just after group j. The trip starts with empty gondolas of group j at the depot and ending by dropping off full gondolas of group i at the depot. The c_{ji} is calculated as follows:

$$c_{ji} = min \begin{cases} d_{01} + d_{13} + min \begin{cases} d_{32} + d_{24} + d_{40} \\ d_{34} + d_{42} + d_{20} \end{cases} \\ d_{03} + d_{31} + min \begin{cases} d_{12} + d_{24} + d_{40} \\ d_{14} + d_{42} + d_{20} \end{cases} \end{cases}$$

$= d_{01} + d_{13} + d_{32} + d_{24} + d_{40}, d_{01} + d_{13} + d_{34} + d_{42} + d_{20}, d_{03} + d_{31} + d_{12} + d_{24} + d_{40}, \ d_{03} + d_{31} + d_{14} + d_{42} + d_{20}).$

As we reorganize c_{21}, it is observed that $c_{12} = c_{21}$. Hence, the problem is symmetric.

Finally, we discuss the distances between groups and the depot, i.e., c_{0i} or c_{i0}. Assuming that the tugger driver is at the depot and the full gondolas of group i are collected. The total distance travelled, c_{i1}, is formulated as $min(d_{02} + d_{24} + d_{40}, d_{04} + d_{42} + d_{20})$. Note that $c_{01} = c_{10}$ holds true.

Next, we introduce the mathematical model for our problem.
Parameters:

N_1 - total number of gondolas,

N_2 - total number of groups,

Node 0 – depot,

$$a_{ij} = \begin{cases} 1 & \text{if gondola } i \text{ is in group } j \\ 0 & \text{o/w} \end{cases} \quad \forall i = 1,2, \dots, N_1 \quad \forall j = 1.2. \dots N_2,$$

c_{ij} - the distance traveled between groups i and j, $0 \leq i \neq j \leq N_2$.
Decision Variables:

$$x_j = \begin{cases} 1 & \text{if group } j \text{ is picked} \\ 0 & \text{otherwise} \end{cases}$$

$$y_{ij} = \begin{cases} 1 & \text{the path from group } i \text{ to group } j \text{ is selected} \\ 0 & \text{o/w} \end{cases}$$

Our mathematical formulation for the recycle container collection problem is as follows:

$$Minimize \sum_{\substack{j=1 \\ j \neq k}}^{N_2} \sum_{k=1}^{N_2} c_{jk} y_{jk}$$

subject to:

$$\sum_{j=1}^{N_2} a_{ij} x_j = 1 \qquad \forall i = 1, \dots, N_1 \qquad \text{(i)}$$

$$\sum_{\substack{k=1 \\ k \neq j}}^{N_2} y_{jk} = x_j \qquad \forall j = 1, \dots N_2 \qquad \text{(ii)}$$

$$\sum_{\substack{j=1 \\ j \neq k}}^{N_2} y_{jk} = x_j \qquad \forall k = 1, \dots, N_2 \qquad \text{(iii)}$$

$$u_i - u_j + N_1 y_{ij} \leq N_1 - 1, 1 \leq i \neq j \leq N_1 \quad \text{(iv)}$$

x_j, y_{jk} binary

The first set of constraints forces that each gondola is picked-up exactly once. The second set of constraints assures that the route leaves the group j, only if the group j is selected, $x_j = 1$. If the group is not selected among the ones to be visited, then the route is not going to pass though the group j. Note that the corresponding constraint in original TSP formulation is $\sum_{\substack{k=1 \\ k \neq j}}^{N_2} y_{jk} = 1, \forall j = 1, \dots, N_2$, since each existing group is visited. Similarly, (iii) assures that the route enters a group only if the group is selected to be visited.

Finally, (iv) represents the subtour elimination constraints. In original TSP, the MTZ subtour elimination constraints are formulated as $u_j - u_k + N_2 y_{jk} \leq N_2 - 1, 1 \leq j \neq k \leq N_2$, given that all the nodes are visited exactly once. However, in our problem not all the groups are visited. Hence, we need to modify the subtour elimination constraints. There are N_2 groups, but the number of groups visited is between $[N_1/2]$ and N_1. Since the optimal number of groups visited may be greater than $[N_1/2]$, in our subtour elimination constraint, we utilize N_1 as a valid upper bound. For the (j, k) arc, where $y_{jk} = 1$, the constraint reduces to $u_j \geq u_i + 1$. If the arc is not included within the optimal route, then the constraint reduces to $u_j \geq u_i - N_1 + 1$. Since $1 \leq i \neq j \leq N_1$, the constraint becomes redundant. Hence, the modified constraints do not eliminate any feasible route. On the other hand, if there exists a subtour that visits 1-2-,…, $n - 1$, then the constraints written for the arcs (1-2), (2-3), …, (n-1) are as follows:

$$u_2 \geq u_1 + 1$$

$$u_3 \geq u_2 + 1$$

$$\vdots$$

$$u_1 \geq u_n + 1$$

When we add these n constraints, we end up with $0 \geq n$. Hence, the subtour elimination constraints avoid all subtours.

5 Conclusions and Future Research

In this paper, we studied the recycling gondola (container) collection problem faced by General Motors (GM) Lake Orion Assembly Plant. Regarding the plant regulations, a tugger driver hauls at most two gondolas and gondolas should be brought back to their original locations right after they are emptied at the depot location. This unique nature of the problem prevents us to use classical Travelling Salesman Problem (TSP) formulation directly. A judicious definition of distances between groups of gondolas enabled us to construct a modified TSP formulation for the gondola collection problem. We also modified subtour elimination constraints in order to obtain tight relaxations. Since similar collection problems are observed in various domains, it is our hope that our model is well received and adopted to solve those problems.

As a future research direction, we plan to solve GM's problem using real data. It is stated by GM representatives that gondolas are picked up at different frequencies. As a next step, we aim to incorporate the frequency parameter to our mathematical formulation.

REFERENCES

Bektas, T. (2004). The multiple traveling salesman problem: an overview of formulations and solution procedures. *Omega*, *34*(3), 209-219.

Bochtis, D., & Sorense, C. (2009). The vehicle routing problem in field logistic part 1. *Bio Systems Engineering*, *104*(4), 447-457.

Brandon, J., & Mercer , A. (1998). The multi-trip vehicle routing problem. *Operation Research Society*, *49*, 799-805.

Dorigo, M., & Gambardella, M. (1997). Ant colony system: A cooperative learning approach to the traveling salesman problem. *IEEE*, *1*(1), 53-63.

Faccaci, F., Lodi, A., & Milano, M. (2002). A hybrid exact algorithm for the TSPTW. *INFORMS Journal on Computing*, *14*(4), 403-417.

Ghaziri, H., & Osman, I. (2003). : A neural network algorithm for the traveling salesman problem with backhauls. *Computers & Industrial Engineering* ,*44*, 267–281.

Laporte, G. (1992). The vehicle routing problem: An overview of exact and approximate algorithms. *European Journal of Operational Research, 59*(3), 345–358.

Lin, S., & Kernighan, W. (1973). An effective heuristic algorithm for the traveling-salesman problem. *Operations Research*, *21*(2), 498-516.

Miller, C., & Tucker, A. (1960). Integer programming formulation of traveling salesman problems. *ACM*,*7*(4),326-329.

Salhi, S., Petche, R. (2007). A GA based heuristic for the vehicle routing problem with multiple trips. *Mathematical Modelling and Algorithms*, *6*(4), 591-613.

MODELING AND ANALYSIS OF USER INTERFACE DESIGN TO SUPPORT WORK PATTERNS IN ELECTRONIC HEALTH RECORDS (EHR'S)

By Jerrell Mitchell
Major: Industrial & Systems Engineering
Mentor: Dr. R. Darrin Ellis, Department of Industrial & Systems Engineering

ABSTRACT

As the medical field continues to navigate in a direction that it has never been before, new services and systems are being implemented for the benefit of workflow, patient waiting durations, and the continuity of medication orders. The benefits that the new systems and services in the medical field are receiving are; efficiency of work-pages and widgets, and complete overhauls of Electronic Health Records Platform. Electronic Health Record Platforms allow for clinicians and medical providers, to complete tasks and daily duties such as; notes, consults, medication orders, chart reviews, imaging, and reviewing of patients' past records with complete diagnosis.

Though the Electronic Health Records allows for a significant ease when maneuvering patient information; reliability, usability, and layout of the content is a problem. The reliability of the Electron Medical Record is questioned because the platform experiences unpredictability and goes offline under certain instances. This unpredictability not only can create bottlenecks. Bottlenecks are what cause waiting rooms to have back-ups. Another example as well is beds that are unavailable to patients, and time crunches. Bottlenecks can also cause patients to have their information processed because of delays.
From unpredictability, time crunches can become a central problem; which can cause patients to have delayed check-outs, and cause back-ups for doctors and clinicians when entering patient information into the Electronic Health Record.

As the Electronic Medical Records continue to become an intricate part of the patient-provider hospital experience, perfecting the Electronic Health Record and its continuity and efficiency must be mastered for the benefit of the workflow of the facility and for the security of patient's information.

INTRODUCTION

Much iteration of Electronic Health Records have been developed, tested, and utilized by clinical providers. These differing Electronic Health Records all have different focuses and medical tasks that they wish to improve upon. Improvements can be made in the area of quality and adding value, such as; increasing the readiness of deliverables, decreasing the amount of clicks that occur within a given task, and diminishing the content that does not service the patient.

An e-prescribing interface is an example of a modern system that allows providers to safely input orders for patients. Benefits of e-prescribing are; more cost-effective medication options for patients, and improvements in error resolution.
Just as there are successes with Electronic Health Records, there are also nuances that have not been solved. For instance Electronic Health Records have, been labeled difficult because in different healthcare settings,

clinicians may have to learn the new Electronic Health Records systems for a designated department. This costs great amounts of funding as clinicians have to be trained on how to operate and function within the new system.

Another concern of the design of current and modern Electronic Health Records is that they are not necessarily acceptable to "care" as much as they are to "care transactions." This essentially means that some Electronic Health Records do not put the health and wellness of the patient as a top priority as much as it puts the sending and receiving of daily deliverables.

Some findings in Research have questioned the functionality of Electronic Health Records based on the formatting and layout of the content on the interfaces of the platforms. The research that has been completed on this study has not compared or contrasted the options of different interfaces.

Electronic Health Records have a great deal of support from all demographics of the population. Healthcare organizations as well as government agencies have endorsed the implementation of Electronic Health Records. According to Vest (2011), "As stated by the President's Council of Advisors on Science and Technology, Data exchange and aggregation are central to realizing the potential benefits of health IT." The parties mentioned view Electronic Health Records as a "game-changer" or a model that can transform the process flow of healthcare. Electronic Health Records have the potential to decrease waiting time, allow clinicians to interact with patients at an efficient level, expedite the check-in process for patients , as well as check-out patients in an efficient manner.

For the potential to be seen as changing in the near future, some common issues must be addressed, which include but are not limited to; lack of standardization and password fatigue. Standardization can save hospital facilities a great amount of funding as clinicians will not have to be trained to operate other interferes from the departments. Instead, all clinicians will be fully capable and cross-trained in the development of the Electronic Health Record. Password fatigue is an issue that plagues clinicians. Within most Electronic Health Records interfaces, clinicians have to put in two or more passwords to reach the portal for their network. This causes a pro-longed clinician-patient experience that is unwarranted for all parties involved.

The purpose of the research that has been conducted is to make the navigation of Electronic Health Records more efficient. Efficiency can be reached in the areas of; loading and completion speed, the reception time of deliverables, the display of the content, the reliability and accessibility of information that is inputted and the reliability of the network that enables the Electronic Health Records.

METHODS

In an effort to develop an Electronic Health Record that is able to achieve a consistent and high level of efficiency and quality, researchers have been known to use Lean principles that have the capability to eliminate waste and non-value added properties. Lean has made its high profile of usage in the manufacturing industry, but still has a success that has yet to be reached in the medical field. For our procedure, we have utilized CogTool software, which enables the Lean principles by taking the time of a simulated user completing a task that is identical to that of a real provider or clinician. Completing these simulations gives a benchmark of what margin of time the tasks should be completed within.

To be specific, we will develop an Electronic Health Record that will model an Electronic Health Record that is called CPRS (Computerized Patient Record System).
To build our model Electronic Health Record system, we must first download CogTool. Once CogTool is downloaded we list all the process that is within the CPRS into our CogTool model. For example, CPRS allows clinicians and providers to complete consults, medication orders, and enter notes on patients. So in our

CogTool model, if we wanted to simulate these tasks, we would input into the new project that we have created. After listing the processes in our new project, we must record and enter the steps for the tasks that we want to simulate in CogTool. Next we must identify the tasks that we will perform in the CogTool design board. Analyzing the steps of each task and process is the next step. Analyzing includes; viewing the amount of clicks per some unit of time, and other key strokes.

These steps are completed in an effort to create a standard that will reduce time for the same task in CPRS, but in CogTool a lesser completed time will be achieved for the same given task.

Allow the task to run in CogTool. Using Windows Snap Shot we capture the images of the screen. Capture enough screen-shots to convert them into frames to build a storyboard. The storyboard will give the research the validity to demonstrate the manner of efficiency in which the tasks could potentially be running. Align all the screen-shots in the chronological manner that they will occur. To run the simulated task, pick the first aligned frame from the storyboard and press "start demonstrating." The next step is to press compute, and you will be given the simulated time for in which it should take a clinician or provider to complete the task.
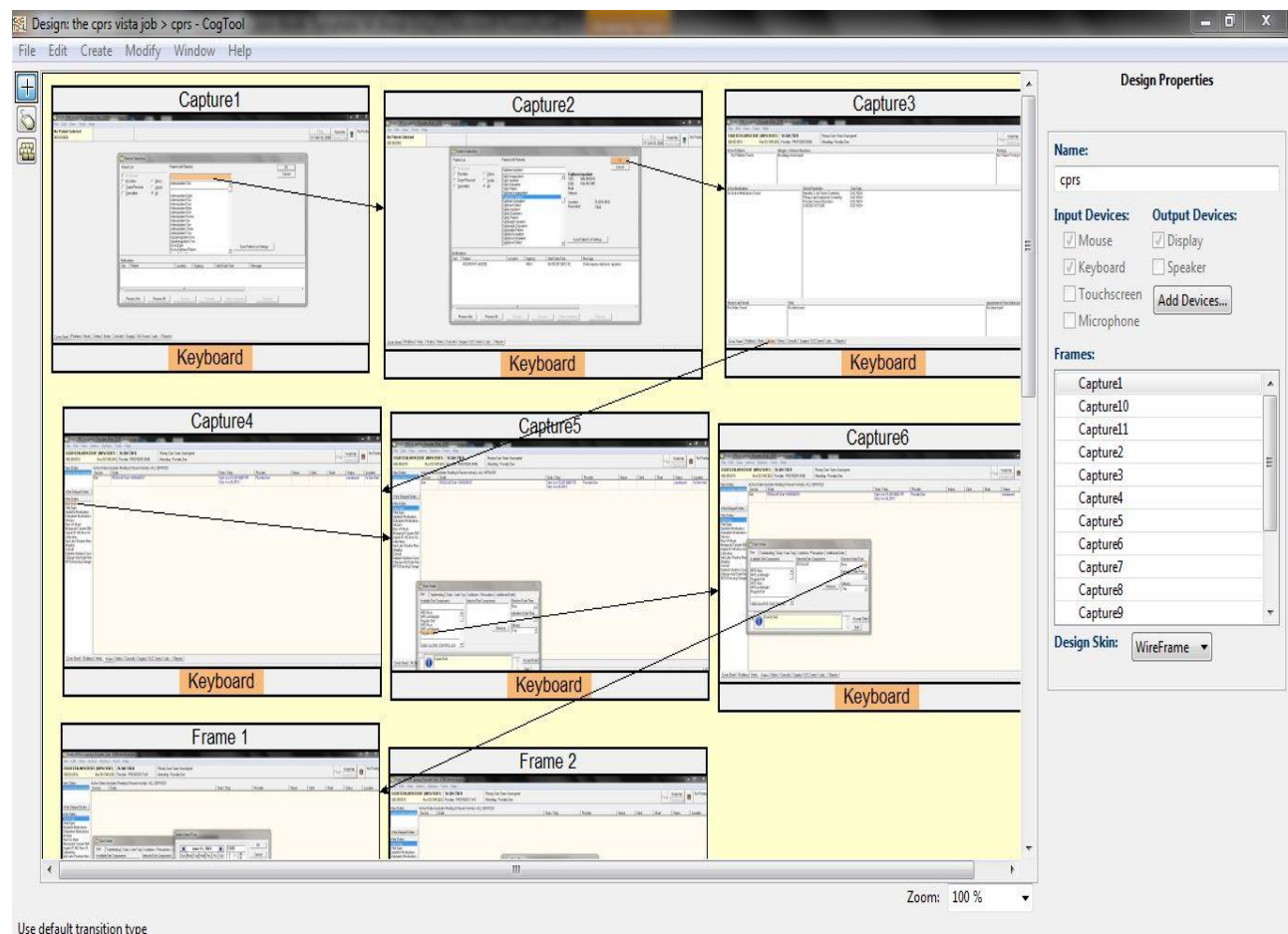
Figure 1. Above is the model storyboard that has been created using CogTool.

RESULTS

Our results follow the formal expectations of our processing and implementation. Results were taken before implementing the Lean principals and results were also taken after implementing Lean principals. The results

from CogTool are theoretical and do not contain the human error factor that occurs daily in the Electronic Health Records platform.

Table 1

Tasks perform.	Time
Writing a diet order	28.8s
Implementing a new problem for a patient.	22.7s
Setting an appointment for a patient.	27.3

The table above shows the time, in seconds, that it would take a provider to complete the given task on a daily basis within an Electronic Health Record platform. The left column displays the task that is being completed. The right column displays the time in which the task has been completed in. This given table demonstrates the results that occur when Lean principals have not been implemented into the Electronic Health Record. Therefore the times of completion showcase inefficiencies within the system and within the user. Whether the inefficiencies occur because of fatigue or lack of knowledge on the part of the user, or whether it be on the unresponsiveness of the systems' interface is unbeknownst. The results do allow us to know that inefficiency does occur.

Table 2

Tasks perform.	Time
Writing a diet order	21.3
Implementing a new problem for a patient.	18.6
Setting an appointment for a patient.	19.6

The table above displays the results that would occur theoretically, utilizing CogTool. The left column displays the tasks that will be simulated in CogTool, while the right column displays the time that it takes to complete the task on our model Electronic Health Record platform. In every task, the time decreased for the model Electronic Health Record that was developed through CogTool. This allows us to know that improvement can be achieved for the Electronic Health Record.

CONCLUSION

The results display that there is great potential to improve the efficiency of the Electronic Health Record. The next method of research is to utilize Lean principals and techniques to examine and identify where the lags and inefficiencies in the system occur. If the CogTool model contained Lean principals and techniques, then the times in table2 would be even lower, which would allow for an even greater Electronic Health Record System. The inefficiencies could be contributed to the unresponsiveness of the interface, or the human err of the provider or clinician. The next steps would be to identify these inefficiencies and diminish them to achieve a timely and efficient Electronic Health Record System.

REFERENCES

- Middleton, B., Bloomrosen, M. (2013). Enhancing Patient Safety and Quality of Care by Improving the Usability of Electronic Health Record Systems. AMIA.
  http://www.jamia.bmj.com

- Vest, John R., Japerson, J. (2011). How are Health Professionals Using Health Information Exchange Systems? Measuring Usage for Evaluation and System Improvement. Springer.

MOBILE APPLICATION DEVELOPMENT WITH ROUTE PLOTTING AND SERVER INTERACTIONS

By Ken Thomas
Major: Electrical Engineering
Mentor: Dr. Cheng-Zhong Xu, Department of Electrical Engineering

ABSTRACT

Public transportation is an important aspect of any major city. Taxis play a vital role in a city's public transportation, because they are able to take passengers directly to their final destination. Unfortunately many places have found that when a person unfamiliar with the area rides in a taxi, the driver will intentionally drive out of the way in order to increase the fare. In this paper, the creation of a mobile application to mitigate the problem will be discussed, and how it is to be used. This application will take information from the taxi's receipt. In order to accomplish this, image processing is run on an image of the receipt, or a user may manually enter it. The application then shows the route taken as well as an ideal route based on current traffic conditions. To determine the taxi's actual route, the application sends a request to a servlet that responds with the GPS data for that trip. The ideal route is found by a function that uses the first and last locations of the GPS data as inputs. This application will give the user the ability to see the route that was taken and whether or not the taxi went the proper way to the final location. This application may be integrated into an existing taxi service application to make it more robust. This application, as well as the one it may be integrated into, has the ability to be applied to any major city for a variety of public transportation means. This mobile application was written in Java for Android Operating System, and uses Google Maps API v2.

INTRODUCTION

Creating the Taxi Receipt Image Processing Application (Name Subject to Change) will require the collaboration of several functions. Each function must be able to operate within the other functions, access data from a server and access the data that was generated in another function. The main functions for this application will include accepting/reading the data that is input, sending that data to the server, receiving data from the server, manipulating the data that is received, and lastly plotting the points and connecting them on the map. Each of these functions can be created independently and later implemented as a whole.

Taxi Receipt Image Processing Application (Name Subject to Change) has three main parts. First is the taxi data acquisition. This will take the taxi receipt and get the information required to find a unique taxi ride. This is the start time, date and taxi license plate number for the ride. The next part of the program takes the data found in the first part, sends it to a servlet, and receives data on the taxi's route as well as an ideal route based on traffic conditions at the time of the trip. The third part of the program takes the route data and plots it on a map.

With these three main parts, our application is able to allow users to look at the taxi ride they took and compare it to an ideal route that could have been taken.

MOTIVATION AND RELATED WORKS

A group that works at the Shenzhen Institute of Advanced Technology (SIAT) has been working on an application that finds taxis relative to the user's location. This application has several purposes for the people

in Shenzhen, China. This application gives the user the ability to track the location of taxis by a Global Positioning System (GPS) coordinate set, book a taxi to their current location, and determine legitimacy of a taxi. This application was made in order to alleviate some of the problems surrounding taxis in Shenzhen.

The city had many issues with the taxi drivers in recent history so it is with a great need that an application like this was to be designed. One of the problems is finding a taxi. Although Shenzhen has many taxis, it is a very big city. Some areas of the city does not have high taxi traffic. In addition, the process of booking a taxi is somewhat cumbersome. First one must call a third party booking agency which takes the location and destination of the caller. The booking agency then looks for taxis relatively close to the starting point and calls all of the individually until one agrees to pick up the caller. In addition, there are many taxis in the city of Shenzhen that are not registered. This means that these taxis may have higher rates, unlicensed drivers, and be dangerous to riders. There have been cases of unregistered taxis picking up people, driving somewhere remote and robbing the rider.

By allowing users to see all registered taxis in the area, SIAT's application helps users bypass the incommodious booking process, as well as avoid unregistered taxis. This application also allows users to send GPS data of the starting and ending point of a desired ride. This allows the third party booking agency to find cars in the area and relay information quickly, making the booking process more efficient. There is also a function which allows users to choose a specific taxi in the immediate area, and call then directly, again bypassing the booking process. Lastly there is also a search function so one can quickly check if a taxi is registered, which serves to protect the user from potentially dangerous taxi rides.

While SIAT's application helps the problems related to taxis immensely, one problem is overlooked. A common problem for taxis in Shenzhen is taking extended routes in order to increase fair when a rider is unfamiliar with the area. This is the problem that Taxi Receipt Image Processing Application (Name Subject to Change) is to address. By making an application that allows users to compare routes taken to ideal routes and report incidents of fraud to the Transportation Department, this problem will also be alleviated.

TAXI RECEIPT IMAGE PROCESSING APPLICATION (NAME SUBJECT TO CHANGE)

As previously stated, this application's function is to have a picture of a Taxi's receipt analyzed. Then, with data found on the receipt, the application will query the server at SIAT for Taxi GPS data and an Ideal Route. Using the GPS data and ideal route, the application will pull up a street map of the route taken and ideal route.

The application needed three different data collection techniques which would then lead to the map and route plots: taking new pictures and processing the image, loading old pictures and processing the image, and text entry boxes. The taking of new pictures is required so the user does not need to take a picture before opening the application in order to use the Image Processing and get the routes plotted. The loading of an old picture is essential in case a user disposed of a previous receipt and is no longer able to take new pictures. The text entry boxes are required in order to have a failsafe available. If the receipt is too damaged to get a picture the Image Processing can read, the user can still look at the routes taken. With all of these data collection methods the user should be able to input the data from the receipt as long as it is somehow available.

The architecture of this application is a main menu with three buttons: "Take New Picture", "Load Picture" and "Manual Entry". Each of these buttons will take the user to one of the data collection methods. After the data collection methods have succeed in getting the data from the taxi receipt, the application sends two queries to the SIAT servers. The first gets the taxi's GPS data, and the second gets the ideal route based on the starting and ending position of the taxi ride. Once the data is collected from the server, the application opens the street map of Shenzhen and uses the collected data to plot the taxi's actual route and the calculated ideal route. Google Maps API v.2 was chosen as the map used for this application. It was chosen because Google

Maps is commonly used in Android devices, it works with the information we have available, and the coding for it is done in the same language as the rest of the application development.

DATA COLLECTION TECHNIQUE

As stated above, the three data collection techniques are taking new pictures and processing the image, loading old pictures and processing the image, and text entry boxes.

The most important is the taking of new pictures. This allows the user to skip the tedious possibility of manual text entry and using another application to take a picture to use in this application. While it is possible to take a picture using a basic camera intent, which calls the phone's default camera application to take a photo, the images from the basic camera application can vary too much to reliably process. This made the development of a custom camera application necessary. The custom application, seen in Figure 1, uses the built-in auto-focus function in order to ensure that the text will be readable. In addition a semi-transparent black overlay was placed over the majority of the screen and text instructing the user exactly how to place the receipt in the picture. These custom additions ensure that the image processing will be able to find the characters it is looking for more reliably.
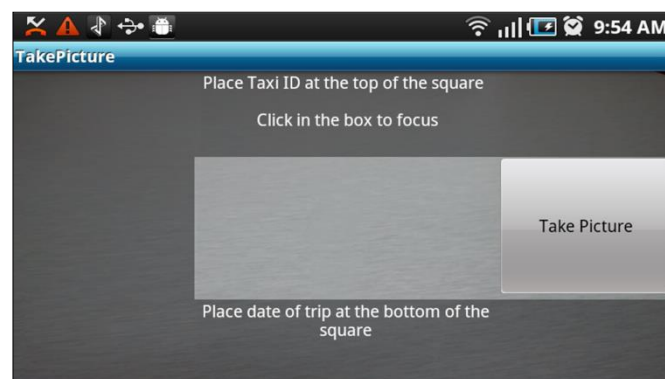
Figure 1. Image capture of the "Take Picture"
function

The other two data collection techniques are simpler. The Load Image option, seen in Figure 3 on the next page, is simply a text box that instructs the user to pick an image of the receipt and a button that says "Load Image". When the button is pressed the main directory for pictures in the phone will open and the user will need to locate the picture of the taxi receipt they want to use. Once the picture is selected, it is sent to the application for image processing. The manual data entry, as seen in Figure 2 of the Figures section, is a series of Text boxes and Edit texts that instruct the user to manually type in the taxi's license plate number, the date of the ride, and the start time of the ride.
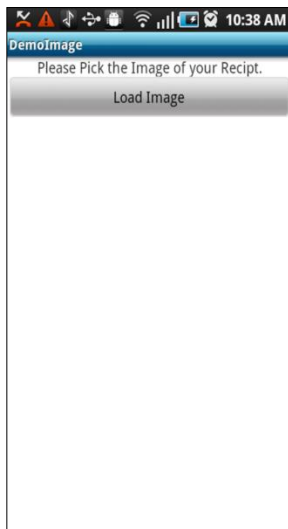
Figure 3. Image capture
of the "Load Image"
function.
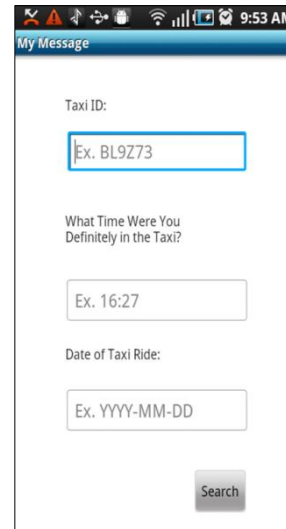
Figure 2. Image capture
of the "Manual Entry"
function.

These three methods are   able to find
the information from the taxi receipt needed to move onto the next part of the application, the query to the
server. It should be mentioned that the image processing function is completed, but not yet integrated into the
application.

GENERATING AND ANALYZING A REQUEST TO THE SERVER

Once the data collection techniques find the necessary data, two requests to SIAT's server are sent. The first
request to the server is sent using the information collected in the data collection methods. This returns a
JSONObject, a class created by the Cloud Computing and Mobile Development Team at SIAT, contains a lot
of information on the taxi ride. The only information currently used is the GPS data, which is saved as a long
string. From this long string we get the first and last GPS points and query the server again. This time the
server returns another JSONObject that contains GPS data can be used to find an ideal path from the starting
GPS point to the ending GPS point based on current traffic conditions, which is again saved as a long string.

These long strings are first separated into an array of string values, each containing a longitude and latitude
point. These longitude and latitude points are used to create the Polyline, a built in Google Maps API class,
that will later overlay the map. We define two Polylines, one for each array of string values. Then, going
through each string array one value at a time, the string containing a longitude and latitude point is split and
converted into numerical values. Unfortunately, because of inconsistencies in Google Maps in China, the road
map and the satellite map do not overlay perfectly. This means that our GPS data is somewhat skewed.
However, because we are only dealing with a relatively small area it was possible to make manual
measurements of how skewed the GPS points are and average it throughout the city of Shenzhen. This
resulted in a constant value to add to the Latitude or longitude values given by the JSONObject. These
modified numerical values are then used to create a LngLat point, another built-in Google Maps API class,
and added to the corresponding Polyline. The program also keeps track of the highest and lowest point used
for both latitude and longitude. These points are used to create two LngLat points at the most southwest and
northeast locations. These are then used to create a bound for the map. The two Polylines and the bound are
then sent to a map object for the application to show.

EMPLOYING THE MAP AND PLOTTING THE ROUTES

The last step for this application is to use the Polylines and bounds sent to the map object to plot the routes on the map. However there is a slight barrier to overcome before using Google Maps. Before a Google Map can even be opened in an application, an access key must be obtained for mobile applications. A new key obtained for each application made.

Once all permission issues are settled the map can be opened. When the map is being created we use the bounds as an input so it opens directly to the location that contains both routes but is not zoomed out too far.

Figure 4. Image capture of
the Polylines showing the
taxi routes.

After the map is placed, the Polylines can be overlaid on the map, as seen in Figure 4 below. The Polylines were given different colors and a 50% transparency so that any overlap between the two would be a mixture of the two colors. For example, if the red for the actual route and blue for the ideal route overlapped a purple route would be seen.

CONCLUSION

Taxi Receipt Image Processing Application (Name Subject to Change) was created to solve one of the problems previously ignored by the application created by SIAT. This problem is taxi drivers purposefully taking long routes in order to increase fair. It is accomplished by allowing the user to view their path taken against a computer generated ideal route based on traffic conditions. The application does this by allowing the user to upload information in one of three ways: taking a new photo, loading a photo, or manually entering the information. If the user chooses to get the information via a photo, image processing takes finds the required data and sends it to the server. The server responds with information that can be used in Google Maps API v2 to plot both routes. Once fully completed, the Taxi Receipt Image Processing Application (Name Subject to Change) will be integrated into the application created by SIAT to form a more robust application.

FUTURE WORK

There is still more work to be done before this application is ready for commercialization. The following tasks should be completed:

- The Image Processing that was developed by another group must be integrated into the existing application.
- The Ideal Route query to the server should give an ideal route based on traffic conditions at the start time of the Taxi, not the time queried.
- A rating system should be implemented, where users are able to give drivers a rating based on their experience for other users and future rides.
- The application should be slightly modified to be more esthetically pleasing.

THE DESIGN OF REALITY GAMES: THE LAND BRIDGE GAME DESIGN PROJECT

By David Warnke
Major: Computer Science
Mentor: Dr. Robert G. Reynolds, Department of Computer Science

ABSTRACT

The Alpena-Amberley Ridge is an ancient land bridge that divided Lake Huron into two smaller lakes, and connected Michigan's Lower Peninsula with Ontario. The Land Bridge was above lake level from approximately 10,000 to 7,500BP. A team of Archaeologists and Engineers from the University of Michigan-Ann Arbor under the direction of Dr. John O'Shea discovered ancient artifacts on this land bridge left behind by hunter-gatherer societies that hunted caribou migrating across the bridge. However, searching a vast underwater area for possible sites was not feasible. Therefore, Dr. Reynolds and a group of his students from the Artificial Intelligence Laboratory at Wayne State University have designed a virtual world model of what the Land Bridge might have looked like at the time of these ancient hunters. They modeled ancient caribou herds and generated predicted migration pathways across the Land Bridge using an A* optimal path planning algorithm. These pathways were then used to predict "hot spots" or locations where the best hunting locations would be, based upon caribou migration behavior. This method had some success. Two of the predicted sites were checked and both were found to yield material remains. However, there were artifacts discovered at locations that were not predicted to be "hot spots" as well.

The hypothesis tested here is that the addition of a machine learning algorithm, specifically Cultural Algorithms, will lead to even greater success in predicting hunting "hot spots". This is because the Cultural Algorithm is able to model the decisions by herds of caribou with regards to the selection of migration paths using cognitive knowledge taken from the experience of simulated caribou and encoded as influence maps..

Our simulated results demonstrate the advantages of using a group-based approach. In particular, we suggest that there are areas on the land bridge that are attractive to herds coming from various directions. These confluences are particularly interesting in terms of the possibility of larger-scale human occupations that might be associated with them.

INTRODUCTION

The Alpena-Amberley Ridge is a natural land-bridge connecting Michigan's Lower Peninsula with Ontario. From 10,000 to 7,000 B.P. the water levels were low enough for the land bridge to be above water, separating Lake Huron into two lakes. This enabled caribou to cross the land bridge during their spring and fall migrations. Ancient hunter-gatherers would set up hunting blinds along the bridge in order to hunt the caribou. Most of the remnants of these civilizations have been destroyed due to weather and modern development, however the land-bridge has been underwater for almost 10,000 years, and the water has preserved much of the hunting sites and artifacts of these ancient peoples. The period of time that the land-bridge was exposed represents a critical turning point in human history when people began to stray from hunting and gathering to fishing and agriculture. Artifacts such as spears and arrowheads can help anthropologists understand this transition better.

The National Oceanic and Atmospheric Administration (NOAA) produced a bathymetry map of the bottom of Lake Huron shown in Figure 1. Dr. John O'Shea, a Professor in the University of Michigan's Museum of Anthropology, discovered archaeological remains on the submerged land-bridge in 2009. What he found resembled the types of structures that modern caribou hunters use, hunting blinds and drive lanes. There are two types of hunting blinds, V shaped blinds and simple closed blinds which can be seen in Figure 2. V shaped blinds point in a particular direction while simple closed blinds encircle the hunters allowing them to hide in any direction. Evidence for another structure, the drive lane, used by modern caribou hunters was found as well. A drive lane is a combination of rocks or other debris that act as a fence-like barrier to guide caribou in a particular direction.
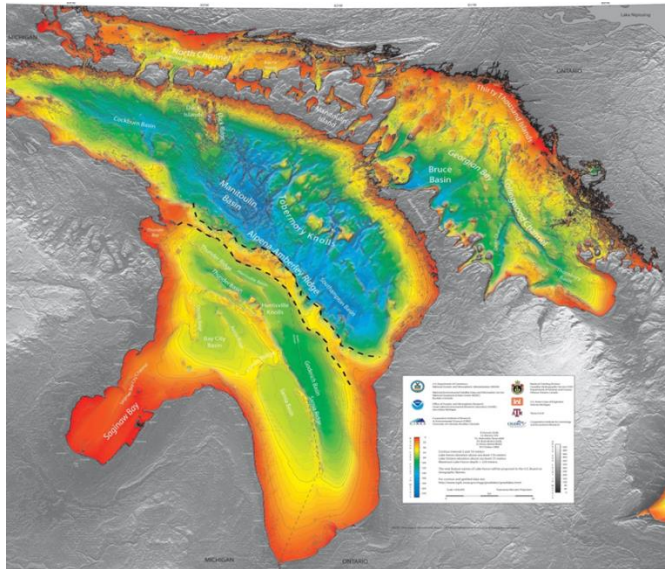

Figure 1: Bathymetry Map of Lake Huron: The Alpena-Amberley Ridge is Between the Dotted Lines

Figure 2: Left: Simple Closed Blind, Right: V Blind

Although the preliminary findings were tantalizing, the task of searching the overall area for other occupational remains was daunting. In order to expedite the search process, Dr. Robert G. Reynolds and a

team of graduate students in the Artificial Intelligence Laboratory at Wayne State University were called in to create a computer model of the Land-Bridge. Next, they developed models of individual caribou and caribou herd behavior that were to be used to predict herd movement across the ancient landscape. The idea was then to use this herd movement information to predict hunting blind locations.

Kevin Vitale designed the original program and used Cultural Algorithms to implement a kinematic or movement algorithm for caribou herds . This allowed the individual caribou to move together as herds in the landscape with herd size and shape changing as individuals moved from one herd to another. [1]

Next, James Fogarty implemented an A* optimal path-finding algorithm to produce a path optimized relative to certain herd goals. These goals were evaluated by using influence maps for terrain traversal and vegetation content. Euclidean distance was used as a heuristic. He then used Cultural Algorithms, a socially motivated evolutionary learning tool, to simulate a flocking behavior. The Cultural Algorithm collected information such as, distance to herd, distance to closest caribou, and herd direction based upon the cognitive experience of the caribous. It also used the kinematic developed by Vitale. First a path was generated based upon herd goals. Next the actual traversal of the path was simulated using the Cultural Algorithm. [2]

Jin Jin extended the A* approach by using Cultural Algorithms to evolve the value that caribou herds placed on various A* components. Both of Fogarty's influence maps, as well as the heuristic were given weights, and The Cultural Algorithm evolved optimal weights. This allowed the caribou to decide the level of importance that food was to them and go graze during their journey, instead of just running straight at the final goal. This version of the A* algorithm is what is currently supported by the virtual world design by Thomas Palazzolo and Gerald Larsen seen in figure 3. [3]

Figure 3: Land Bridge Game

The next step was to use information about simulated herd movement to predict where various occupational and hunting site remains might be located. S. Dustin Stanley then used Cultural Algorithms to predict the

location of hunting blinds using herd behavior produced by the A* algorithm alone without the use of Cultural Algorithms. This was viewed as a baseline for a comparison with the Cultural Algorithm generated results. These "hot spots" were then given to the archaeologists to guide their search. Subsequently they found remains at two of the predicted sites. In addition remains were discovered at sites not predicted to be "hot spots" by A* alone. This suggested that the use of the Cultural Algorithm guided A* might be able to expend on these baseline results. [4]

In this study we then employed a Cultural Algorithm to evolve optimal paths for the caribou herds. As before Cultural Algorithms were then used to extract "hot spots" for settlement. We then compared the "hot spots" produced by both approaches. The use of the Cultural Algorithms allowed us to identify confluences or overlaps in herd movement based upon shared cognitive information that was produced through the use of the influence maps.

METHODS

Reality Game Framework:

Game design is based on a pyramidal structure where each layer overlays the previous layer seen in figure 4. The bottom of the pyramid consists of the geometry of the game. In our case the geometry is created by using the data points collected from NOAA, and generating a landscape based on those data points. The land is then smoothed and water is added at the base water level. The next layer is physics. In our program simple gravity is implemented and water is dropped on top of the land directed by that gravity to create ponds. The resultant water levels then determine where certain types of vegetation can grow. On top of that is the bio mechanics layer. In our program caribou herds are added to the landscape, and interact with it by walking along the ground, where the gravity keeps them. And the top layer is behavior. This is where we implement A*, Cultural Algorithms and other algorithms that determine what motivates the various agents in the game as well as how they interact with each other.

Figure 4: Game Programming Pyramid Scheme

Cultural Algorithm Framework:

Cultural Algorithms, created by Reynolds, is an evolutionary algorithm that is based on Genetic Algorithms. Like Genetic Algorithms there is a population space, but there is also an additional component named the belief space. These two influence each other through an interaction protocol, which consists of an influence function and an acceptance function, whereby the two evolve together to create agents which excel at completing the given task. Figure five provides a graphical representation.
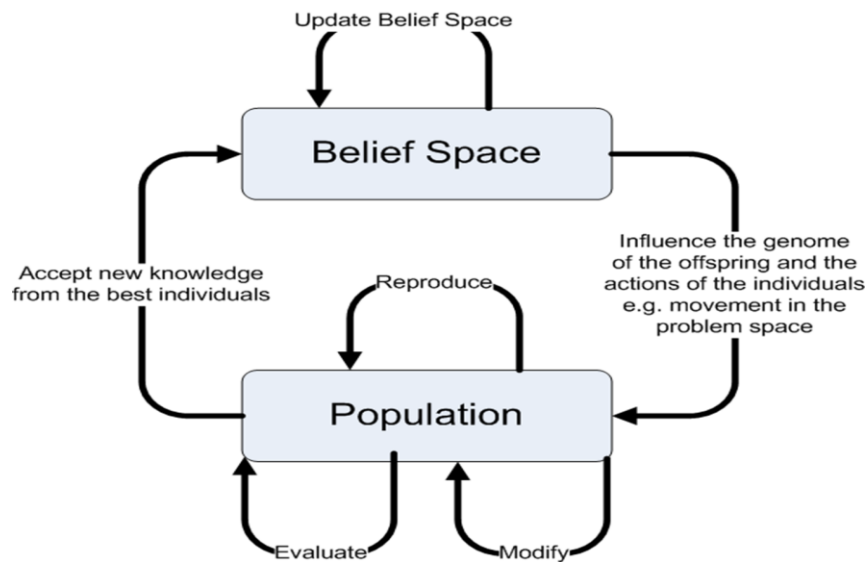
Figure 5: Cultural Algorithms

The population space consists of the agents that make up the population. Each Agent contains a genome that contains malleable information about how to solve a problem. The population reproduces and can evaluate and modify their genome on each successive generation.

The belief space consists of the shared knowledge of the population and represents culture. There are five types of knowledge types that can be represented in the belief space: normative knowledge determines the range of parameter values; situational knowledge stores the values of the best fit agents from the population; domain knowledge contains information about the problem space; historical knowledge keeps track of values in the search space determined at run-time; and topographical knowledge contains information about the geometry of the search space.

The Acceptance function determines which agents are used, and how their knowledge is used, to update the belief space. The Influence function determines what knowledge is used to influence the next generation of the population.

The pseudocode for Cultural Algorithms is as follows…

    Begin

        t = 0

        InitPop(t)   // initialize population

        InitBelief(t)   // initialize belief space

        Repeat

                EvaluatePop(t)

Vote(Belief(t), Accept(Pop(t)))

Adjust(Belief(t))

Evolve(Pop(t), Influence(Belief(t)))

t++

Select Pop(t) from Pop(t − 1)

Until (termination condition)

End

Generating Optimal Caribou Migration Paths:

The path-planning used by Stanley was a simple A* algorithm. The heuristic function was admissible, and based on Euclidean distance, so it was guaranteed to produce an optimal path. However, it is difficult to decide what optimal caribou behavior is. The cost function used two influence maps, ease of traversal and vegetation nutrition. There were no weights used on any of the functions so the algorithm simply valued getting to the destination as fast as possible.

Jin updated the path-planning to allow weights on all of the functions. He also made the vegetation map negative so that it was more appealing to the caribou. Equation 1 shows the total value of a cell in Jin Jin's A* formula. These changes allowed the caribou to seek out food instead of just finding the easiest path to the destination. Jin Jin then used Cultural Algorithms to calculate which weight values produced the best outcome.

$$= EuclidianDistance * finalGoalWeight$$
$$+ \left(\sum_{i=0}^{n-1} movementvalue_i + g_i * geometryWeight \right) + (movementvalue_n + g_n$$
$$* geometryWeight - v_n * foodWeight)$$

$$movementvalue = \begin{cases} 1.0000 & \text{if move in the normal direction} \\ 1.4142 & \text{if move in the diagonal direction} \end{cases}$$

Equation 1: Jin A* formula for total cell score with weighted functions

The population space in this case is a set of caribou herds, where each herd is an agent in the population. Each herd is represented by a chromosome that has one gene for each of the three weights distanceWeight, foodWeight, and finalGoalWeight.

The acceptance function in this case decides which herd does the best according to the fitness function:
score of the herd = total nutrition value – total topographical effort.

Equation 2: Jin Cultural Algorithms Fitness Function

The function then sends the values of the weights determined in the genome to the belief space.

The belief space is the combined knowledge of the caribou herds and the best genomes. The normative knowledge sets the range that the weights contained in the genome can take. The top 20% of genomes from each population are stored to the situational knowledge via the acceptance function. The domain knowledge is represented in the influence maps, which consist of the vegetation map, and the topographical map; topographical knowledge is contained in the topographical map as well; the historical knowledge modifies the influence maps during run-time. Each of these knowledge sources is updated according to the update function which keeps them up to date as each generation makes changes to their genome and the influence maps.

The influence function is based on a roulette wheel approach. At each generation the roulette wheel is updated in order to give better performing sources more space on the wheel and poorer performing sources less space on the wheel. The wheel is spun for each agent in the new population, randomly choosing a source as its base point. The agents then influence their neighbors as well, to create variations in the gene pool.

Predicting Hunting Blind Locations:

Stanley ran one A* path repeatedly to test for hunting blind locations. He used Cultural Algorithms to test which hunting blinds were best suited for hunting caribou. Each agent in this population space is a chromosome for one hunting blind builder. The acceptance function evaluates the fitness of a hunting blind according to the following function:

$F(H) = -C1A1 + C2A2 + C3A3$ *(if H is above water), OR*

$F(H) = -\infty$ *(if H is underwater)*

Equation 3: Stanley Cultural Algorithms Fitness Function

In this function A1 is distance to closest caribou approach, A2 is the height above or below the closest caribou approach, and A3 is the distance to the nearest other hunting blind, and C1-C3 are constants set by Stanley as C1=-30, C2=50, and C3=8.

The belief space in this case represents the shared knowledge of the hunting blinds. It is implemented by incorporating a genome into each node in the search space. The belief space genome, and the population space chromosome work together to influence the algorithm, and create the following weight function.

$W(T) = W1B1 - W2B2 - W3B3 - Log10(W4B4) \mid (W1, W2, W3, W4 \geq 0)$

Equation 4: Stanley Belief Space Weight Function

In this function, each of B1-B4 is determined by the belief space genome where B1 is distance to closest caribou approach, B2 is the height above or below the closest caribou approach, and B3 is the distance to the nearest other hunting blind and B4 is the distance to the nearest underwater location. Each of W1-W4 is

determined by the population space chromosome. The influence function decides where an agent will build a hunting blind by evaluating each node in the search space for each agent according to the weight function.

Stanley then evaluated the search space, and produced a "heatmap" where the more times a hunting blind hit a particular coordinate in the search space the hotter that coordinate becomes. This produces a number of "hotspots" which prove to be good location to search for real hunting blinds and artifacts. Stanley's results yielded accurate predictions, however there were artifacts discovered at unpredicted sights as well.

Our method:

We modified the program, to allow Stanley's "heatmap" function to be run with multiple paths. We also set it up so that the "heatmap" could be ran with either A* or with the version of Jin Jin's Cultural Algorithms described earlier. We focused on the same area of the land bridge as Stanley, shown in Figure 6.
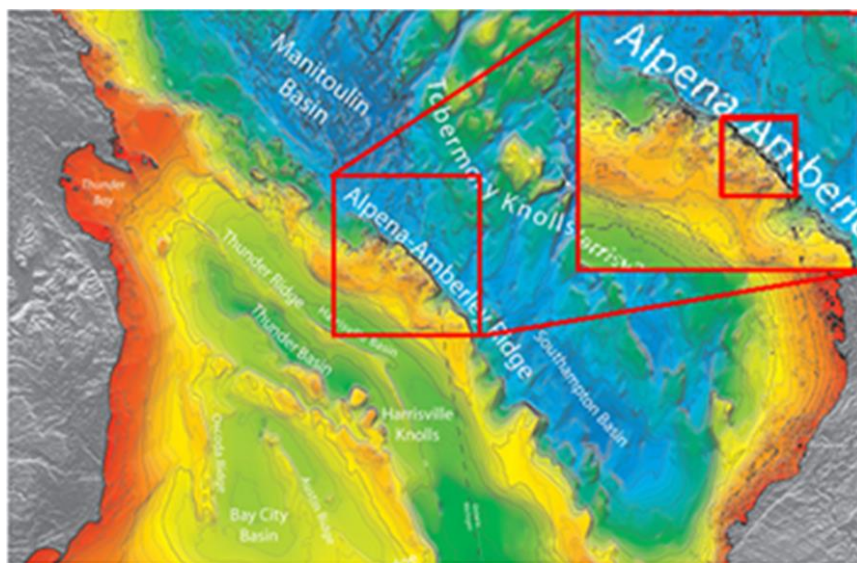
Figure 6: Search area used

We then set up two experimental runs which focused on the fall migration. This is due to the fact that the majority of the hunting blinds found were V-blinds facing the fall migration. In the first we ran Stanley's "hot spot" algorithm using 3 entry points to create a broader spectrum of analysis. In the second, we used the same entry points, but applied Jin's Cultural Algorithms path-planning algorithm instead of Fogarty's A* to better simulate caribou behavior. Due to the overhead involved in adding additional paths, we were not able to use the same level of detail in the search space, and were required to scale it down.

RESULTS/FINDINGS

Figure 7 shows Stanley's initial path relating to the movement of a herd coming in from the Northwest corner. Figure 8a shows our 3 A* paths and figure 8b shows our 3 Cultural Algorithms paths. The black dots in each represent current hunting blind locations. The red dot in each represents their goal. The reason our paths are larger is because our map is scaled down (as I mentioned earlier).
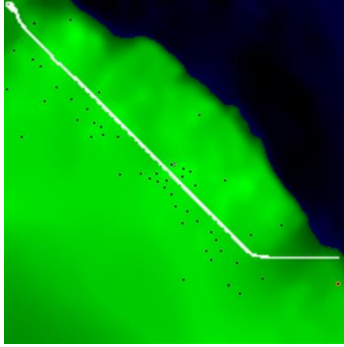
Figure 7: Stanley's one path
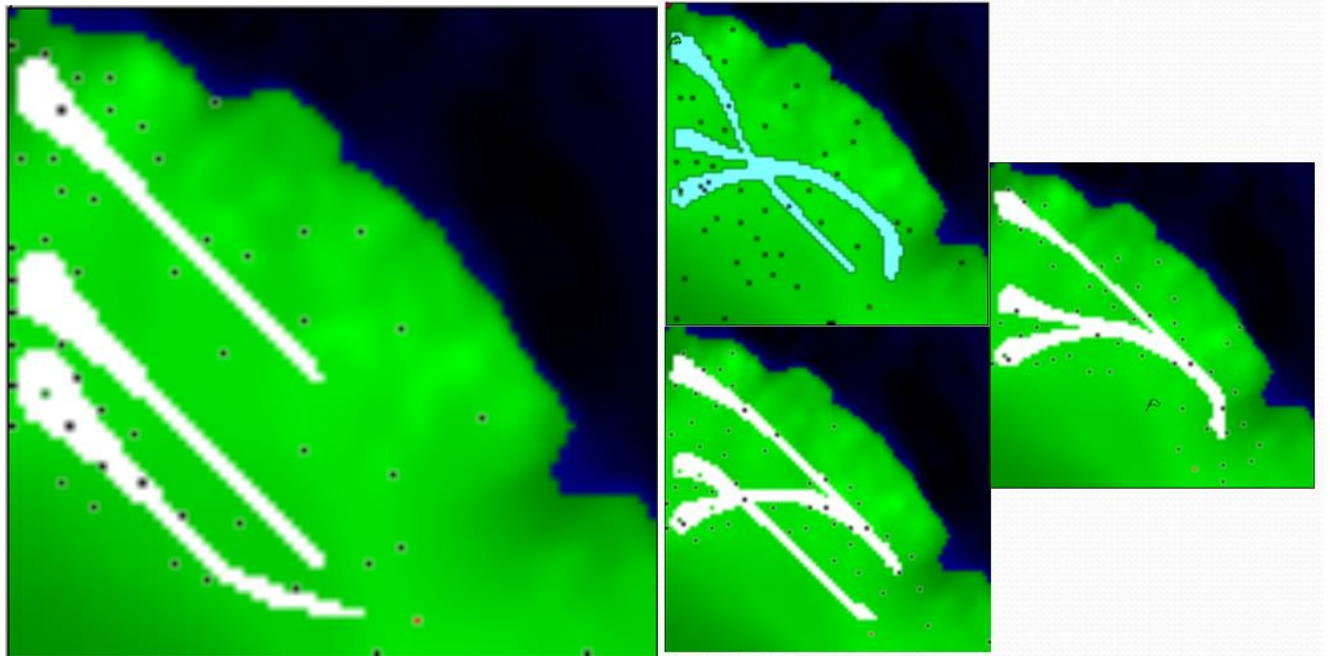
Figure 8 a: Our 3 A* paths **b:** 3 examples of the Cultural Algorithms runs

We can immediately see that our method produces a wider range of hunting blinds to the south and west of Stanley's. We can also see that the A* herds run in a straight line for their goal, however the Cultural Algorithms herds seem to have other interests. This shows how implementing Cultural Algorithms for path planning creates intelligent looking agents that have values, in this case food. We can also see a confluence of different paths and different points where the herds have a tendency towards confluence, which we call here, areas of confluences.

In figure 9 we see Stanley's "heatmap;" it is only the first quadrant which has been enlarged for visibility. In figure 10a we see our A* "heatmap," and in figure 10b we see our Cultural Algorithms "heatmap." In all three, yellow dots represent less hunting blind activity, and red dots represent more hunting blind activity. Ours contain more and larger data points because Stanley used a program, that we did not have access to, that evaluated a file produced by his algorithm. It essentially produces cleaner more concise results.

Figure 9: Stanley's "heatmap", 1st quadrant only
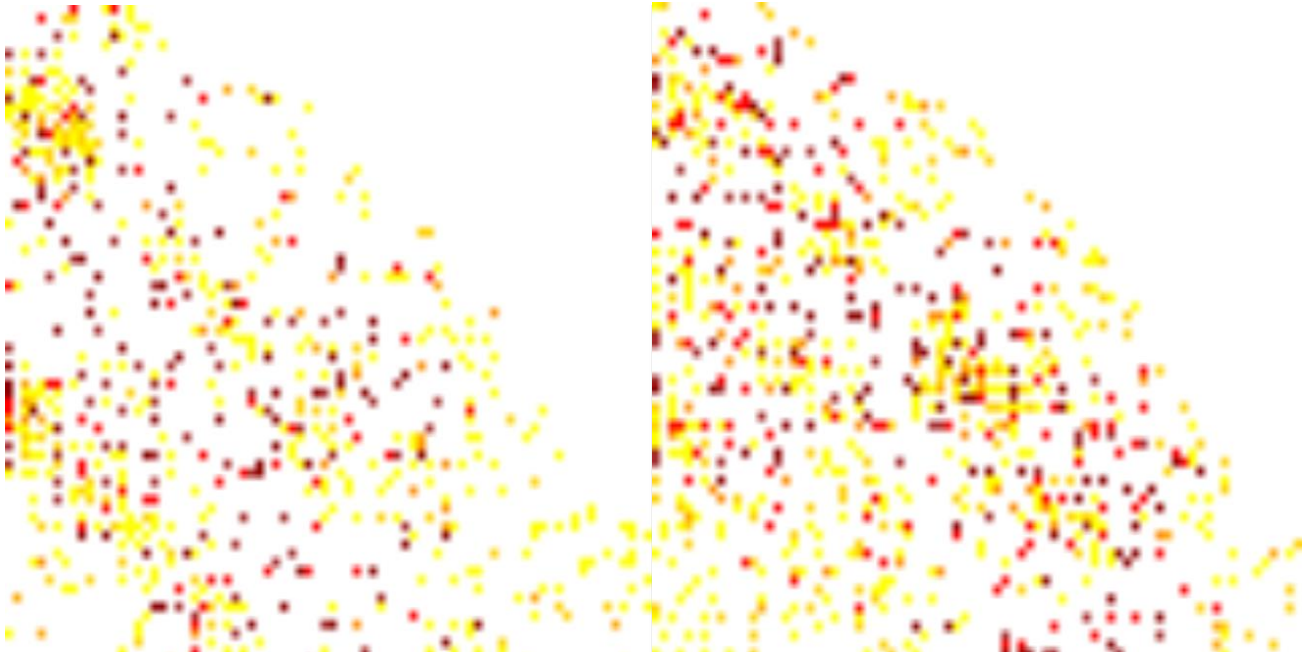
Figure 10 a: Our A* "heatmap" **b:** Our Cultural Algorithms "heatmap"

Although our maps contain far more data points, we can still see that our method creates a far greater tendency to produce "hotspots" to the South and West of Stanley's predictions. It is also interesting to note that the Cultural Algorithms approach produces more and hotter "hotspots" than the A* approach, and that these locations line up with the areas of confluence mentioned earlier.

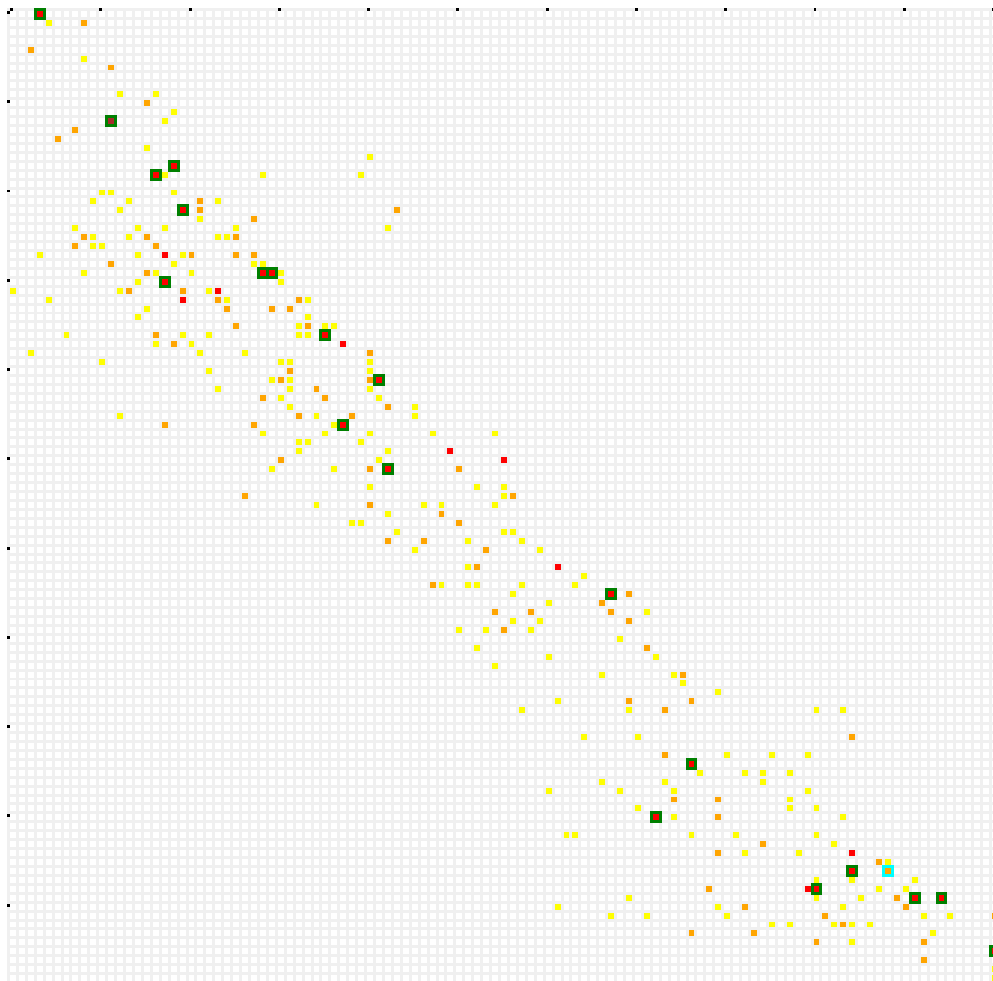Our three path - Cultural Algorithms approach produced hot spots in, or near, all of the locations that O'Shea discovered hunting blinds and artifacts so far including the original location found in 2009, the predicted locations by Stanley, and the locations Stanley did not predict.

DISCUSSIONS/CONCLUSIONS

By using more entry points we are able to collect a more expansive range of predictions across the search space. However, these predictions may have been inaccurate using the A* approach, due to the fact that the caribou do not seem to exhibit any intelligent behavior. By using Cultural Algorithms we are better able to predict the motivations of the caribou (they eat when they are hungry) and thus increase the accuracy of our hunting blind predictions.

Due to time constraints Stanley's "heatmap" analysis program was not used, the number of generations that Jin Jin's algorithm runs is currently only five and should be increased to at least 20, and the map used was scaled down and should be scaled back up. These could all be fixed in later work given enough time and computer memory.

We currently only implement a caribou herds desire to move easily across the terrain, and a desire for food. We could use the many-objective approach to caribou goal setting in order to add motivations such as: desire water, avoid dead caribou, avoid bugs (because they carry disease), avoid human smell, and many more.

REFERENCES

[1] Kevin Vitale, "Learning group behavior in games using Cultural Algorithms and the land bridge simulation example" (January 1, 2009). ETD Collection for Wayne State University. Paper AAI1470274. http://digitalcommons.wayne.edu/dissertations/AAI1470274

[2] Fogarty, James "Serious game modeling of caribou behavior across Lake Huron using cultural algorithms and influence maps" (January 1, 2011). *ETD Collection for Wayne State University.* Paper AAI1488884. http://digitalcommons.wayne.edu/dissertations/AAI1488884

[3] Jin, Jin (2011) "Path Planning in Reality Games Using Cultural Algorithm: The Land Bridge Example." *Wayne State University Thesis.*

[4] Stanley, S. Dustin (2013) "Path Planning in Reality Games Using Cultural Algorithm: The Land Bridge Example." *Wayne State University Thesis.*

ADDITIONAL BIBLIOGRAPHY

Ali, M., Reynolds, R. G. Embedding a social fabric component into cultural algorithms toolkit for an enhanced knowledge-drive engineering optimization. International Journal of Intelligent Computing and Cybernetics, 1, 4 (2008), 563-597.

Barth, Amy. "Top 100 Stories of 2009." Discover Magazine December 17th, 2009, Accessed October 22nd 2010 http://discovermagazine.com/2010/jan-feb/095

Benedict, J. B. Tundra Game Drives: An Arctic-Alpine Comparison, Arctic, Antarctic, and Alpine Research, Vol. 37, No. 4 (Nov., 2005), pp. 425-434).

Bergman, Carita M., Schaefer, J., and Luttich, S. Caribou Movement as a Correlated Random Walk. Oecologia, Vol 123, 3 (2000), 364-274.

Best, Christopher. Multi-Objective Cultural Algorithms. Master Thesis, Wayne State University, Detroit. (2009)

Bliss, L. C., Courtin, G. M., Pattie, D. L., Riewe, R. R., Whitefield, D. W. A., and Widden, P. Arctic Tundra Ecosystems. Annual Review of Ecology and Systematics, Vol 4 (1973), 359-399.

Chung, C. J., Reynolds, R. G. A testbed for solving optimization problems using cultural algorithms, Evolutionary Programming, 1996, pp. 225-236.

Cowling, S. A., Sykes, M. T., Bradshaw, R. H. W. Palaeovegetation-Model Comparisons, Climate Change and Tree Succession in Scandinavia over the past 1500 year, Journal of Ecology, Vol. 89, No. 2 (Apr., 2001), pp. 227-236)

Griffin, L. D. Proceedings: Mathematical, Physical and Engineering Sciences. Vol. 456, No. 2004 (Dec. 8, 2000), pp. 2995-3004).
Haupt, R. L., Haupt, S. E. Practical Genetic Algorithms. Wiley-Interscience, 2nd Edition, 1998.

Jain, A. Fundamentals of Digital Image Processing, Prentice-Hall, 1986, Chapter 7.

Jin, X., Reynolds, R. G. Using Knowledge-based evolutionary computation to solve nonlinear constraint optimization problems: a cultural algorithm approach. Proceedings of the 1999 Congress on Evolutionary Computation (1999), 1672-1678.

Lester, P. A* Pathfinding for Beginners. July, 2005.

Lewis, C. F. M., Heil Jr., C. W., Hubeny, J. B., King, J. W., Moore Jr., T. C., Rea, D. K. The Stanley unconformity in Lake Huron Basin, Journal of Paleolimnology, Vol. 9, 2004.

Lobao, A. S., Evangelista, B. P., Leal de Farias, J. A., Grootjans, R. Beginning XNA 3.0 Game Programming: From Novice to Professional, Apress, 1 Edition (2009).

Loiacono, D., Togelius, J., Lanzi, P. L., Kinnaird-Heether, L., Lucas, S. M., Simmerson, M., Perez, D., Reynolds, R. G., and Saez, Y. The WCCI 2008 Simulated Car Racing Competition.

McInnes, C. R. Velocity field path-planning for single and multiple unmanned aerial vehicles. The Aeronautical Journal, July 2003, pp 419-426.

Microsoft XNA Education Catalogue. June 30th, 2010. http://creators.xna.com/en-US/education/
Ochoa, A., Padilla, A., Gonzalez, S., Castro, A., and Hal, S. Improve a Game Board based on Cultural Algorithms. The International Journal of Virtual Reality, 2008, 7(2). pp. 41-46.

O'Shea, J. Ancient Hunters and the Lake Stanley Causeway: A Pilot Study. NSF High-Risk Grant #BCS-0829324, University of Michigan, Ann Arbor. (2008).

Pettit, C. J., Sheth, F., Harvey, W., and Cox, M. Building a 3D Object Library for Visualizing Landscape Futures. 18th World IMACS/MODSIM Congress, 2009.

Price, D. T., Halliwell, D. H., Apps, M. J., Peng, C. H. Adapting a Path Model to Simulate the Sensitivity of Central-Canadian Boreal Ecosystems to Climate Variability, Journal of Biogeography, Vol. 26, No. 5 (Sep., 1999), pp. 1101-1113.

Reynolds, R. G., Ali, M., and Jayyousi, T. Mining the social fabric of archaic urban centers with cultural algorithms. Computer, 41, 1 (January, 2008), pp. 64-72.

Reynolds, R. G., An Introduction to Cultural Algorithms, in [EO94], pp. 131-139.
Reynolds, R. G. (1999). Chapter Twenty-Four; Cultural Algorithms: Theory and Applications, In: New Ideas in Optimization, Corne, D., Dorigo, M. & Glover F., pp.367-377, McGraw-Hill Ltd., ISBN 0-07-709506-5, UK, England.

Reynolds, R. G., Craig W. Flocks, Herds, and Schools: A Distributed Behavioral Model. Computer Graphics, Vol 21, 4 (1987).

Reynolds, R. G., O'Shea, J., Fotouhi, F., Fogarty, J., Vitale, K., Meadows, G. R. Agile Design of Reality Games Online. Supported in part by NSF High-Risk Grant #BCS-0829324.

Reynolds, R. G., Peng, B. Knowledge learning and social swarms in cultural algorithms. Journal of Mathematical Sociology, 29 (2005), 1-18.

Reynolds, R. G., Peng, B., Whallon, R. Emergent Social Structures in Cultural Algorithms.

Reynolds, R. G., Saleem, S. M. The impact of environmental dynamics on cultural emergence. In Perspectives on Adaptations in Natural and Artificial Systems. Oxford University Press, 2001.

Saranoha, D. A. Mathematical Models of Tundra Communities and Populations. Laboratory of Mathematical Ecology, Computer Center, USSR Acad. Sci, Vavilova 40, 117333 Moscow USSR.

Sirois, L., Bonan, G. B., Shugart, H. H. Development of a Simulation Model of the Forest-Tundra Transition Zone of Northeastern Canada, Can. J. For. Res. Vol. 24 (4), pp. 697-706 (1994).

Stout, B. Smart Moves: Intelligent Pathfinding. Game Developer Magazine, July, 1997.
Tozour, P. "Influence Mapping," Game Programming Gems 2, 2001.

Vitale, Kevin. Learning Group Behavior in Games Using Cultural Algorithms and the Land Bridge Simulation Example. Master Thesis, Wayne State University, Detroit. (2009)

Walters, Carl J., Hilborn, R., and Peterman, R. Computer Simulation of Barren-Ground Caribou Dynamics. Ecological Modeling, 1 (1975), 303-315.

Zobrist, A. L. "A model of visual organization for the game of go," AFIPS Conf. Proc., 1969, pp. 34, 103–112.

COMPARISON OF TOPOLOGY-BASED PATHWAY ANALYSIS TOOLS IMPLEMENTED IN R

By Alyssa Wilkins, Wayne State University

Major: Computer Science

Mentors: Sorin Draghici, PhD, Department of Computer Science
Ms. Cristina Mitrea, Department of Computer Science

ABSTRACT

Pathway analysis methods typically use gene expression data from an experiment comparing a condition to control, and a set of pathways, and try to identify the pathways that are significantly perturbed in the given condition. Even though these methods have gained a lot of popularity in recent years, there are no benchmark gene expression datasets or pathway databases to compare them. The goal of this study is to provide an objective comparison of some of these methods. We use methods with R implementation available. We discuss the challenge due to the lack of standard data sets and uniformity between the input and output of the tools which led to the necessity to implement conversion methods. Furthermore, we talk about the limitations and challenges related to the minimum number of samples required or different default significance cut-offs that arose when trying to run the tools on the same pathway data and on the same gene expression data. We run the tools using mouse knockout gene expression datasets and signaling pathways from the Kyoto Encyclopedia of Genes and Genomes (KEGG). To compare, we use the precision and recall measures computed using the pathways retrieved by the methods and the known relevant pathways, which contain the knockout gene. Results show that, when using gene expression data from a knockout experiment, these methods are not well designed to identify as relevant the pathways that contain the knockout gene.

1 INTRODUCTION

Fundamental notions of molecular biology are the deoxyribonucleic acid (DNA), the ribonucleic acid (RNA) and proteins, which represent the three major life essential macromolecules. DNA encodes instructions used by all living cells for their development and activity. DNA is a chemical compound, a molecule, 2 meters long that resides in the nucleus of mammalian cell. Genes are functional stretches of DNA, that contain the code for a polypeptide (protein). A gene is expressed when the protein it encodes is produced, and repressed when the production is stopped. RNA performs important roles like the expression and repression of genes. Proteins consist of one or more chains of amino acids and are fundamental components of all living cells. They include hormones and antibodies, which are necessary for the proper functioning of an organism. Antibodies are used by the immune system to identify and neutralize bacteria and viruses. Hormones transport a signal from one cell to another through blood. The general flow of biological information is: DNA can be copied to DNA (replication), DNA information can be copied into messenger RNA (transcription), and proteins can be synthesized using the information from the messenger RNA as a template (translation).[12]

Pathway analysis methods try to identify the pathways that are significantly perturbed in the given condition by use of a set of pathways and experiment data comparing control and condition data. Pathways are functional modules, that describe specific cellular processes such as insulin signaling. The genes in a specific pathway are more related to each other than to the ones on other pathways. A pathway can be defined as a set of genes and their interactions, and can be represented as a graph. Genes are nodes, and interactions are edges.

Examples of such interactions are the before mentioned expression (activation) and repression (inhibition). These are actions that the product of a gene can perform on another gene. Biological pathways are typically curated by molecular biology experts and stored in public databases such as the Kyoto Encyclopedia of Genes and Genomes (KEGG) [8, 9]

Biological studies have yielded information about the different systems present in the human body. One type of information we have knowledge is differentially expressed genes or proteins. The information is very useful in identifying genes that have many roles in a given phenotype. However, the information does not give investigators the insights of the biology of the condition being studied. A challenge occurs, extracting meaning from the long list of differentially expressed genes and proteins. One way to tackle this specific challenge is to reduce the long individual lists of genes to smaller sets of related genes or proteins. This will reduce both the noise and the search space; however it does not make use of the important knowledge stored in pathway databases.

There are no standard or benchmark data sets therefore there is no previous study to compare topology-based analysis methods and no uniformity between different data sets. A recent study takes the first step forward in providing a set of 24 benchmark datasets for gene set analysis methods [18]. However, for each of these datasets there is only one target pathway selected based on the phenomena under study, e.g colorectal cancer. Such phenomena are generic and the mechanism may not be limited to the specific pathway. Another study [16] tries to unify several pathway analysis methods in a single R package; nevertheless, they are ran on different experiment datasets and different pathway databases. Researchers face a great challenge in validating a new pathway analysis method since there is no objective way to determine which analysis is better at finding significant pathways given a set of pathways and gene expression data comparing disease with control. Uniformity of data would allow the use of different organisms, because some experiments are best suited for a specific organism. For example, knockout experiments are unlikely to be performed in vivo in humans; however they are readily performed in mice. Having such standards and benchmarks will allow comparisons to find the analysis methods to further in accuracy, precision, and reliability.

A number of databases are available for both pathway information, such as Kyoto Encyclopedia of Genes and Genomes (KEGG), or for experiment data, such as Gene Expression Omnibus (GEO) [6, 2]. The pathway knowledge bases describe the biological processes, the components, or structures of the genes or proteins that are known to be involved in how gene products interact with each other. One way to use this idea is to identify gene groups which function in the same pathways. Analyzing biological pathways has two reasons for why it is appealing. The first reason is the grouping of thousands of genes and proteins by pathways reduces the complexity. From the thousands of genes or proteins to maybe several hundred pathways, the complexity for an experiment is greatly reduced. The second reason is the explanation of active pathways that differ between two conditions is greater than looking through a simple list of different genes or proteins.

Khatri et al. [11] categorized pathway analysis tools into three categories. The first generation consists of tools that evaluate a fraction of genes in a pathway among the genes showing a change in expression. Second generation tools are an improvement over first generation methods. They take into consideration that large changes in individual genes can have huge significant effects on pathways and coordinated changes in functionally related genes can also have significant effects. The third generation tools include the information of the topology of the genes in the computations of significant pathways in a given data set. The tools that were used are the third generation tools. The tools are pathway topology (PT)-based approaches which utilize additional information that first or second generation tools cannot process such as Over-Representation Analysis (ORA) and Functional Class Scoring (FCS). The additional information PT-based methods use are gotten from pathway databases such as the Kyoto Encyclopedia of Genes and Genomes (KEGG). Pathway topology-based methods perform the same the same three general steps that FCS does. The three steps are computation of the gene-level statistic using the measurements from an experiment, gene-level statistics are

averaged into a single pathway-level statistic, and the statistical significance is assessed from the pathway-level statistic. The key difference between the two is the usage of pathway topology to compute the gene-level statistic. The difference allows a greater perception of pathways significance in diseases.

Important milestones in topology-based pathway analysis are: the first method developed for metabolic networks [14], the first method developed for signaling pathways [10, 5], the first method that applies topology-based multivariate hypothesis tests [17], and the first method based on multi-type graphs from heterogeneous sources [20].

The tools used in this study are presented in Table 1.

Tools name	Abbreviation	Version	Available
R Onto-Tools suite	ROntoTools	1.0.0	bioconductor
DEGraph	DEGraph	1.12.0	bioconductor
Clipper	clipper	1.0.0	bioconductor
Signaling Pathway Impact Analysis	SPIA	2.12.0	bioconductor

Table 1: Table of topology-based analysis tools compared in this study, their version in R and availability

The knockout datasets used in this study are presented in Table 2.

Dataset ID	KO Gene Symbol		
GSE19793	MyD88		
GSE10849	Cav1		
GSE21691	HDAC3		
GSE33162	Adam17		

Table 2: Table of knockout datasets used in this study, Gene Expression Omnibus (GEO) ID and the knockout gene symbol.

2 MATERIALS

To compare the methods we used mouse knockout datasets from GEO and the first data set that was used is GSE19793 [15]. MyD88 mouse (mmu) is an adapter protein that can promote equilibrium in the cell or it can produce cancer. If MyD88 signals certain receptors it can cause the onset of cancer. One such cancer that MyD88 has a role is colitis associated cancer. A total of 12 samples that were the untreated. Six were the untreated wild type (control) while the remaining six were the untreated MyD88 knockout (condition). In the wild type mice the gene performs its normal function, it produces its protein. In the condition, the gene is turned off, it is not producing its protein. There are 16 KEGG pathways that contain the MyD88 gene, these are listed in Table 3.

KEGG ID	Name
mmu04064	NF-kappa B signaling pathway - Mus musculus (mouse)
mmu04210	Apoptosis - Mus musculus (mouse)
mmu04620	Toll-like receptor signaling pathway - Mus musculus (mouse)
mmu05132	Salmonella infection - Mus musculus (mouse)
mmu05133	Pertussis - Mus musculus (mouse)
mmu05134	Legionellosis - Mus musculus (mouse)
mmu05140	Leishmaniasis - Mus musculus (mouse)
mmu05142	Chagas disease (American trypanosomiasis) - Mus musculus (mouse)
mmu05143	African trypanosomiasis - Mus musculus (mouse)
mmu05144	Malaria - Mus musculus (mouse)
mmu05145	Toxoplasmosis - Mus musculus (mouse)
mmu05152	Tuberculosis - Mus musculus (mouse)
mmu05161	Hepatitis B - Mus musculus (mouse)
mmu05162	Measles - Mus musculus (mouse)
mmu05164	Influenza A - Mus musculus (mouse)
mmu05168	Herpes simplex infection - Mus musculus(mouse)

Table 3: Table of KEGG pathways IDs and names that contain the MyD88 gene.

The second data set we used is GSE33162 [4]. These data may have relevance for the use of selective HDAC inhibitors as anti-inflammatory agents. Histone deacetylase 3 is an enzyme that in humans is encoded by the HDAC3 gene. This protein can also down-regulate the function of the known tumor suppressor, p53, function and thus modulate cell growth and apoptosis. This gene is regarded to have a potential protective role against cancer. The dataset contains 3 wild type samples and 3 knockout samples. There are 2 KEGG pathways that contain the HDAC3 gene, these are listed in Table 4.

KEGG ID	Names
mmu05034	Alcoholism
mmu05203	Viral carcinogenesis

Table 4: Table of KEGG pathways IDs and names that contain the HDAC3 gene.

The third data set that was used is GSE10849 [1]. The dataset is the result of a study on mice hearts lacking the protein called Caveolin-1. Results of the study show that these mice develop hypertrophy with normal cardiac substrate metabolism. Cav-1 drives caveolae formation, by interacting with other genes. Cav-1 is also a good candidate to protect the cell from becoming cancerous. The dataset contains 3 wild type samples and 3 knockout samples. There are 5 KEGG pathways that contain the Cav1 gene, these are listed in Table 5.

KEGG ID	Name
mmu04144	Endocytosis
mmu04510	Focal adhesion
mmu05100	Bacterial invasion of epithelial cells
mmu05205	Proteoglycans in cancer
mmu05416	Viral myocarditis

Table 5: Table of KEGG pathways IDs and names that contain the Cav1 gene.

The last data set that is used is GSE21691 [3]. Adam17 is a gene that show a lot of change in expression during inflammation and cancer. The experiment is designed to capture the effect of Adam17 knock out on the in mice colon and skin. Ethanol may affect Adam17 expression by inhibiting it. In the human colon Adam 17 is ubiquitously expressed, with high activity in the colonic mucosa of ulcerative colitis patients. Ulcerative colitis is a main form of inflammatory bowel disease. The dataset contains 6 wild type samples and 6 knockout samples. There are 2 KEGG pathways that contain the Adam17 gene, these are listed in Table 6.

KEGG ID	Names
mmu04330	Notch signaling pathway
mmu05010	Alzheimer's disease

Table 6: Table of KEGG pathways IDs and names that contain the Adam17 gene.

3 METHODS

3.1 GRAPH Interaction from pathway Topological Environment

Sales at al. [16] describes GRAPH Interaction from pathway Topological Environment (graphite) as an R package that is built to provide networks for four databases: Biocarta, KEGG, NCI/Nature Pathway Interaction Database and Reactome. This approach differentiates between different gene set types, includes chemical compounds interactions and selection of the edge attributes, as well as allows the conversion of node identifiers to entrez IDs, or gene symbols. It provides R functions to run Clipper, SPIA, DEGraph and toplogyGSA. A major limitation for this package is that all pathway information is available only for human. There are several important model organisms (e.g. mouse, rat, fruit fly) which are the subject of important research, yet pathway data for them is not available in this implementation. We downloaded mouse pathways using the KEGGGRAPH R package and we implemented a method to convert objects of graphNEL-class from the *graph* package to objects of pathway-class from the *graphite* package.

```
graphNEL2Pathway=function(mygraphNEL)
{
  pathwayName=as.character(pathsKEGG2[names(mygraphNEL),])
  pathurl=gsub(paste("path:",organism,sep=""),"",names(mygraphNEL))
  pDF <- parseKGML2DataFrame(getKGMLurl(pathurl,organism=organism))
  pathwayEdges=data.frame(src=gsub(paste(organism,":",sep=""),"",pDF\$from),
          dest=gsub(paste(organism,":",sep=""),"",pDF\$to),
          direction=rep(mygraphNEL[[1]]@graphData\$edgemode,dim(pDF)[1]),
          type=paste("process(",pDF\$subtype,")"), stringsAsFactors=F)
  mypathway=new(Class="pathway",
          title=pathwayName,
          nodes=gsub(paste(organism,":",sep=""),"",mygraphNEL[[1]]@nodes),
```

```
            edges=pathwayEdges,
            ident="entrez",
            timestamp=Sys.Date(),
            database="KEGG")
  return(mypathway)
}
```

The object mygraphNEL is a list object that has the name of the pathway and the graphNEL object containing the pathway information.

3.2 The novel Signaling Pathway Impact Analysis

Signaling Pathway Impact Analysis (SPIA) is an analysis method is a variation of its predecesor impact analysis [5]. Impact analysis that was created as an improvement to methods such as over-representation analysis (ORA) and the gene set enrichment analysis (GSEA). ORA and GSA treat the pathways as simple sets of genes and do not consider the complex gene interactions that the pathways describe. Tarca et al. [19] demonstrates that SPIA combines two types of evidence, the over-representation of differentially expressed genes in a pathway and the perturbation of gene expression change through that pathway. The input of the SPIA implementation is the log2 fold changes of the differentially expressed genes, list of all the genes measured during the experiment, list of pathways described by connectivity matrices, and the organism symbol. The fold change for a gene is the ratio of disease (condition) over normal (control). The list of pathways is represented by the signaling pathways from KEGG. The connectivity matrices are the genes in the rows and columns and an element of the matrix can be 1 if the genes interact or 0 if the genes do not interact. With this input, the tool computes the gene perturbation factors. There are two steps to compute the gene perturbation factor. The gene perturbation factor formula is $PF(g_i) = \Delta E(g_i) + \sum_{j=1}^{n} \beta_{ij} \times PF(g_i)/N_{ds}(g_i)$. First, the net perturbation accumulation is computed with $Acc(g_i) = PF(g_i) - \Delta E(g_i)$. The subtraction makes sure that the differently expressed (DE) genes are not considered twice. The accumulation equation is written for each gene in the pathway and the system of equations is solved, providing a pathway accumulation by summing the accumulation of all genes in the pathway. The second step is to use a bootstrap procedure to compute the significance of pathway accumulation $P_{PERT} = P(T_A \geq t_A | H_O)$. The third step is to perform the hypergeometric test to assess how likely it is to have the observed number of differentially expressed (DE) genes in a pathway just by chance. The last step is to combine the two types of evidence in a global p-value a combination of p-values from the two types of evidence. The formulas used are $P_G(i) = c_i * ln(c_i)$ and $c_i = P_{NDE} * P_{PERT}(i)$ for each pathway i. The output is a data frame containing the following columns: pSize, NDE, tA, pNDE, pPERT, pG, pGFdr, pGFWER, STATUS and KEGGLINK. pSize column is the number of genes on the pathway. The NDE column is the number of DE genes per pathway. The total perturbation accumulation in the pathway is the column tA. pPERT is the probability of observing total accumulation more extreme that tA by chance. The column pG is the p-value that is obtained from the combination of pNDE and pPERT. pGFdr and pGFWER are the columns that are the False Discovery Rate and Bonferroni adjusted global p-values. The STATUS column gives the direction of the pathway is perturbed (activated or inhibited.) The last column, KEGGLINK, give a web link to the pathway image, from the KEGG website, with DE genes marked in red for over-expression, green for under-expression.

3.3 R Onto-Tools suite

R Onto-Tools suite (ROntoTools) is a topology-based pathway analysis tool that is an improvement on SPIA proposed by Tarca et al. [19]. ROntoTools incorporates the significance (p-value) of each gene. Voichita et al. [21] describe how to capture it motivating that incorporating the significance of each gene increases the accuracy of the method. ROntoTools also proposes to use the gene significance as a weighting factor that would reduce the noise, therefor the whole list of measured genes will be used in the analysis without a

preliminary gene selection. The input ROntoTools is the list of differently expressed genes (IDs and log fold change, here we may use the list of all genes), list of all genes entrez IDs, and the list of pathways. The first step in the ROntoTools algorithm is to compute the gene perturbation factor using the formula $PF(g) = \alpha_g \times \Delta E(g) + \sum_{u \epsilon USg} \beta_{ug} \times \text{PF}(u)/ \text{N}_{ds}(u)$ for each gene i. Here, the significance value for the measured expression change of a gene g is computed with the formula: $\alpha_g = 1 - (\text{P}_g /\alpha_t)$, where α_t is the significance threshold used for the selection of DE genes. The second step of ROntoTools is to compute the pathway accumulation using the formula $Acc(g_i) = PF(g_i) - \alpha_g \times \Delta E(g_i)$. The third step is to use a bootstrap procedure to compute the significance of pathway accumulation $P_{PERT} = P(T_A \geq t_A | H_O)$. The fourth step is to perform the hypergeometric test to assess how likely it is to have the observed number of DE genes in a pathway just by chance. The last step is to combine the two types of evidence in a global p-value a combination of p-values from the two types of evidence using $P_G(i) = c_i * ln(c_i)$ and $c_i = P_{NDE} * P_{PERT}(i)$ for each pathway i. The output for ROntoTools is a data frame with the columns totalAcc, totalPert, totalAccNorm, totalPertNorm, pPert, pAcc, pORA, pComb, pPERT.fdr, pACC.fdr, and pComb.fdr. The first column total Acc is the value of total accumulation if it can be computed. totalPert column is the values of the total perturbation. totalAccNorm and totalPertNorm are the columns that have been normalized using bootstrap. pPert is the significance of the total perturbation after bootstrap permutations. pAcc is the significance of total accumulation after bootstrap permutations. pORA is the values of over-represented p-values. pComb is the combination of p-values. pPERT.fdr, pACC.fdr, and pComb.fdr are the columns that have False Discovery Rate applied to the pPert, pAcc, and pComb columns.

3.4 DEGraph

DEGraph is a pathway analysis method that uses a two sample graph test under alternative hypotheses that takes in account the graph structure. Jacob et al. [7] describe the alternative hypothesis testing using the Hotelling's T^2-test which considers the null hypothesis $H_0 : \mu_1 = \mu_2$ against the alternative hypothesis $H_0 : \mu_1 \neq \mu_2$. It is important to consider the graph structure as part of analysis since it can be used to detect systemic changes between two conditions. An example would be detecting the DE genes of a patient who is receiving treatment for a condition that is effective and the DE genes of patients who are resistant to the treatment. This would give insight about the resistance mechanisms of the condition to create treatments to target where the condition is resistant. The method input is a list of pathways. In this case, it would be the MyD88 list that was taken from GEO. The process of DEGraph is described as follows: Hotelling T^2-test and the T^2 test in the new graph-based space that only retains the first 20 percent coefficients ($k = 0.2p$), then the unadjusted p-values are computed under nominal F-distributions $F_0(p, n_1 + n_2 - p - 1)$ and $F_0(k, n_1 + n_2 - k - 1)$ and the Benjamini and Hochberg procedure was then applied to control the false discovery rate (FDR) at level 0.05. The output data frame is a list of the results of the pathways and a list of generated errors.

3.5 Clipper

Clipper is a topology based analysis tool that tries to fill the gap of information about the pathways involved with the biological problem. Clipper takes the problems of GSA with the multivariate approach. The multivariate approach considers only the genes in the gene set and hypotheses that no gene in the gene set is associated with the phenotype. Clipper disagrees with the multivariate approach and claims that the phenotype is presented and the pathway of the biological problem can be mapped. The input is a gene data set. The first step of the Clipper process is to test the whole pathway. To test the whole pathway you must compute the covariance matrices and means. To compute covariance matrices and means, you have to see which ones are significantly different between experimental conditions. The second step is to identify relevant signal paths. The way to identify relevant signal paths is to construct junction trees, identifying of paths and corresponding sub-paths, and computation of relevance of sub-pathways. The output is the list of ranked pathways that are ranked by the p-values. The pathways are the ones that are deregulated (associated with the phenotype). The significant pathways are selected after a correction for multiple comparisons, considering the number of

pathways; a false discovery rate (FDR) correction is applied. The output data frame of Clipper is a matrix of the significant pathways.

3.6 Measures for the performance assessment

The analysis methods above were ran through different data sets (see section 3 to gauge their efficiency. Equations were written to take the results gathered from the methods and compare them to the data sets to see if the significant pathways that should appear would. The assessment statistics used are true positive, true negative, false positive, false negative, precision, and accuracy. True positive checks the results of the methods gathered and see how many pathways are truly significant for the condition. True negative takes the results and check to see what pathways are truly not significant for the condition. A false positive equation is written to go through the results and determine how many incorrect significant pathways that should not be significant are documented. False negative is the checking of how many significant pathways in the results was labeled as insignificant pathways. Precision is how well our results are close to actual results of the data sets. Recall with our results is how many significant pathways were corrected identified by the analysis methods.

The true positives are presented for each dataset in section 3. Using the pathways IDs from the results of each method we can compute Precision and Recall as follows: *Precision = TP/(TP + FP)* and *Recall = TP/(TP +FN)*, where TP is the number of true positives, FP is the number of false positives, and FN is the number of false negatives.

4 RESULTS

Unlike most gene set analysis methods which are validated by a human interpretation of the results, the validation employed here uses different data sets and a completely objective assessment scheme that makes minimal assumptions and eliminates the need for possibly biased human assessments of the analysis results.

4.1 MyD88 knockout analysis results

Results for the analysis of Myd88 knockout data are presented in Table 7 and show that the precision and recall are very low. For the only method with precision and recall different than 0, SPIA, the precision and recall are 16.66% and 6.25% respectively.

	Precision	Recall	TP	FP	TN	FN
SPIA	0.1666667	0.0625	1	5	114	15
ROntoTools	0.0000000	0.0000	0	4	135	16
DEGrpah	0.0000000	0.0000	0	61	78	16
Clipper	0.0000000	0.0000	0	18	121	16

Table 7: The results for the GSE19793 dataset where the MyD88 gene is the knockout.

4.2 MyD88 knockout analysis results

Results for the analysis of Cav1 knockout data are presented in Table 8 and show that the precision and recall are very low. For the only method with precision and recall different than 0, SPIA, the precision and recall are 27.27% and 60% respectively. Which shows SPIA performs better than on the MyD88 dataset, however still poor performance.

	Precision	Recall	TP	FP	TN	FN
SPIA	0.2727273	0.6	3	8	122	2
ROntoTools	0.0000000	0.0000	0	11	139	5
DEGrpah	0.0000000	0.0000	0	29	121	5
Clipper	0.0000000	0.0000	0	30	120	5

Table 8: The results for the GSE10849 dataset where the Cav1 gene is the knockout.

4.3 HDAC3 knockout analysis results

Results for the analysis of HDAC3 knockout data are presented in Table 9 and show that the precision and recall are very low. For the only method with precision and recall different than 0, SPIA, the precision and recall are 1.78% and 100% respectively. Which shows SPIA performs better than on the previous two datasets in terms of recall, however still poor performance since it retrieves a lot of pathways just by chance it may retrieve the two true positives.

	Precision	Recall	TP	FP	TN	FN
SPIA	0.01785714	1	2	110	23	0
ROntoTools	0.0000000	0.0000	0	18	135	2
DEGrpah	0.0000000	0.0000	0	24	129	2
Clipper	0.0000000	0.0000	0	34	119	2

Table 9: The results for the GSE33162 dataset where the HDAC3 gene is the knockout.

4.4 Adam17 knockout analysis results

Results for the analysis of Adam17 knockout data are presented in Table 10 and show that no method was able to identify any of the pathways containing the knockout gene, which is a remarkably poor performance.

	Precision	Recall	TP	FP	TN	FN
SPIA	0	NaN	0	36	99	0
ROntoTools	0	NaN	0	9	146	0
DEGrpah	0	NaN	0	57	98	0
Clipper	0	NaN	0	1	154	0

Table 10: The results for the GSE21691 dataset where the Adam17 gene is the knockout.

5 DISCUSSION AND CONCLUSIONS

This approach allows a comparison of analysis methods in terms of precision and recall. Such a comparison is: a) objective, b) reproducible, and c) independent of the accuracy and thoroughness of a literature search. Using this approach, we were able to compare existing methods for topology-based pathway analysis based on high-throughput gene expression data. Pathway analysis is a core strategy of bioinformatics research. A major step forward in pathway analysis is the integration of molecular interaction data, which is done through mathematical algorithms that try to assess the perturbation in biological systems when two phenotypes are compared. All R implementations of topological pathway analysis methods we compare were published in the last 5 years, evidence that there is great interest in this area.

The validation of pathway analysis results is an important challenge researchers face when trying to develop such methods. Biologists depend on pathway analysis methods to support their hypotheses, however they are called to validate the pathway analysis results, which is a paradox. For this reason, we attempted to compare four topology-based analysis method implemented in the R programming language. The first challenge we encountered was that many knockout experiments use genes that are not in any KEGG pathway, such as GSE10634 (GEO dataset), which is a study of aquaporin 11 (Aqp11) knockout in mice. The second challenge we encountered was a requirement of a minimum number of samples to be able to run topologyGSA [13]. Another challenge was given by the number input format for the expression data, which required either the EntezID or the Symbol for the genes, and also ranged from probe data, to gene data, to differentially expressed gene data, all log fold change. The major challenge was to interpret the results, which showed a poor performance for the selected tools using knockout data. One might consider that the mechanism

triggered in a cell during a gene knockout cannot be captured with snapshot data, or that some of that pathways are tissue-specific, so that should be included as a criteria in the selection of target pathways (truly affected pathways).

Biological pathways representation differs among databases, that is why an objective assessment should be done on the same set of pathways. For instance, inconsistent conversions for pathways that come from different databases might provide unreliable results. The current efforts to address the problem through the creation of unified formats are led by the BIO-PAX community. Nevertheless, available tools are not compatible with all database formats and either the modification of pathway input or alteration of the underlying algorithm is required in order to accommodate the differences.

High-throughput technologies, developed for biological experiments, are improving in accuracy. Here, we chose to use microarray data which is the most abundant in experiment databases. However, such data is still error prone, and because of that, the results of analyses using these data includes a significant amount of noise. There are more accurate technologies, such as RNAseq, that are catching up in terms of amount of data and cost.

To conclude, we (re-)state that the goal of this study was to survey topology-based tools, with an R implementation available and designed to identify the most significant pathways in a comparison between phenotypes. In other words, the goal was to identify, review and compare topology-based pathway analysis methods that are implemented in the R programming language and *attempt to assess their performance*.

REFERENCES

[1] Ayanna S Augustus, Jonathan Buchanan, Ellen Gutman, Giuseppe Rengo, Richard G Pestell, Paolo Fortina, Walter J Koch, Andre Bensadoun, E Dale Abel, and Michael P Lisanti. Hearts lacking caveolin-1 develop hypertrophy with normal cardiac substrate metabolism. *Cell cycle*, 7(16):2509–2518, 2008.

[2] Tanya Barrett, Stephen E Wilhite, Pierre Ledoux, Carlos Evangelista, Irene F Kim, Maxim Tomashevsky, Kimberly A Marshall, Katherine H Phillippy, Patti M Sherman, Michelle Holko, et al. Ncbi geo: archive for functional genomics data sets—update. *Nucleic Acids Research*, 41(D1):D991–D995, 2013.

[3] Athena Chalaris, Nina Adam, Christian Sina, Philip Rosenstiel, Judith Lehmann-Koch, Peter Schirmacher, Dieter Hartmann, Joanna Cichy, Olga Gavrilova, Stefan Schreiber, et al. Critical role of the disintegrin metalloprotease adam17 for intestinal inflammation and regeneration in mice. *The Journal of experimental medicine*, 207(8):1617–1624, 2010.

[4] Xuefen Chen, Iros Barozzi, Alberto Termanini, Elena Prosperini, Antonio Recchiuti, Jesmond Dalli, Flore Mietton, Gianluca Matteoli, Scott Hiebert, and Gioacchino Natoli. Requirement for the histone deacetylase hdac3 for the inflammatory gene expression program in macrophages. *Proceedings of the National Academy of Sciences*, 109(42):E2865–E2874, 2012.

[5] Sorin Draghici, Purvesh Khatri, Adi Laurentiu Tarca, Kashyap Amin, Arina Done, Calin Voichita, Constantin Georgescu, and Roberto Romero. A systems biology approach for pathway level analysis. *Genome Research*, 17(10):1537–1545, 2007.

[6] Ron Edgar, Michael Domrachev, and Alex E Lash. Gene expression omnibus: Ncbi gene expression and hybridization array data repository. *Nucleic Acids Research*, 30(1):207–210, 2002.

[7] Laurent Jacob, Pierre Neuvial, and Sandrine Dudoit. Gains in power from structured two-sample tests of means on graphs. *arXiv*, 2010.

[8] Minoru Kanehisa and Susumu Goto. Kegg: kyoto encyclopedia of genes and genomes. *Nucleic Acids Research*, 28(1):27–30, 2000.

[9] Minoru Kanehisa, Susumu Goto, Yoko Sato, Miho Furumichi, and Mao Tanabe. Kegg for integration and interpretation of large-scale molecular data sets. *Nucleic Acids Research*, 40(D1):D109–D114, 2012.

[10] Purvesh Khatri, Sivakumar Sellamuthu, Pooja Malhotra, Kashyap Amin, Arina Done, and Sorin Draghici. Recent additions and improvements to the Onto-Tools. *Nucleic Acids Research*, 33(suppl 2):W762–W765, 2005.

[11] Purvesh Khatri, Marina Sirota, and Atul J Butte. Ten years of pathway analysis: current approaches and outstanding challenges. *PLoS Computational Biology*, 8(2):e1002375, 2012.

[12] H.F. Lodish. *Molecular Cell Biology*. W. H. Freeman. W.H. Freeman, 2012.

[13] Maria S Massa, Monica Chiogna, and Chiara Romualdi. Gene set analysis exploiting the topology of a pathway. *BMC Systems Biology*, 4(1):121, 2010.

[14] Jorg Rahnenfuhrer, Francisco S Domingues, Jochen Maydt, and Thomas Lengauer. Calculating the statistical significance of changes in pathway activity from gene expression data. *Statistical Applications in Genetics and Molecular Biology*, 3(1):1055, 2004.

[15] Rosalba Salcedo, Andrea Worschech, Marco Cardone, Yava Jones, Zsofia Gyulai, Ren-Ming Dai, Ena Wang, Winnie Ma, Diana Haines, Colm O'hUigin, et al. Myd88-mediated signaling prevents development of adenocarcinomas of the colon: role of interleukin 18. *The Journal of Experimental Medicine*, 207(8):1625–1636, 2010.

[16] Gabriele Sales, Enrica Calura, Duccio Cavalieri, and Chiara Romualdi. graphite-a bioconductor package to convert pathway topology to gene network. *BMC Bioinformatics*, 13(1):20, 2012.

[17] Ali Shojaie and George Michailidis. Analysis of gene sets based on the underlying regulatory network. *Journal of Computational Biology*, 16(3):407–426, 2009.

[18] Adi L Tarca, Sorin Draghici, Gaurav Bhatti, and Roberto Romero. Down-weighting overlapping genes improves gene set analysis. *BMC Bioinformatics*, 13(1):136, 2012.

[19] Adi Laurentiu Tarca, Sorin Draghici, Purvesh Khatri, Sonia S Hassan, Pooja Mittal, Jung-sun Kim, Chong Jai Kim, Juan Pedro Kusanovic, and Roberto Romero. A novel signaling pathway impact analysis. *Bioinformatics*, 25(1):75–82, 2009.

[20] Charles J Vaske, Stephen C Benz, J Zachary Sanborn, Dent Earl, Christopher Szeto, Jingchun Zhu, David Haussler, and Joshua M Stuart. Inference of patient-specific pathway activities from multi-dimensional cancer genomics data using paradigm. *Bioinformatics*, 26(12):i237–i245, 2010.

[21] Calin Voichita, Michele Donato, and Sorin Draghici. Incorporating gene significance in the impact analysis of signaling pathways. In *Machine Learning and Applications (ICMLA), 2012 11th International Conference on*, volume 1, pages 126–131. IEEE, 2012.

THE CONTRIBUTION OF OXIDATIVE STRESS TO THE DEVELOPMENT OF CISPLATIN RESISTANCE IN EPITHELIAL OVARIAN CANCER

By Yousif Younan

Major: Biology

Mentor: Dr. Ghassan M. Saed, Department Obstetrics and Gynecology

ABSTRACT

Epithelial ovarian cancer (EOC) is the most lethal gynecologic disease today. Oxidative stress is caused from an imbalance among the production of reactive oxygen species and the biological system's ability to readily detoxify the reactive intermediates or easily repair the resulting damage. If there are changes in the normal redox state, toxic effects such as free radicals can damage the entire cell. The goal of this study was to determine the mechanisms by which oxidative stress, specifically inducible nitric oxide synthase (iNOS), contributes to the development of cisplatin resistance in EOC. Two parent EOC cell lines (SKOV-3 and MDAH-2774) and their chemoresistant counterparts were used. Total RNA from these cells was extracted and subjected to real-time RT-PCR to evaluate the expression of iNOS as well as media collected and levels of nitrate/nitrite detected. Samples were subjected to real-time RT-PCR to evaluate the expression of iNOS.

The results of this study showed nitrate/nitrite levels to be significantly increased in SKOV-3 cisplatin resistant EOC cells as compared to their sensitive counterpart. There was no change observed in nitrate/nitrite levels in MDAH-2774 sensitive EOC cells as compared to its cisplatin resistant counterpart. iNOS mRNA levels were significantly increased in MDAH-2774 cisplatin resistant EOC cells as compared to their sensitive counterpart. There was an increased trend, however not significant, observed in iNOS mRNA levels in SKOV-3. In conclusion, oxidative stress contributes to the development of cisplatin resistance in EOC.

INTRODUCTION

Epithelial ovarian cancer (EOC) is the most lethal gynecologic disease today [1]. Cancer is one of the leading causes of death in the United States today. It affects all of us in some way; everyone in this country knows someone or has met someone with some type of cancer. There are almost 100 different types of cancer known so far, and the list keeps on growing. Merriam-Webster defines cancer as a malignant tumor of potentially unlimited growth that expands locally by invasion and systemically by metastasis. Thus far, no cure has been found for this evil disease. Many research facilities are working everyday throughout the world to try and defeat cancer, but most have failed to do so. The origins and how EOC is developed are not understood at this time which makes it even harder to figure out. It's believed to be originated from the ovaries or more specifically the surface of the ovaries which is why it's called epithelial ovarian cancer [1]. There are a few different ways to treat EOC. If the case is being treated in an advanced stage then complete surgical tumor debulking is the single most important prognostic factor; then it can be followed by the use of chemotherapy, more specifically with cisplatin [2].

Evidence from several studies has suggested that cancer cells, as compared to normal cells, are under increased oxidative stress, which is associated with oncogenic transformation, alterations in metabolic activity, and increased generation of reactive oxygen species including superoxide ($O_2^{\cdot-}$), hydrogen peroxide (H_2O_2), and the hydroxyl radical [3]. Oxidative stress is defined as a disturbance in the equilibrium between free radicals, reactive oxygen species, and endogenous antioxidant defense mechanisms, or more simply, it is a disturbance in the balance between oxidant-antioxidant states favoring the oxidant environment [4, 5]. Enzymes that preserve a reducing environment through metabolic energy are responsible for this. If there are changes in the normal redox state, toxic effects such as free radicals can damage the entire cell. Oxidative

stress can also cause many neurodegenerative disorders such as Parkinson's, Alzheimer's, etc. Also, heart failure, atherosclerosis and many other diseases are caused by oxidative stress [5].

The causes of EOC are still unknown, but there are many risk factors that are being studied. Some of those factors are older women who don't give birth, relatives with the disease, and more importantly mutation in specific genes such as BRCA1 and BRCA2. Signs and symptoms of EOC are pain in the abdomen or the pelvis and also gastrointestinal problems are very common as well [6].

The overall project investigates the mechanisms by which oxidative stress contributes to the development of cisplatin resistance in EOC.

MATERIALS AND METHODS
Cell Culture

Two parent human EOC cell lines (SKOV-3 and MDAH-2774 from American Type Culture Collection (ATCC), Manassas, VA) were utilized in developing cells resistant to cisplatin. Cells were exposed to a stepwise increase in cisplatin (Sigma Aldrich, St. Louis, MO) over the course of a year, with a final concentration 50 µM. Conformation of resistance was determined by the Trypan Blue Dye Exclusion Method following a two week incubation without cisplatin and subsequent replacement of cisplatin. Cells were cultured in 60-mm^2 dishes with McCoy's 5A medium (Invitrogen, Grand Island, NY) supplemented with 10% fetal bovine serum (FBS, Atlanta Biologicals, Lawrenceville, GA) and 1% penicillin and streptomycin) (Invitrogen). For measurement of iNOS mRNA and nitrate/nitrite levels, cells (2.5×10^6) were seeded in 150 mm dishes (Corning) and allowed to rest for 24 hrs followed by media replacement and cell collection 24 hrs later.

Measurement of Nitrate/Nitrite Levels

The nitrate/nitrite colorimetric assay (Cayman Chemical, Ann Arbor, MI) was used to measure the levels of stable NO by-products, nitrate ($NO2^-$) and nitrite ($NO3^-$), as an indication of NO production. Due to the fact that the proportion of $NO2-$ and $NO3-$ is variable and cannot be predicted with certainty, the sum of both NO by-products is a more accurate indicator of NO production. The assay was performed utilizing cell culture media according to the manufacturer's protocol. Absorbance was detected at 540 nm and a standard curve for nitrite was utilized to determine total $NO2-$ and $NO3^-$.

Reverse Transcription Real-time Polymerase Chain Reaction (RT-PCR)

RNA isolation: Total RNA was extracted from EOC cells using the RNeasy Mini Kit (Qiagen, Valencia, CA) according to the protocol provided by the manufacturer.
Reverse transcription: A 40-µL-cDNA-reaction volume utilizing 2 µg RNA was prepared using the QuantiTect Reverse Transcription Kit (Qiagen), as described by the manufacturer's protocol.

Real-time RT-PCR primer design and controls: Optimal oligonucleotide primer pairs for real-time RT-PCR amplification of reverse-transcribed cDNA were selected with the aid of the software program, Beacon Designer (Premier Biosoft Int., Palo Alto, CA). Human oligonucleotide primers, which amplify variable portions of the protein coding regions, were used. Sequences of the oligonucleotides used for amplification of iNOS are described in Table 1. Quantitative real-time RT-PCR was performed using a QuantiTect SYBR Green RT-PCR kit (Qiagen) and Cepheid 1.2f Detection System. RT-PCR was performed in a 25 µl total reaction volume including 12.5 µl of 2 x QuantiTect SYBR Green RT-PCR master mix, 2 µl of cDNA

template, and 0.2 μM each of target specific primers designed to amplify a part of each gene. Standards with known concentrations and lengths (base pairs (bp)) were designed specifically for iNOS (103 bp) using the Beacon Designer software (Premier Biosoft, Palo Alto, CA), allowing for construction of a standard curve using a tenfold dilution series. A specific standard for each gene allows for absolute quantification of the gene in number of copies, which can then be expressed per μg of RNA. RT-PCR reaction conditions were programmed as follows: An initial cycle was performed at 95°C for 900 sec followed by 35 cycles of denaturation at 95 °C for 15 sec, annealing for 30 sec at 58°C. This was followed by a final cycle at 72 °C for 30 sec to allow completion of product synthesis. Following RT-PCR, a melting curve analysis was performed to demonstrate the specificity of the PCR product as a single peak. A control, containing all the reaction components except for the template, was included in all experiments. All experiments were performed in triplicate.

Statistical analysis: Data were analyzed with SPSS 19.0. Unpaired t-tests were utilized to compare the controls and the resistant cell lines. Probability values are expressed at $\alpha < 0.05$ for significance.

Table 1. Oligonucleotide primers for iNOS.

Locus	Sense (5$'$ – 3')	Antisense (3$'$ – 5')	Size (bp)
iNOS	GGCACAGAACTTAAGGATGG	TTGTTAGGAGGTCAAGTAAAGG	145

RESULTS

iNOS mRNA levels were significantly increased in MDAH-2774 cisplatin resistant EOC cells (0.28 + 0.01 fg/ug RNA) as compared to their sensitive counterpart (0.39 + 0.00 fg/ug RNA)(p<0.05, Figure 1). There was an increased trend, however not significant, observed in iNOS mRNA levels in SKOV-3 as compared to its cisplatin reisistant counterpart.

Nitrate/nitrite levels were significantly increased in SKOV-3 cisplatin resistant EOC cells (13.7 + 0.2 μM) as compared to their sensitive counterpart (8.2 + 0.0 μM) (p<0.05, Figure 2). There was no change observed in nitrate/nitrite levels in MDAH-2774 sensitive EOC cells as compared to its cisplatin reisistant counterpart.
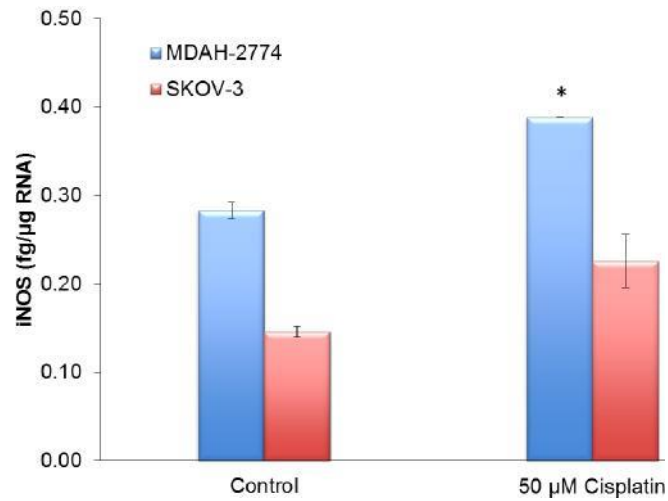
Figure 1: Real-time RT-PCR for inducible nitric oxide synthase (iNOS). Sensitive (control) and (resistant) (50 uM), cisplatin resistance correlates with iNOS mRNA levels. (* P<0.05)
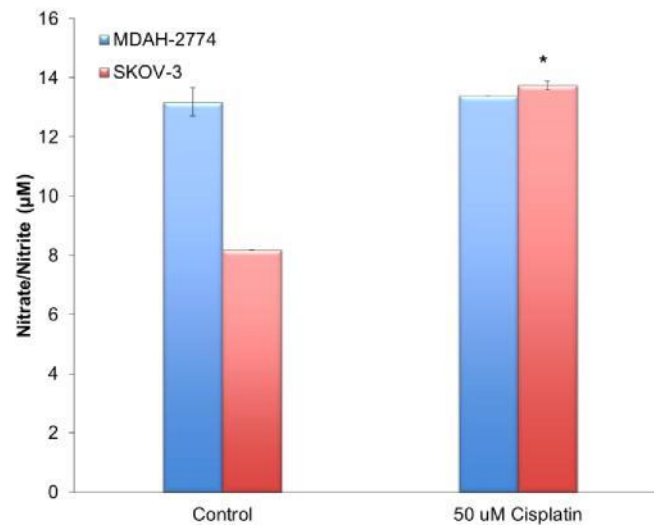

Figure 2. Nitrate/nitrate levels in EOC cells. Sensitive (control) and (resistant) (50 uM), cisplatin resistance correlates with nitrate/nitrite levels. (* P<0.05)

DISCUSSION

Oxidative stress contributes to the development of cisplatin resistance in EOC. Two parent EOC cell lines (SKOV-3 and MDAH-2774) and their chemoresistant counterparts were used. Nitric oxide is produced by three different isoforms of nitric oxide synthase (NOS). iNOS can be expressed in response to proinflammatory agents which produces high levels of nitric oxide (NO). Over expression of iNOS has been linked to tumor growth and metastasis in in vitro models. This overexpression leads to aggressive tumors and poor prognosis. Thus, inhibitors of NO have been potential cancer chemopreventive and therapeutic agents [7]. Many physiological functions require NO to perform. Depending on many different situations in the body nitric oxide plays both the facilitator and the inhibitor. High levels of NO can also inhibit cell growth and division of tumor cells, which leads to apotosis [8]. In a previous study, it was demonstrated that treatment of EOC cell lines with L_NAME, a specific iNOS inhibitor, significantly reduced nitrate/nitrite levels and iNOS mRNA levels [7]. Treatment with L-NAME for 24 hours also resulted in a significant inhibition of VEGF mRNA in EOC cells as well as increased apoptosis [7]. Therefore, the importance of iNOS in the persistence of EOC has been demonstrated.

This data shows that with the presence of oxidative stress may play a role in the acquisition of chemoresistance (cisplatin) in EOC. Increased levels of iNOS and NO may play a role in the development of resistance to chemotherapy in EOC. Cisplatin has dramatically improved the clinical outcome for testicular germ cell tumors and remains the first line treatment of several tumors such as, ovarian, breast, head and neck, and small cell lung cancers [9]. However, in many cases, cancer cells develop a resistant phenotype, and the outcome for these patients is very poor [9].

In conclusion, as stated before, oxidative stress is caused from an imbalance among the production of reactive oxygen species and the biological system's ability to readily detoxify the reactive intermediates or easily repair the resulting damage. Collectively, this work further demonstrates the role of oxidative stress, as demonstrated by an increase in iNOS and its downstream product nitrate/nitrite, in the pathogenesis of ovarian cancer as well as in the acquisition of chemotherapy resistance.

REFERENCES

1. Kurman, R.J. and M. Shih le, *The origin and pathogenesis of epithelial ovarian cancer: a proposed unifying theory.* Am J Surg Pathol, 2010. 34(3): p. 433-43.
2. *Investigators at Turku University Hospital Detail Research in Chemotherapy* 2013. p. 127.
3. Saed, G.M., et al., *Dichloroacetate induces apoptosis of epithelial ovarian cancer cells through a mechanism involving modulation of oxidative stress.* Reprod Sci, 2011. 18(12): p. 1253-61.
4. Ahmed Abdal Dayem, H.-Y.C., Jung-Hyun Kim and Ssang-Goo Cho, *Role of Oxidative Stress in Stem, Cancer, and Cancer Stem Cells.* 2010: p. 860-884.
5. Ivana S. Trbojevic1, B.I.O., NATAŠA Z. ĐORĐEVIĊ1, SNEŽANA D. MARKOVIĊ1, A.Š. ŠTAJN1, JELENA P. GAVRIĊ2, and ZORICA S. SAIĊIĊ2*, *Effects of Cisplatin on Lipid Peroxidation and the Glutathoione Redox Status in the Liver of Male Rats: the Protective Role of Selenium.*, 2010: p. 75-82.
6. Society, C. Ovarian Cancer, 2011 Jan 2011 [cited 2013 10 Aug 2013]; Available from: http://www.cancernz.org/assets/files/_ISOvarianCancerJan11.pdf.
7. Malone, J.M., et al., *The effects of the inhibition of inducible nitric oxide synthase on angiogenesis of epithelial ovarian cancer.* Am J Obstet Gynecol, 2006. 194(4): p. 1110-6; discussion 1116-8.
8. Anttila, M.A., et al., *Prognostic significance of iNOS in epithelial ovarian cancer.* Gynecol Oncol, 2007. 105(1): p. 97-103.
9. Noel, E.E., et al., *The association of CCND1 overexpression and Cisplatin resistance in testicular germ cell tumors and other cancers.* AM J Pathol, 2010. 176(6): p. 2607-15.

EXPLORING THE EFFECTS OF CATION TYPE

AND CONCENTRATION ON LIPID BILAYERS

By William Zygmunt
Major: Chemical Engineering
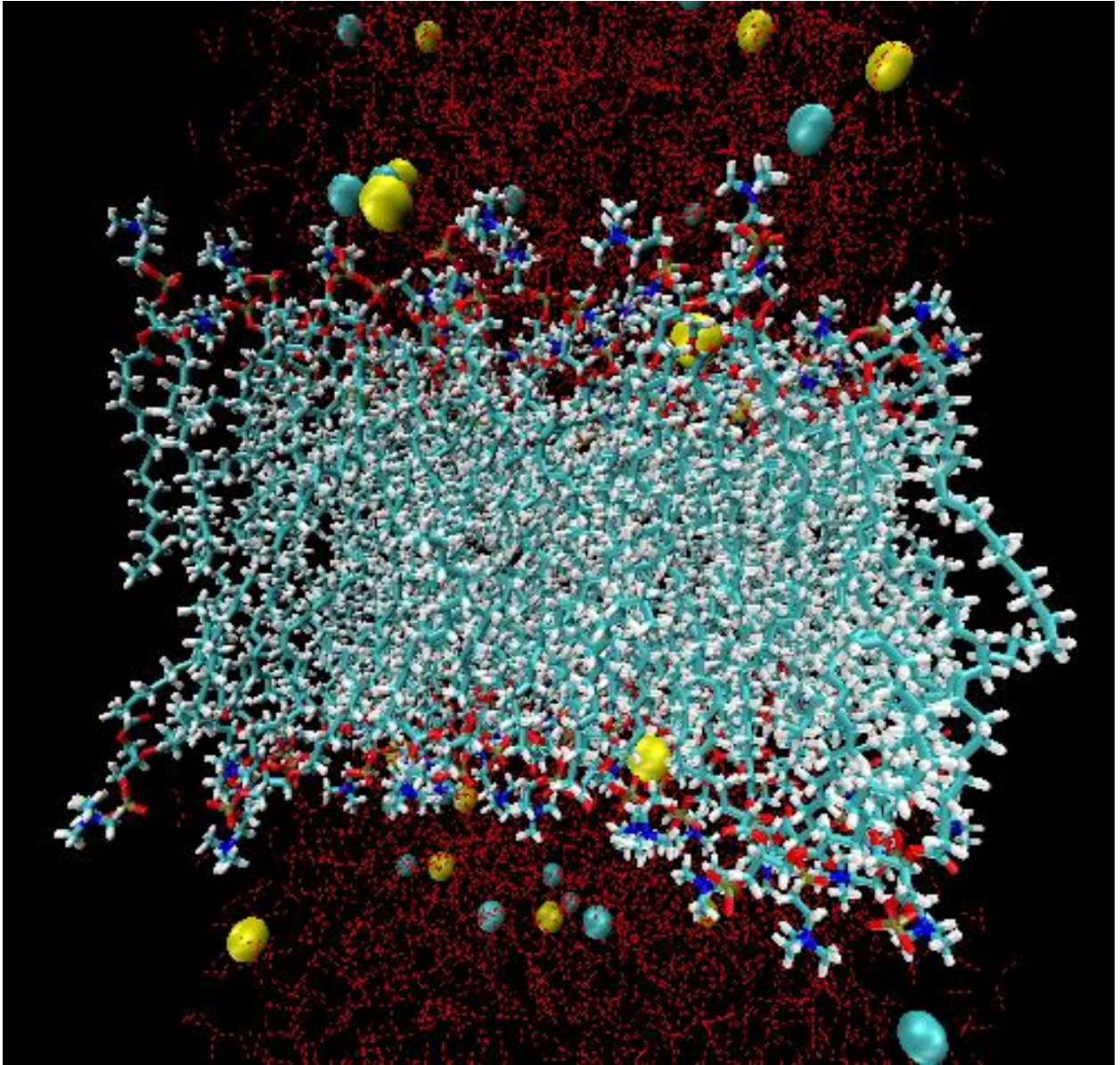Mentor: Dr. Jeffrey Potoff, Department of Chemical Engineering & Materials Science

Figure 1: POPC Lipid Bilayer

1. INTRODUCTION

Lipids are one of four macromolecules (large collections of smaller molecular units) that are essential to the human body and to life in general. Lipids themselves are responsible for keeping order in cells and provide many different functions in the cell environment such as the containment of the various organelles inside of the cell, acting as a barrier to foreign agents that should not be entering the cell, and by acting as a regulation tool to allow certain materials into the cellular environment. The lipid bilayer is the primary concern of this work; a lipid bilayer is a double row of lipids that is responsible for holding in place the many proteins and ion channels necessary to cell function and health.

Given the obvious necessity of the lipid bilayer and all the important things that it does for the cell and its contents, a solid understanding of the cellular environment (what surrounds the cell itself) and how this environment affects the barrier (the lipid bilayer) is necessary. The cytosol that surrounds the cell is an electrolytic solution composed of ions such as sodium, calcium, and many others. Each ion has an effect on not only the structure of the bilayer but also the behavior of the bilayer as it attempts to allow material into the cell and regulate the fusion of cells to others. There are numerous ways to quantify these effects, but the most effective and comprehensive tool that can be utilized is molecular simulation.

Molecular simulation can be used to explore the various interactions of molecules with other molecules by building a system and allowing it to act as it would in real time. The simulations performed here are with the lipid 1-palmitoyl-2-oleoyl-sn-glycero-3-phosphocholine (POPC) and with various concentrations of ions including sodium and calcium and later the ions magnesium and potassium. The simulations were performed using the CHARMM ver. 36 force field parameters the molecular simulation tool NAMD ver. 2.9. The goal is to quantify various parameters about the systems described above and to draw conclusions about what effects ions have on the lipid POPC and how this may affect cell regulation and fusion. This research is currently ongoing, so general analysis will be discussed as to how it will be used to answer these questions at a later date.

2. LITERATURE REVIEW

The following articles were deemed relevant to the studies performed in this research and are listed below as reference:

- Papahadjopoulos, D. & Poste, G. (1975) Calcium-Induced Phase Separation and Fusion In Phospholipid Membranes. *Biophysical Jounral Volume 15 1975*

Papahadjopoulos and Poste (1975) performed an analysis of the effects of calcium on lipid bilayers, particularly the effects it has on phase separation and membrane fusion. The overall effect of calcium is an earlier formation of crystalline phase behavior when added to lipid membranes that are in the liquid-phase. The "solid" phase of lipids is the gel-crystalline phase and the more-ordered phase than the "liquid" phase (the liquid-crystalline phase). Additionally, calcium is found to induce membrane fusion between different layers of lipids, as demonstrated by an experiment with phosphatidylserine vesicles. This article (written in 1975) would later have many of its hypotheses verified by molecular dynamics simulations.

- Bockmann, R. A. & Grubmuller, H. (2004). Multistep Binding of Divalent Cations to Phospholipid Bilyers: A Molecular Dynamics Study. *Angew. Chem. Int. Ed. 2004, 43, 1021-1021*

Bockmann and Grubmuller (2004) examined the various effects that divalent cations (cations that have a charge of +2 due to a lack of two electrons) have on phospholipid bilayers, in this study the lipid 1-palmitoyl-2-oleoyl-sn-glycero-3-phosphocholine (POPC). The study placed the POPC lipid in two different electrolytic solutions, one containing a mixture of sodium cation and chloride counterion and the other a mixture of calcium cation and chloride counterion. The two systems were

simulated for about 200 nanoseconds and then the bonding of the ions to various oxygen atoms was observed. The calcium ion took longer to bond to the carbonyl oxygen of the phospholipid headgroups than the sodium ion, but both were found to order the lipid tails and reduce the amount of self-diffusion in the lipids.

- Gurtovenko, A.A. (2005). Asymmetry of lipid bilayers induced by monovalent salt: Atomistic molecular-dynamics study. *The Journal of Chemical Physics 122, 244902 (2005)*

Gurtovenko (2005) observed the effects of monovalent cations (in this case the sodium ion) on lipid bilayers. Sodium ion was used on a double bilayer system of dimyristoylphosphatidylcholine (DMPC) which has a makeup of water-DMPC-water-DMPC-water with ions placed at various water sections. The purpose was to see how monovalent cation such as sodium distorts the bilayer depending on their position in the system. Addition of salt to both bilayers resulted in an 8% area compression, while addition to just one bilayer only resulted in a 4% compression; both systems experienced an ordering of the acyl tails. In both cases, the sodium cation found themselves attracted to the carbonyl oxygen of the DMPC headgroups. The shrinking of the area per lipid and the ordering of the lipid tails are consistent with a lipid bilayer that is becoming more ordered

- Gurtovenko, A. A., Miettinen, M., Karttunen, M. & Vattulainen, I. (2005). Effect of Monovalent Salt on Cationic Lipid Membranes As Revealed by Molecular Dynamics Simulations. *J. Phys. Chem. B 2005, 109, 21126-21134*

Gurtovenko, Miettinen, Karttunen, and Vattulainen (2005) studied the effects of sodium ion on lipid bilayers that were cationic in nature, in this study a mixture of dimyristoyltrimethylammonium propane (DMTAP) and dimyristoylphosphatidycholine (DMPC). This is unique because most studies of lipid bilayers are on anionic (negatively charged) or zwitterionic (charge neutral with local charge balancing). Their studies were performed to shed light on the possible effects that lipid concentration (amounts of different types) and the presence of ions would have on the construction of liposomes, which are vesicles used in material transportation and drug delivery. Molecular simulation using the GROMACS suite showed that no oxygen-ion binding is shown toward the cationic DMTAP but is shown toward the zwitterionic DMPC in low concentrations of DMTAP. Additionally, the lower concentrations of DMTAP allowed for lipid systems with more order in their acyl chains and compression of their area per lipid.

- Issa, Z. K., Manke, C. W., Jena, B. P. & Potoff, J. J. (2010). Ca^{2+} Bridging of Apposed Phospholipid Bilayers. *J. Phys. Chem. B 2010, 114, 13249-13254*

Issa, Manke, Jena, and Potoff (2010) observed the effects of calcium ion on apposed bilayers and the complexes that subsequently formed there. Simulations were performed on the zwitterionic DMPC in the presence of calcium ion using the CHARMM force field system (isothermal, isobaric system in the liquid-crystalline phase). The results displayed the effects of calcium on lipid bilayer-bridging in the formation of complexes formed between the calcium ion and the lipid headgroups (similar simulations with sodium did not display this complex formation). The calcium ion also showed a pathway for dehydration of the area around the bilayer by calcium displacing water oxygen around the lipid headgroups. The formation of the complexes, dehydration of the area around the headgroups, and other observations displayed evidence for easier membrane fusion in the presence of calcium.

- Mao, Y., Du, Y., Cang, X., Wang, J., Chen, Z., Yang, H. & Jiang, H. (2012). Binding Competition to the POPG Lipid Bilayer of Ca^{2+}, Mg^{2+}, Na^+, and K^+ in Different Ion Mixtures and Biological Implication. *J. Phys. Chem. B 2013, 117, 850-858*

Mao, Du, Cang, Wang, Chen, Yang, and Jiang (2012) explored the roles that various ions located in the cytosol around the lipid bilayer play in quantitative terms. In their molecular simulations, two mixtures of Ca2+, Mg2+, Na+, and K+ on a 1-palmitoyl-2-oleoyl-sn-glycero-3-phosphoglycerol (POPG) bilayer were performed using the CHARMM force field system with the GROMACS simulation software. It was found that calcium ion seemed to be the most willing to bind to the headgroup carbonyl oxygen and would often bind to the most lipid oxygen in each system. Additionally, the aggressive binding of calcium to the oxygen molecules often impeded the ability of the other ions to bind, displaying that in physiological-correct systems calcium takes precedence. Calcium was shown to take precedence in both systems, even over the other divalent cation magnesium.

- Yang, H., Xu, Y., Gao, Z. Mao, Y. Du, Y. & Jiang, H. (2010). Effects of Na^+, K^+, and Ca^{2+} on the Structures of Anionic Lipid Bilayers and Biological Implication. *J. Phys. Chem. B 2010, 114, 16978-16988*

Yang, Xu, Gao, Mao, Du, and Jiang (2010) explored the effects of various ions (Na^+, K^+, and Ca^{2+}) in various mixtures on the anionic lipid bilayer 1-palmitoyl-2-oleoyl-sn-glycero-3-phosphoglycerol (POPG) in order to see the structural effects that each ion has on an anionic lipid bilayer. Their studies were conducted using the GROMACS simulation suite along with the Berger force field system to model lipid behavior, with seven different ion systems (three pure and four mixtures). Comparing the different simulations, they determined that potassium and sodium did not show a preference for location inside of the lipid headgroups, while the calcium ion all buried themselves deep within these headgroups. In systems where the calcium ion was present in a mixture it seemed to take precedence over the other ions present and had several effects on the lipid bilayer greater than the others. These effects included an affinity for oxygen-lipid bonds in the headgroups regions, a compression of the area per lipid, and an ordering of the acyl chains.

3. PURPOSE

The literature review provided gives many examples of studies conducted on various types of lipids with various ion environments. The lipid bilayer can include many mixtures of different lipids and often does in nature, including anionic bilayers (1-palmitoyl-2-oleoyl-sn-glycero-3-phosphoglycerol or POPG), cationic bilayers (dimyristoyltrimethylammonium propane or DMTAP), and zwitterionic bilayers (1-palmitoyl-2-oleoyl-sn-glycero-3-phosphocholine or POPC). There are also many ions present in the electrolytic cytosol such as sodium, calcium, potassium, magnesium, and chloride (among others), so there are many different types of lipid-ion systems to choose from.

In order to fully understand the ion effects on zwitterionic lipid bilayers, the lipid POPC is used exclusively in this study (although it many expand to include others and possibly mixtures of others later on). The ions chosen for interaction were sodium and calcium (although studies may include magnesium later on), due to their observed effects on lipid bilayers and the possibility that some of these effects on zwitterionic lipid bilayers is still unknown. It is unlikely that potassium will be studied in this work in the future, due to the large amount of information dismissing its effects as low-key (Mao, 2012).

The simulations described in this work are simulations of the POPC lipid bilayer with no ions present, simulations of the POPC bilayer with sodium ion present (0.1 M and 0.5 M, along the appropriate counterions), and simulations of the POPC lipid bilayer with calcium ion present (0.1 M and 0.5 M, along with the appropriate counterions). The concentrations were chosen to mirror and then to exceed the normal ion concentration in the human body (0.1 M and then 0.5 M). The desired outcome of this work is to gain knowledge of the effects that these various ions will have on the structure of the zwitterionic POPC bilayer. In order to properly understand the ion mechanics behind membrane

fusion and bilayer structure, these first few simulations will create a starting point for more complicated simulations (more ions, different lipids) in the future.

4. METHODS

Each system is made up of a lipid bilayer (no proteins or ion channels) that is solvated in water in the presence of some form of ion, created with the CHARMM-GUI ver. 36 utility. The choice of POPC was made as to focus on some of the specific effects that certain ions have on the zwitterionic lipid bilayers and to make easier the charge balancing of the created systems; the zwitterionic lipid bilayer POPC has a net charge of zero, so the only counterion required are those needed to balance out the charges of the cation. The CHARMM (ver. 36) force field was used to model of all the interactions between the lipids, water, and the ions. In each system, 128 POPC lipids were used and split between two monolayers to form the bilayer; for each lipid, 100 water molecules were assigned to it, placing 12,800 water molecules for each system.

The five systems are listed in fig.2:

System Name	Type of Ion	Amount of Ion (M)	Equilibration Time Required (ns)	Current Simulation Time (ns)
A	None	-	50	40
B	Sodium	0.1	100	85
C	Sodium	0.5	100	75
D	Calcium	0.1	100	30
E	Calcium	0.5	100	55

Figure 2: Ion Systems

The systems consisting of sodium ion are close to the time required for equilibration and will be used in this report to demonstrate the analysis tools to be used. The systems consisting of calcium ion and the system with no ions have not yet passed the long-time simulation required to pass equilibrium (use of the NAMD simulation software requires roughly three days for 10 nanoseconds of simulation time). For this reason, this report is limited in scope and will be expanded in the future when these simulations complete the necessary equilibration time.

Simulations were performed using the NAMD (ver. 2.9) simulation suite, which allows for the specification for many system properties before the actual simulation is performed. Simulations were run at 2 femtosecond/step once a proper assembly was achieved to resolve any patch-grid errors. Each system was placed in an isothermal and isobaric ensemble, with a temperature of 303.15 K and a pressure of 1 bar. The temperature was chosen to place the lipid-water-ion system in the liquid-crystalline phase, over the POPC lipid phase transition temperature of 271.15 K; a temperature lower than this would place the lipid in the gel phase. All pressure controls were performed using the Langevin piston method. Lennard-Jones interactions were truncated at 12 Å and electrostatic interactions were modeled using the particle-mesh Ewald (PME) system. The created systems are also anisotropic, which means movements are allowed in the x-y plane of the simulation window. Each system will eventually run for about 20 nanoseconds post-equilibration, but only the sodium-based systems have gotten close to this goal. All data that will be considered will utilize this 20 nanosecond post-equilibration time in the future results.

5. RESULTS

It should be noted early on that this experiment is still ongoing and most of the simulations are not finished. The results section will try to summarize all of the different analysis that will occur once the simulations are completed. The final 10 nanoseconds of the 0.1 M sodium-based systems will be used as an example of how this data will be analyzed, and what types of things that are expected from both sodium and calcium according to previous results. The area per lipid, the acyl chain order parameter, the lipid-ion association, and other factors will be analyzed.

5.1 Area per Lipid

The area per lipid is a characteristic of the lipid bilayer which collectively can describe whether or not the bilayer itself is getting larger or smaller. Different ions have different effects on the area per lipid, but all cation will shrink the bilayer in some way (Yang 2010). The study by Yang et. al showed that the type of ion used as well as the amount of that ion used can significantly alter the area per lipid. The results for the anionic POPG bilayer used in this research might differ from the results that will be retrieved from tests on POPC, but tests on the zwitterionic POPC have shown that calcium does have a pronounced effect on the area (Gurtovenko 2005)
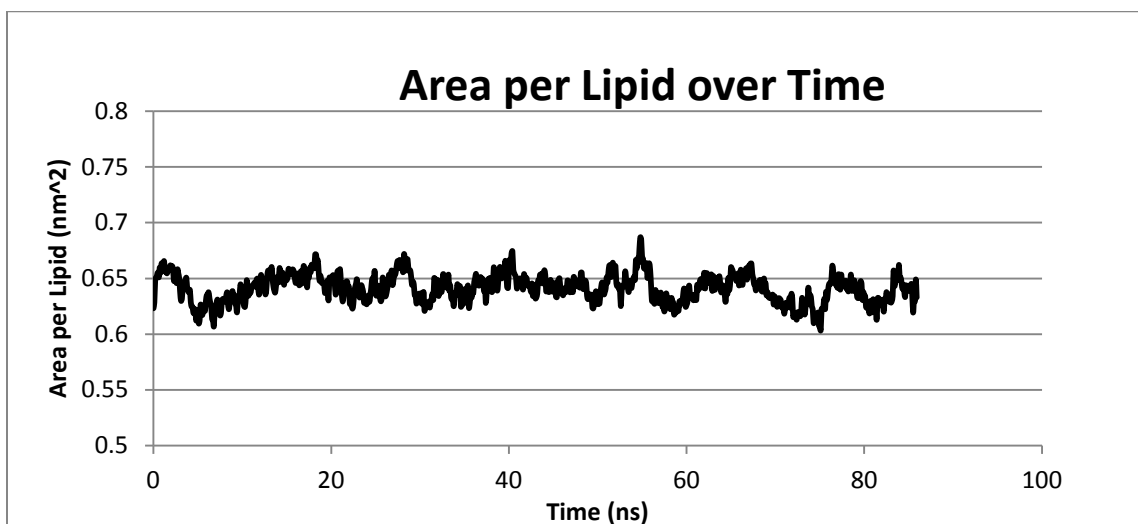

Figure 3: Area per Lipid (last 10 nanoseconds)

The graph shows the fluctuations of the bilayer area over the entire simulation time, which includes the pre-equilibration period. This data is shown to demonstrate the importance of the equilibrating the bilayer, and should smooth out more near 100 ns of simulation time. The compression of the area of POPC is expected in both of the systems containing sodium and calcium, but will be expected to be much further compressed in the systems with calcium. Part of this can be attributed to the phase transition that is induced by calcium to form a more-ordered crystalline phase (Papahadjopoulos 1975). The system with no ions will eventually act as a control over this compression, for comparison of systems with sodium and calcium.

5.2 Order Parameter of the Acyl Chains

The acyl chains are the two tails of each lipid with the names of sn1 and sn2. The tails of these lipids are visually prominent during simulation as they move around rapidly between other lipids until they equilibrate. Once they do equilibrate, the lipid tails can order themselves within the bilayer which compresses the area per lipid and also eases the process of fusion into the bilayer. The order parameter S_{CD} is a way to quantify this behavior; the larger the value of S_{CD}, the more pronounced the

ordering of the lipid tails are. The addition of sodium does order the lipid tails to a certain extent (Gurtovenko 2005), and this ordering can be seen in the order parameter plots of each tail below:
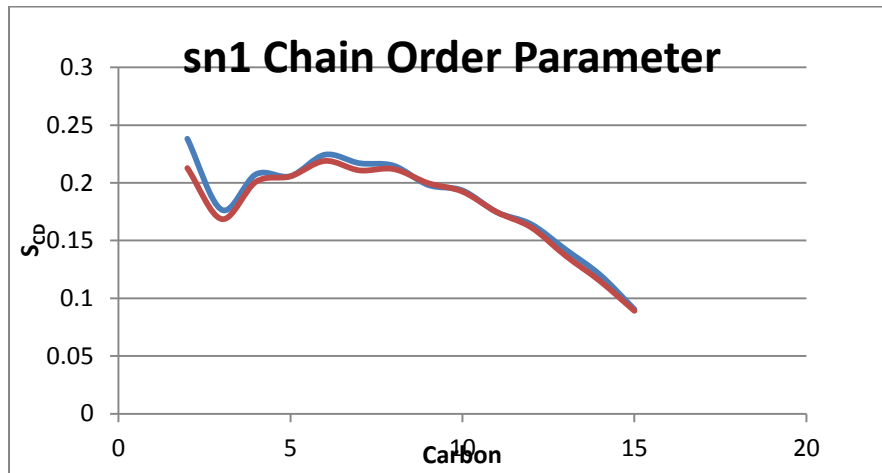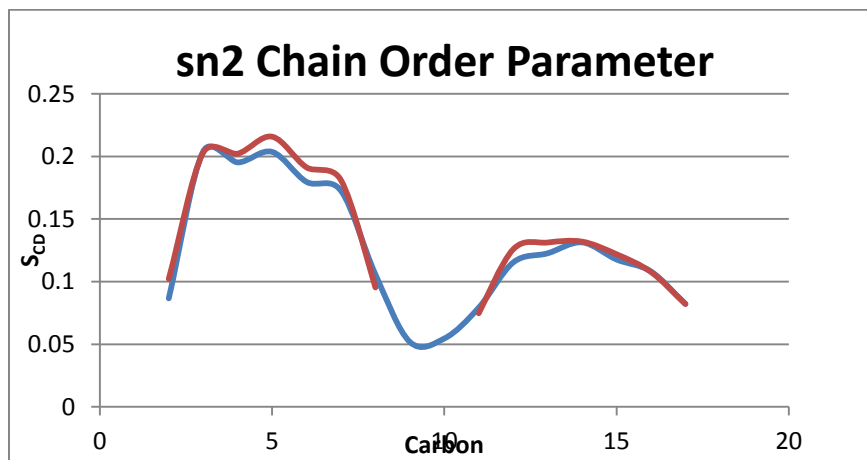

Figure 4: sn1 Order Parameter

Figure 5: sn2 Order Parameter

The order parameter for the sn1 chain is similar to what it would look like at equilibrium, since the chemical tail structure is uniform and should overall appear parabolic. The depression in the sn2 parameter is due to the double bond which appears only in this chain. Future studies will help to confirm that the order parameter is an effective way to quantify the ordering of the lipid tails in various ion systems.

5.3 Ion-Lipid Interactions

The interaction between ions and lipids are one of the most crucial things that must be considered, since this shows that the ions are interacting with the oxygen of the lipid bilayers. The presence of ions near oxygen in POPC (especially near the oxygen on the phosphate headgroups) helps to stabilize the bilayer (Yang, 2010) It is also important to note the relative positions of the cation near the oxygen in order to attempt to develop mechanisms for the binding/unbinding of cations (Bockmann 2004), which can help to understand how cations can affect fusion by moving themselves. The formation of calcium bridges also depends on the relative position of these ions (Issa, 2010).
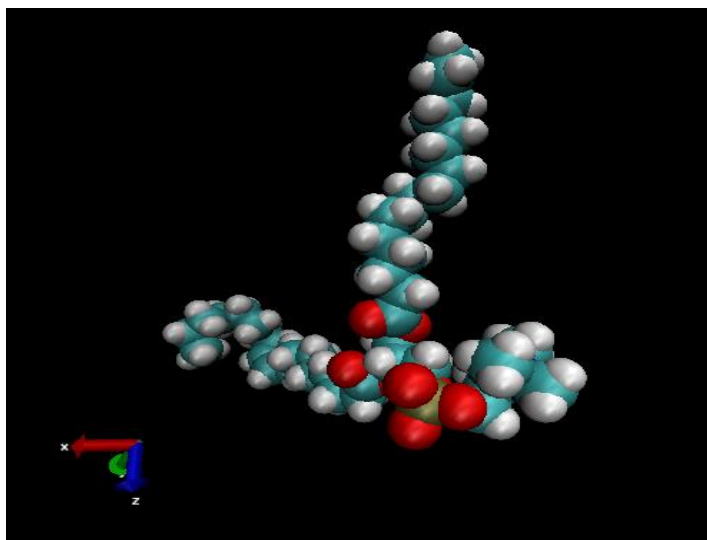
Figure 6: Single POPC Lipid

The molecule above has the phosphorus atom in brown with two of the red carbonyl oxygen (designated as O13 and O14) attached to it. The other two carbonyl oxygen are the two red atoms sticking out of each chain respectively (designated as O22 and O32). In order to determine the cutoff for interactions with the oxygen lipid pairs, radial distribution functions can be used to determine the minimum distance required for interactions:
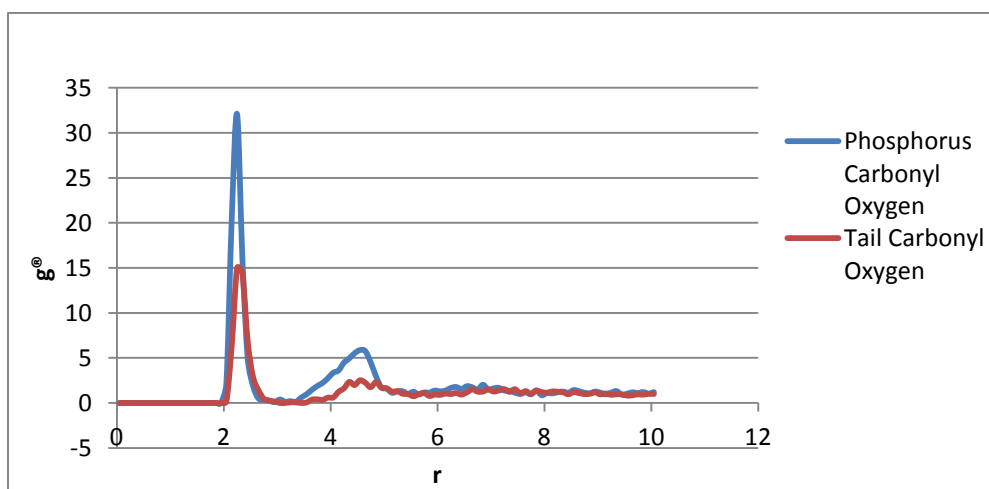

Figure 7: Radial Distribution Function for Oxygen

The first minimum of the radial distribution function is called the cutoff distance of that oxygen, and any ions found within this distance are said to be bound to that particular oxygen. Results of neighbor-finding programs are tabulated below:

Oxygen Designation	Radial Distribution Cutoff	Number of Associated Sodium Ions
O22	3.05	2
O32	3.05	3
O13	2.95	2
O14	2.95	2

Figure 8: Ion Association

The low amount of sodium ion association is expected when compared to experimental data and to previous simulation data, but is even lower compared to data from POPG binding (Yang, 2010). Sodium does not generally form bonds with these oxygen molecules due to its monovalent status (where divalent calcium does), but it still does relatively associate with the oxygen atoms. Studies have shown that in terms of divalent cation, calcium is preferred to magnesium in terms of effective bonds (Mao 2012). Future simulation will likely show increased sodium association (slightly), but much more association with calcium ion. Additionally, the zwitterionic POPC bilayer has less ion-lipid interaction when compared to the anionic POPG.

5.4 Future Work

Additional parameters for characterizing the structure and functionality of the lipids bilayer are under consideration and will be developed as research continues. These parameters include:

- Bilayer thickness, which fluctuates in a manner similar to the area per lipid and can be used alongside the area to see how lipids are pushing themselves into the bilayer. This allows for insight into the area compression that was discussed previously

- Bilayer density, which will be used to track and quantify the locations of ions, lipids, and other molecules at their relative positions in the lipid bilayer

- Headgroup orientation, which is a measure of the angle between the phosphorus atom of the headgroup and the vector normal to the bilayer. This depends strongly on the charge of the bilayer and is a way to see how the headgroups are arranging themselves due to ionic presence

6. CONCLUSIONS

At this time, no definite conclusions can be made as to the outcome of these experiments. Past simulations and experiments have suggested many different conjectures related to calcium and its effects on lipid bilayers, but these studies have included other lipids (with different charges), different ions and amounts, and different simulation environments. Until these experiments have concluded, nothing can be said about the possible effects ions such as sodium, calcium, etc. will have on the zwitterionic POPC lipid bilayer. Ultimately, the effects of calcium will be explored to determine how it effects the fusion of lipid bilayers and their structures in later work.

7. REFERENCES

Bockmann, R. A., Grubmuller, H. (2004). "Multistep Binding of Divalent Cations to Phospholipid Bilayers: A Molecular Dynamics Study." Agnew. Chemie Int. Ed. **2004**(43): 1021-1024.

Gurtovenko, A. A. (2005). "Asymmetry of lipid bilayers induced by monovalent salt: Atomistic molecular-dynamics study." The Journal of Chemical Physics **122**(244902).

Gurtovenko, A. A., Miettinen, M., Karttunen, M., Vattulainen, I. (2005). "Effect of Monovalent Salt on Cationic Lipid Membranes As Revealed by Molecular Dynamics Simulations." The Journal of Physical Chemistry B **2005**(109): 21126-21134.

Issa, Z. K., Manke, C. W., Jena, B. P., Potoff, J. J. (2010). "Ca^{2+} Bridging of Apposed Phospholipid Bilayers." The Journal of Physical Chemistry B **2010**(114): 13249-13254.

Mao, Y., Du, Y., Cang, X., Wang, J., Chen, Z., Yang, H., Jiang, H. (2012). "Binding Competition to the POPG Lipid Bilayer of Ca^{2+}, Mg2+, Na$^+$, and K$^+$ in Different Ion Mixtures and Biological Implication." The Journal of Physical Chemistry B **2013**(117): 850-858.

Papahadjopoulos, D., Poste, G. (1975). "Calcium-Induced Phase Separation And Fusion in Phospholipid Membranes." Biophysical Journal **15**: 945-948.

Yang, H., Xu, Y., Gao, Z., Mao, Y., Du, Y., Jiang, H. (2010). "Effects of Na$^+$, K$^+$, and Ca^{2+} on the Structures of Anionic Lipid Bilayers and Biological Implication." The Journal of Physical Chemistry B **2010**(114): 16978-16988.